ESL-TR-88-25

FUEL COMPONENT EFFECTS ON COMBUSTER SOOT FORMATION

G. S. SAMUELSON

UCI COMBUSTION LABORATORY
DEPARTMENT OF MECHANICAL ENGINEERING
UNIVERSITY OF CALIFORNIA
IRVINE CA 92717

AUGUST 1990

FINAL REPORT

DECEMBER 1982 - SEPTEMBER 1986

AIR FORCE ENGINEERING & SERVICES CENTER
ENGINEERING & SERVICES LABORATORY
TYNDALL AIR FORCE BASE, FLORIDA 32403

NOTICE

PLEASE DO NOT REQUEST COPIES OF THIS REPORT FROM HQ AFESC/RD (ENGINEERING AND SERVICES LABORATORY). ADDITIONAL COPIES MAY BE PURCHASED FROM:

NATIONAL TECHNICAL INFORMATION SERVICE
5285 PORT ROYAL ROAD
SPRINGFIELD, VIRGINIA 22161

FEDERAL GOVERNMENT AGENCIES AND THEIR CONTRACTORS REGISTERED WITH DEFENSE TECHNICAL INFORMATION CENTER SHOULD DIRECT REQUESTS FOR COPIES OF THIS REPORT TO:

DEFENSE TECHNICAL INFORMATION CENTER
CAMERON STATION
ALEXANDRIA, VIRGINIA 22314

Unclassified

SECURITY CLASSIFICATION OF THIS PAGE

REPORT DOCUMENTATION PAGE

Form Approved
OMB No. 0704-0188

1a. REPORT SECURITY CLASSIFICATION Unclassified	1b RESTRICTIVE MARKINGS
2a. SECURITY CLASSIFICATION AUTHORITY	3. DISTRIBUTION/AVAILABILITY OF REPORT Approved for Public Release Distribution Unlimited
2b. DECLASSIFICATION/DOWNGRADING SCHEDULE	
4. PERFORMING ORGANIZATION REPORT NUMBER(S)	5. MONITORING ORGANIZATION REPORT NUMBER(S) ESL-TR-88-25
6a. NAME OF PERFORMING ORGANIZATION UCI Combustion Laboratory 6b. OFFICE SYMBOL (If applicable)	7a. NAME OF MONITORING ORGANIZATION Air Force Engineering and Services Center
6c. ADDRESS (City, State, and ZIP Code) Dept. of Mechanical Engineering University of California Irvine, CA 92717	7b. ADDRESS (City, State, and ZIP Code) HQ AFESC/RDVS Tyndall AFB FL 32403
8a. NAME OF FUNDING/SPONSORING ORGANIZATION 8b. OFFICE SYMBOL (If applicable)	9 PROCUREMENT INSTRUMENT IDENTIFICATION NUMBER Contract # F08635-83-C-0052
8c. ADDRESS (City, State, and ZIP Code)	10. SOURCE OF FUNDING NUMBERS PROGRAM ELEMENT NO. / PROJECT NO / TASK NO. / WORK UNIT ACCESSION NO.

11. TITLE (Include Security Classification)
Fuel Component Effects on Combuster Soot Formation(U)

12. PERSONAL AUTHOR(S)
G.S. Samuelson

13a. TYPE OF REPORT	13b. TIME COVERED	14. DATE OF REPORT (Year, Month, Day)	15. PAGE COUNT
Final	FROM 12/82 TO 9/86	August 1990	129

16. SUPPLEMENTARY NOTATION
Availability of this report is specified on reverse of the front cover

17. COSATI CODES			18. SUBJECT TERMS (Continue on reverse if necessary and identify by block number)
FIELD	GROUP	SUB-GROUP	Combustor Soot, Jet Fuel, Gas Turbine Engine

19. ABSTRACT (Continue on reverse if necessary and identify by block number)

The principal objective of this program was to obtain information on the effect of fuel composition and combustor operating conditions on soot formation in a model laboratory combustor which is representative of aircraft gas turbine engines (GTEs). Work included the development of a laboratory scale combustor that reflects the characteristics of practical GTEs and the blending of a fuel surrogate from pure hydrocarbons to stimulate JP-4. The results show that the soot yield is affected by fuel molecular structure, loading, engine aerodynamics, and pattern of fuel injection. The performance of the combustor was shown to be highly sensitive to the atomizing air conditions of the fuel nozzle.

20. DISTRIBUTION/AVAILABILITY OF ABSTRACT ☒ UNCLASSIFIED/UNLIMITED ☐ SAME AS RPT ☐ DTIC USERS	21. ABSTRACT SECURITY CLASSIFICATION Unclassified	
22a. NAME OF RESPONSIBLE INDIVIDUAL Mr Paul Kotanchik	22b. TELEPHONE (Include Area Code) (904) 283-6029	22c. OFFICE SYMBOL HQ AFESC/RDVS

SUMMARY

INTRODUCTION:

Emissions from GTEs are harmful in combat, as they help disclose the aircraft's position, and in peacetime, they create an environmental hazard. Changes in fuel composition necessitated by diminishing crude oil stocks will cause increased soot forming tendencies. This project investigated the effect of fuel composition and combustor (engine) operating conditions on soot formation in a laboratory scale combustor representative of GTEs.

APPROACH:

These five areas were identified as in need of attention.

(1) Diagnostics. The extent to which a soot collecting probe perturbs the flow field of a combustor and the role of the probe sampling operation on the final result must be established.

(2) Parametric Sensitivity. The effect of the flow patterns within the GTE on soot formation needs to be determined.

(3) Fuel Simulation. A synthetic fuel is needed; a known mixture of pure hydrocarbons that simulates the physical and chemical properties of the parent fuel.

(4) Atomizer Characterization. Establishing the relationship between combustor nozzle (atomizer) operation and soot formation requires the development, verification, and application of diagnostics for the characterization of atomizer performance.

(5) Model Combustor. The design, verification, and operation of a laboratory scale wall jet can combustor (WJCC) was necessary to provide a model combustor with all the relevant features of a full scale system.

TEST DESCRIPTION:

The experiments were run on an Axisymmetric Can Combustor (ASCC) featuring an aerodynamically controlled, swirl-stabilized recirculation zone to simulate important features of practical combustors (e.g., swirl and highly turbulent recirculation). A spray characterization chamber was used to characterize a liquid fuel atomizer under isothermal conditions. Soot samples were taken with a water cooled electrically-grounded sample probe. The optical soot probe used scattering intensity rationing for the point-measurement of particle size and number density of soot was scattering intensity rationing. Incorporate a two-component Laser Anemometer (LA) system such that measurements of axial and azimuthal velocity can be made simultaneously with particle size. The measurement method used for droplet sizing and droplet velocity is phase Doppler (PD) interferometry.

RESULTS/CONCLUSIONS:

The conclusions for each task are delineated in Section III. The salient conclusions for the program are summarized below:

1. The sampling conditions of an extractive probe are important to soot morphology.

2. The blending of a fuel surrogate to simulate a petroleum derived JP-4 is viable.

3. Doping of the surrogate with small amounts of select compounds can increase the yield of soot.

4. A wall jet can combustor (WJCC) has been designed with clean boundary conditions, optical access, and performance that reflects the basic characteristics of practical gas turbine can combustors.

5. Isothermal characterization of spray behavior does not reflect the performance of the atomizer in gas turbine combustors. In situ measurements are required.

6. The behavior of fuel sprays is likely dependent upon the specific characteristics of the combustor in which they are operated.

7. The spatial distribution of soot, as well as the soot yield in a complex flow combustor, is a function of not only fuel molecular structure and fuel loading, but of flow aerodynamics and pattern of fuel injection.

8. The performance of the model gas turbine can combustors used in the present study are especially sensitive to the atomizing air conditions of the fuel nozzle.

PREFACE

This report was prepared by the UCI Combustion Laboratory, Department of Mechanical Engineering, University of California, Irvine CA 92717, under Contract Number F08635-83-C-0052, for the Air Force Engineering and Services Center, Engineering and Services Laboratory (AFESC/RDVS), Tyndall Air Force Base FL 32403-6001.

Work on this program was performed between 12 December 1982 and 29 September 1986. Major Paul Kerch and Capt Wayne P. Chepren were the AFESC/RDV project officers.

The individuals who participated in and provided major contributions to the program include graduate students Randall A. Smith, Thomas A. Jackson, Roger C. Rudoff, and Vince G. McDonell; laboratory staff Craig P. Wood; and Department of Mechanical Engineering staff Verna Bruce and Janice Johnson.

This report has been reviewed by the Public Affairs Office and is releasable to the National Technical Information Service (NTIS). At NTIS, it will be available to the general public, including foreign nationals.

This technical report has been reviewed and is approved for publication.

Paul Kotanchik

PAUL KOTANCHIK, GS-12
Project Officer

MICHAEL L. SHELLEY, Maj, USAF, BSC
Chief, Environics Division

Wayne P. Chepren

WAYNE P. CHEPREN, Capt, USAF
Chief, Environmental Compliance R&D

Frank P. Gallagher III

FRANK P. GALLAGHER, Colonel, USAF, BSC
Director, Engineering and Services Laboratory

Accesion For	
NTIS CRA&I	X
DTIC TAB	☐
Unannounced	☐
Justification	
By	
Distribution /	
Availability Codes	
Dist	Avail and / or Special
A-1	

(The reverse of this page is blank.)

TABLE OF CONTENTS

TABLE OF CONTENTS

(continued)

TABLE OF CONTENTS

(continued)

TABLE OF CONTENTS

(continued)

LIST OF FIGURES

LIST OF FIGURES

(concluded)

LIST OF TABLES

(The reverse of this page is blank.)

SECTION I
INTRODUCTION

A. OBJECTIVE

A recent trend of aircraft toward greater soot production has been traced, at least in part, to changes in the properties of current fuels. The projected use by Air Force aircraft of shale-derived or broadened-specification fuels having an increased tendency to produce soot means greater difficulty in meeting the future USAF aircraft smoke emission goals.

The principal objective of this program was to obtain information on the effect of fuel composition and combustor operating conditions (e.g., nozzle conditions), on soot formation in a model laboratory combustor which is representative of aircraft gas turbine engines (GTEs). This information is needed to evaluate and develop models destined for gas turbine design, and to provide a basis for estimating the impact of fuel and composition changes on the sooting tendency of GTEs.

To meet the objective of the program, the following five areas were identified as in need of investigation:

- Diagnostics. Although nonintrusive measurements are available for acquiring most of the required data, the determination of soot morphology and gravimetric analyses rely on extractive probe sampling. **The extent to which an extractive probe perturbs the flowfield of a combustor, and the role of probe sampling operation on the final result needs to be delineated.**
- Parametric Sensitivity. The sensitivity of soot production on parameters amenable to control in gas turbine combustors must be determined if effective control strategies are to be established. **The sensitivity of soot production in combusting flows typical of gas turbine combustors needs to be established.**
- Fuel Simulation. The exploration of fuel composition on soot formation requires compositional control of the fuel. Practical jet fuels are comprised of over 300 constituents, most of which are less than 1 percent by volume. **A surrogate is needed, a multicomponent mixture of pure hydrocarbons, that simulates the physical and chemical properties of the parent fuel, as well as the combustor aerothermochemical performance.**

- Atomizer Characterization. A principal contributor to combustor performance is the nozzle used to inject, atomize, and distribute the fuel within the dome. **Establishing the relationship between nozzle operation and soot formation requires the development, verification, and application of diagnostics for the characterization of atomizer performance.**
- Model Combustor. To develop the proposed data base a model combustor is required to provide (1) optical access for laser diagnostics, (2) clean boundary conditions for modeling, and (3) features representative of practical devices. Before the present program, a two-dimensional axisymmetric can combustor (ASCC) was developed to meet these criteria. A key feature, wall jet injection, was excluded to present axisymmetry for two dimensional modeling. Wall jets are likely critical in the evolution of the soot in practical systems. As a result, **the design, verification, and operation of a wall jet can combustor (WJCC) is necessary to provide a model combustor with all the relevant features of a practical system.**

B. BACKGROUND

The recent trend of aircraft toward greater soot production has been traced, in part, to changes in the properties of current jet fuels. At the same time, the combined pressures of rising jet fuel prices, diminishing oil reserves, and increasing dependence on foreign crude oil suppliers increase the interest in alternative sources of fuel, such as oil shale, or in relaxing current jet fuel specifications to permit a greater yield of jet fuels from present crude stocks. In light of a possible future use by Air Force aircraft of such alternative fuels, it is prudent to determine the potential of these fuels for increased soot production, and to develop methods for controlling soot production in aircraft gas turbine engines.

A number of investigations have been conducted to determine the effects of hydrocarbon fuel variations on aircraft gas turbine engine combustion. These studies have shown that alternative fuels display an increased tendency to form soot. The increased soot formation appears to be a direct result of changes in the characteristics of the fuels, particularly their decreased hydrogen content and increased final boiling point. Increased aircraft smoke emissions are undesirable in combat, where the smoke trail gives away the

aircraft position, and in peacetime, since smoke emissions from aircraft and associated engine test cell facilities can present a significant pollution problem and violate national or local environmental regulations. Air Force Regulation 19-1 promulgates the Air Force goal to maintain aircraft engine smoke emissions below the visibility threshold. The smoke-producing potential of alternative fuels will seriously hamper achievement of this goal.

C. SCOPE

Efforts to reduce smoke from aircraft gas turbine engines operating on alternative fuels include modification of the engine combustor design and the use of smoke suppressant fuel additives. Determination of the optimal control approach requires experimental evidence to (1) identify and interrelate the various effects of fuel characteristics, additive properties, and combustor operating conditions on soot formation, and (2) evaluate and develop analytical models destined for application to gas turbine engine design. Previous studies on full-scale combustors have been able to identify some general trends of soot formation but do not provide an opportunity for either theoretical analysis or modeling (limiting their application for predictive purposes), or in-situ measurements (limiting their application for detailed flowfield measurements). Studies to date which have attempted a thorough analysis of soot formation are limited to simple combustion systems such as flat flames or well-stirred reactors which do not include the complex aerodynamics present in gas turbine engine combustion and could yield results which are not representative of such combustion. To bridge this gap, the present program employed laboratory combustors which include the fuel injection and recirculating flow typical of gas turbine combustors while retaining the capability for optical access and modeling.

SECTION II
APPROACH

The approach was to address the areas previously identified in a systematic, coordinated sequence of tasks. In this section, the tasks are delineated and the organization of the experimental and results section is outlined.

A. PROGRAM TASKS

The effort was divided into the following seven tasks:

1. Task 1. Probe Perturbation

This task was established to quantitatively assess the perturbation of an extractive probe in a complex flow by using a nonintrusive optical measurement of local soot concentration and particle size. The extractive probe represents the classical method for the measurement of soot weight concentration and, because of its simplicity and relative ease of use, will continue to be the principal technique employed into the foreseeable future. The nonintrusive optical instrument available in the proposed program provides a unique opportunity to formally address two major questions associated with the use of extractive probes, that of the perturbation produced by the presence and operation of the physical probe on the local number density and particle size. Such an assessment is important in establishing: (1) the quality and credibility of the extractive probe data collected and analyzed under Tasks 2, 3, 4, 5, 6 and 7 of the present study, and (2) the information necessary to guide investigators in future studies with respect to the limits of applicability of extractive probes in measuring soot weight concentration and size produced in gas turbine type combustors.

2. Task 2. Parametric Sensitivity

Soot production in gas turbine combustors depends on a variety of parameters, including fuel composition, atomization quality, and pressure. This task was directed to the question of parametric sensitivity. Using a diagnostic developed under a prior program for the optical measurement of soot, a parametric study of fuel composition, nozzle atomizing conditions, and

fuel injection state was undertaken to assess the extent to which these parameters affect soot production.

3. Task 3. Fuel Simulation

The extent to which the sooting performance of blends of pure hydrocarbons can be used to represent practical jet fuels was established under this task. The use of blends composed of pure hydrocarbons in simulating a practical fuel has the advantage of allowing the fuel composition to be accurately controlled and monitored. In contrast, the practical fuels are chemically complex and the partitioning of the individual hydrocarbon species resident in the fuel mixture is difficult. A blend of pure hydrocarbons which simulates the sooting performance removes this ambiguity and focuses attention on those compositional constituents that dominate the sooting propensity of the next generation fuels.

4. Task 4. Fuel Atomization

In addition to fuel composition, the atomization quality is important to the sooting performance. Atomization quality includes the drop size distribution produced, as well as the spatial distribution of the fuel relative to the recirculation zone. This task was directed to establishing the functional dependence of drop size and distribution on the atomizing air and fuel pressure using optical droplet sizing interferometry, first under cold conditions. Secondly, the sooting propensities of the fuels in the combustor were documented as a function of atomizing performance with the goal of establishing sensitivity of soot formation and soot burnout on the nozzle operation.

5. Task 5. Wall Jet Dilution

In an earlier program, a two-dimensional, axisymmetric can combustor (ASCC) was developed with features representative of the primary zone of a gas turbine combustor: strong swirl, strong backmixing, and liquid fuel spray injection. These features govern the formation and early oxidation of soot. The final burnout of soot occurs in the secondary zone of a practical combustor, a zone characterized by injected jets by air from the side wall. These jets influence the aerodynamics in the secondary zone and determine the distribution of oxygen. The inclusion of wall jet injection and

assessment on the sooting performance was determined under this task. The combustor was modified to include wall jet injection while maintaining sufficient optical access to allow radial mapping of soot size and number density at key axial locations. The modified version was dubbed the wall jet can combustor (WJCC).

The ASCC is designed to operate at one atmosphere to facilitate the use of the extensive diagnostic support of the present experiment, examples of which include optical and extractive probe access. Practical combustors are operated at elevated pressures, generally with an increase in soot production. As a result, pressure was included as a design parameter in the WJCC to allow the results of the present experiment to be more effectively extrapolated to the pressure levels encountered in practical systems.

6. Task 6. Simulation Optimization

Under this task, the combination of atomizer operating condition, and air flow splits in the WJCC was evaluated to assess the extent to which the model combustor simulated actual aircraft gas turbine combustor performance. In addition, a preliminary assessment of the sooting performance was determined and critically compared to the two-dimensional can configuration.

7. Task 7. Analysis

This task ran in parallel with Tasks 1 through 6, and included the effects of probe perturbation on soot particle sampling, the applicability of the results to actual gas turbine engines, and the use of the ASCC and WJCC for predicting the sooting propensity of fuels in practical gas turbine combustors. The objective of the analyses was to provide and interpret the experimental evidence required to (1) identify and interrelate the combustor operating conditions on soot formation and burnout, and (2) evaluate and develop model combustors for application to gas turbine design.

B. PROGRAM IMPLEMENTATION

The tasks were implemented in sequence with overlap as necessary and appropriate to optimize the program plan. Section III presents the experimental components, while Section IV presents the results, task by task:

1. Probe Perturbation

2. Parametric Sensitivity
3. Fuel Simulation
4. Fuel Atomization
5. Wall Jet Dilution
6. Simulation Optimization

The analysis task, Task 7, is intertwined within the presentation of the basic six tasks.

SECTION III
EXPERIMENT

A. COMBUSTOR

The combustor employed was a model laboratory complex flow combustor developed in a series of tests (References 1 and 2). The configuration is presented in Figure 1. The Axisymmetric Can Combustor (ASCC) features an aerodynamically controlled, swirl-stabilized recirculation zone to simulate important features of practical combustors (e.g., swirl and highly turbulent recirculation).

For the present work, the housing consisted of an 80 mm inner diameter cylindrical stainless steel tube that extended 32 cm from the plane of the nozzle. Rectangular, flat windows (25 by 306 mm) were mounted perpendicular to the horizontal plane on both sides of the combustor tube to provide a clear, optical access for the laser measurements.

A set of swirl vanes (57 mm outer diameter) were concentrically located within the tube around a 19 mm outer diameter centrally positioned fuel delivery tube. Dilution and swirl air were metered separately. The dilution air was introduced through flow straighteners in the outer annulus. The swirl air passed through swirl vanes with 100 blockage which imparted an angle of turn to the flow of 60 degrees. For the swirl-to-dilution air flow ratio of 1.66 used in the present study, the swirl number obtained by integrating across the swirl vanes was 1.3; that obtained by integrating the total inlet mass flux was 0.5.

B. ATOMIZER

The air-assist nozzle used in this evaluation (Parker Hannifin Part No. 6830604) was designed to fill a requirement for a low-flow, two-phase nozzle with a high degree of atomization for use in an atmospheric, laboratory combustor. The atomizer consists of two principal components (Figure 2). The outer body houses a set of swirl vanes and one complete air circuit. Within this, a fuel insert is fitted which contains a hollow tube surrounded by a set of swirl vanes on the outside surface. In conjunction with a shroud, the insert forms a second air circuit. Fuel is injected radially as high velocity jets through three discrete ports located 120 degrees apart in the tip of the hollow fuel insert. These jets impinge on the inner surface of the shroud

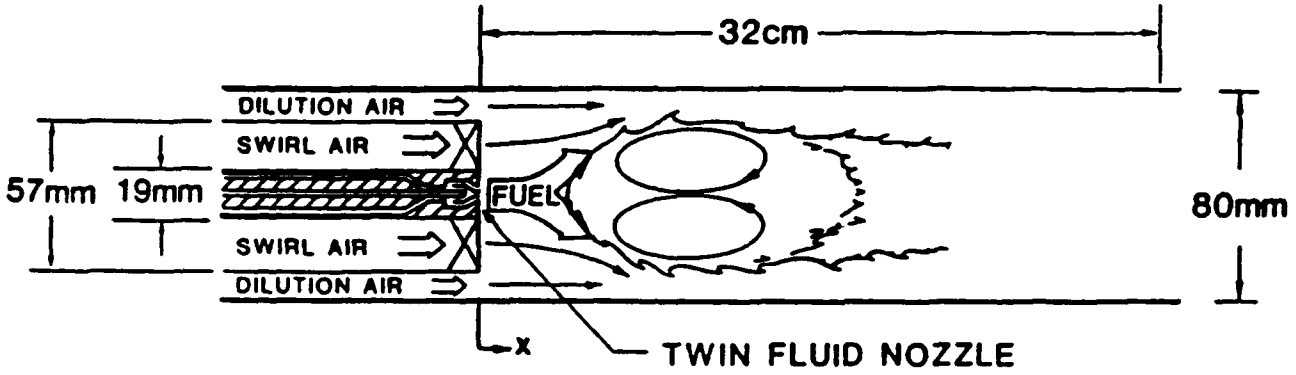

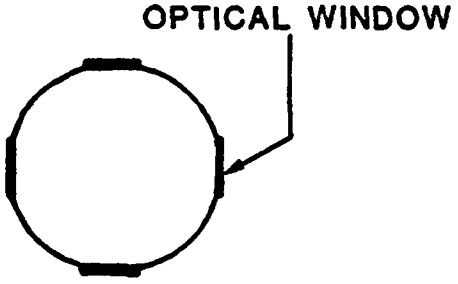

Figure 1. Axisymmetric Can Combustor (ASCC).

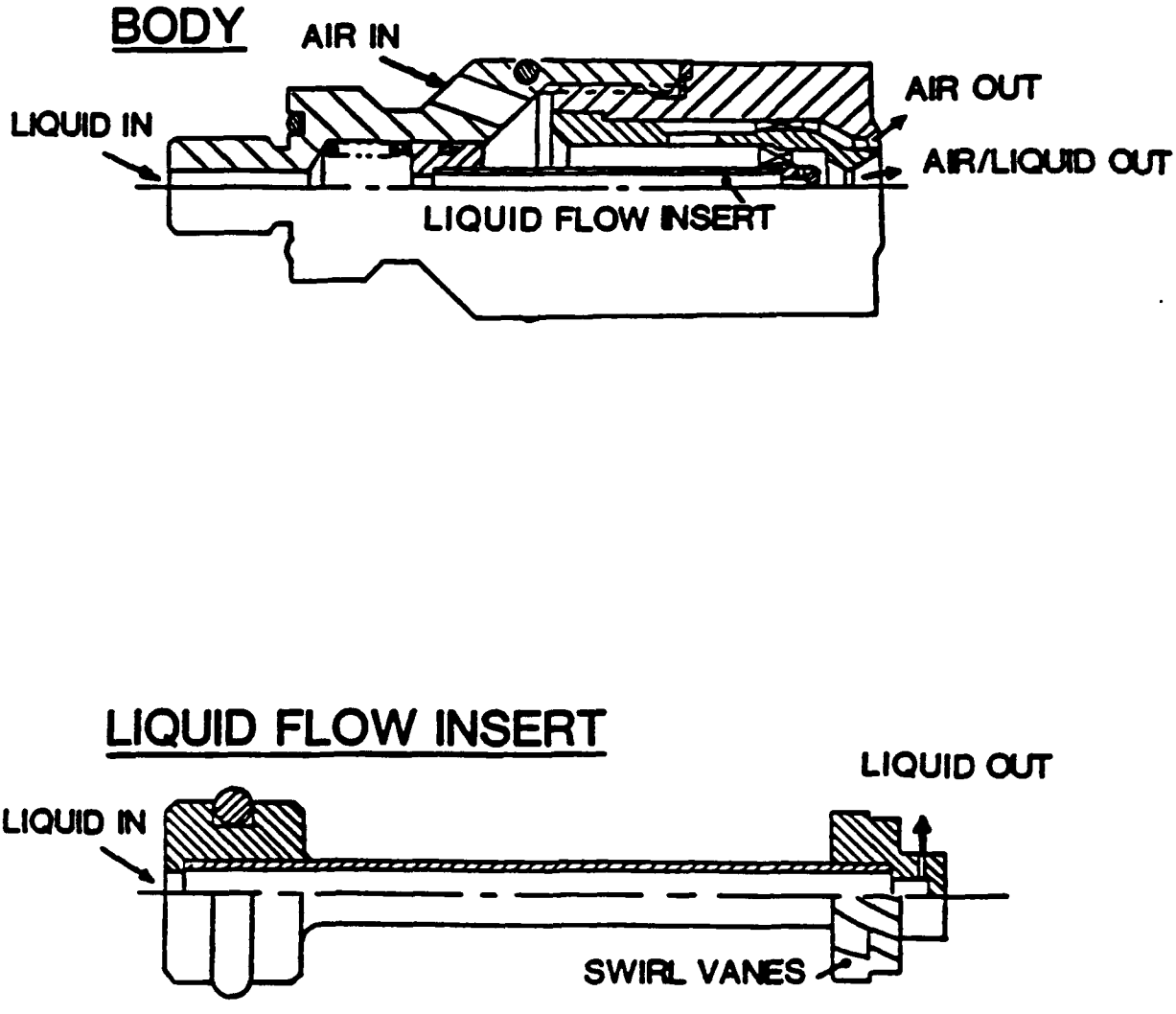

Figure 2. Atomizer.

that separates the two air circuits. The two atomizer swirlers and the combustor swirler each impart a counterclockwise tangential velocity (looking into the face of the combustor and nozzle).

C. SPRAY CHARACTERIZATION CHAMBER

The spray facility (Figure 3) is designed to characterize a liquid fuel atomizer under isothermal conditions (References 3 and 4). The chamber consists of a 30.5 cm inner diameter by 152 cm long Plexiglas® tube positioned vertically at the center of an optical platform. The tube rests in a fuel collection basin, connected to an exhaust system via a fuel vapor trap. The chamber and basin assembly is mounted on a precision platform permitting movement with one degree of freedom in the horizontal plane for radial traverses of the spray.

The atomizer is centrally positioned within the chamber in a fixture that permits vertical movement for axial traverses. The atomizer is assembled in the end of a 19 mm outer diameter fuel delivery tube plumbed to supply JP-4 fuel and atomizing air. Screen air is introduced into the top of the chamber and, coupled with the exhaust system in a push-pull manner, provides a bulk reference velocity of approximately 0.5 m/s to eliminate mist accumulation caused by recirculation at the atomizer inlet plane and/or wall recirculation at the measurement plane.

D. EXTRACTIVE PROBE

The extractive probe and sample train utilized in this study are slight modifications of those used previously (References 5 and 6). The probe is of stainless steel, with an overall outside diameter of 9.5 mm (3/8 inch) and a 3.0 mm (1/8-inch) inside diameter sampling tube. The overall length of the probe is 616 mm (24-1/4 inches) including a large radius bend of 508 mm (20 inches) to clear the combustor exhaust stream. A schematic of the inlet section is presented in Figure 4a.

The probe is water cooled to approximately 80°C (175°F) to insure its structural integrity and provide a convective quench to the sample, while preventing the condensation of water and heavier hydrocarbons from the sample stream. Additional quenching is provided by inert gas addition to the sample stream. Nitrogen is injected through thirty-two, 0.79 mm (0.031-inch) diameter ports in the sample tube wall. The number and diameter of holes are

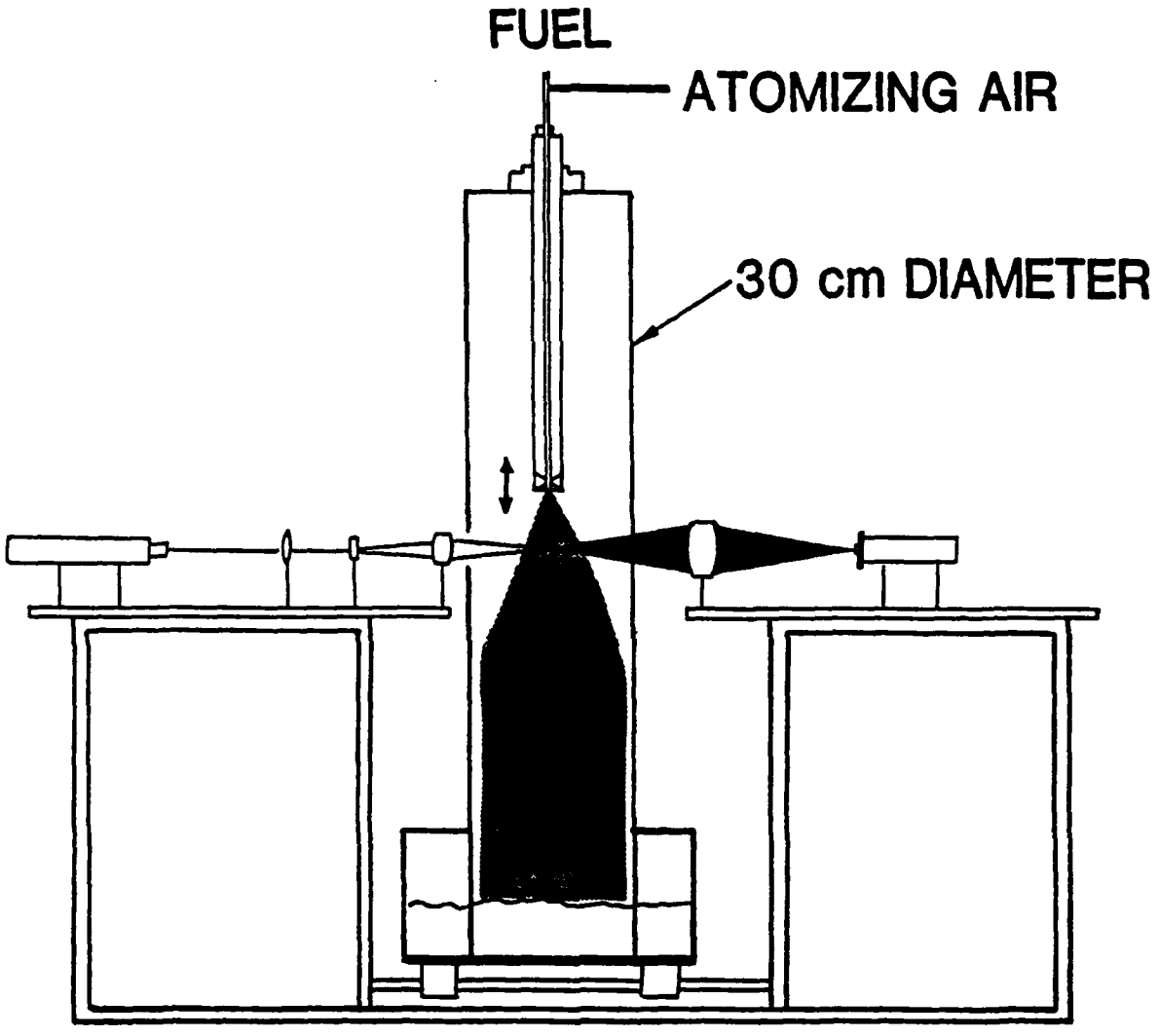

Figure 3. Spray Characterization Chamber.

(a) Extractive Probe

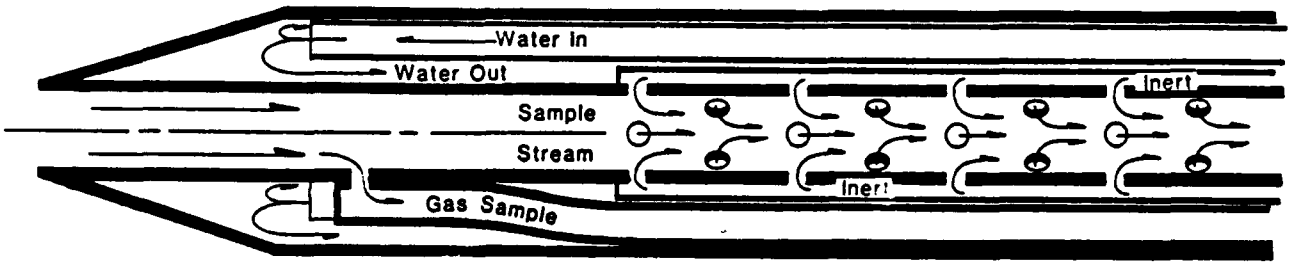

Figure 4. Extractive Probe.

(b) Sample System

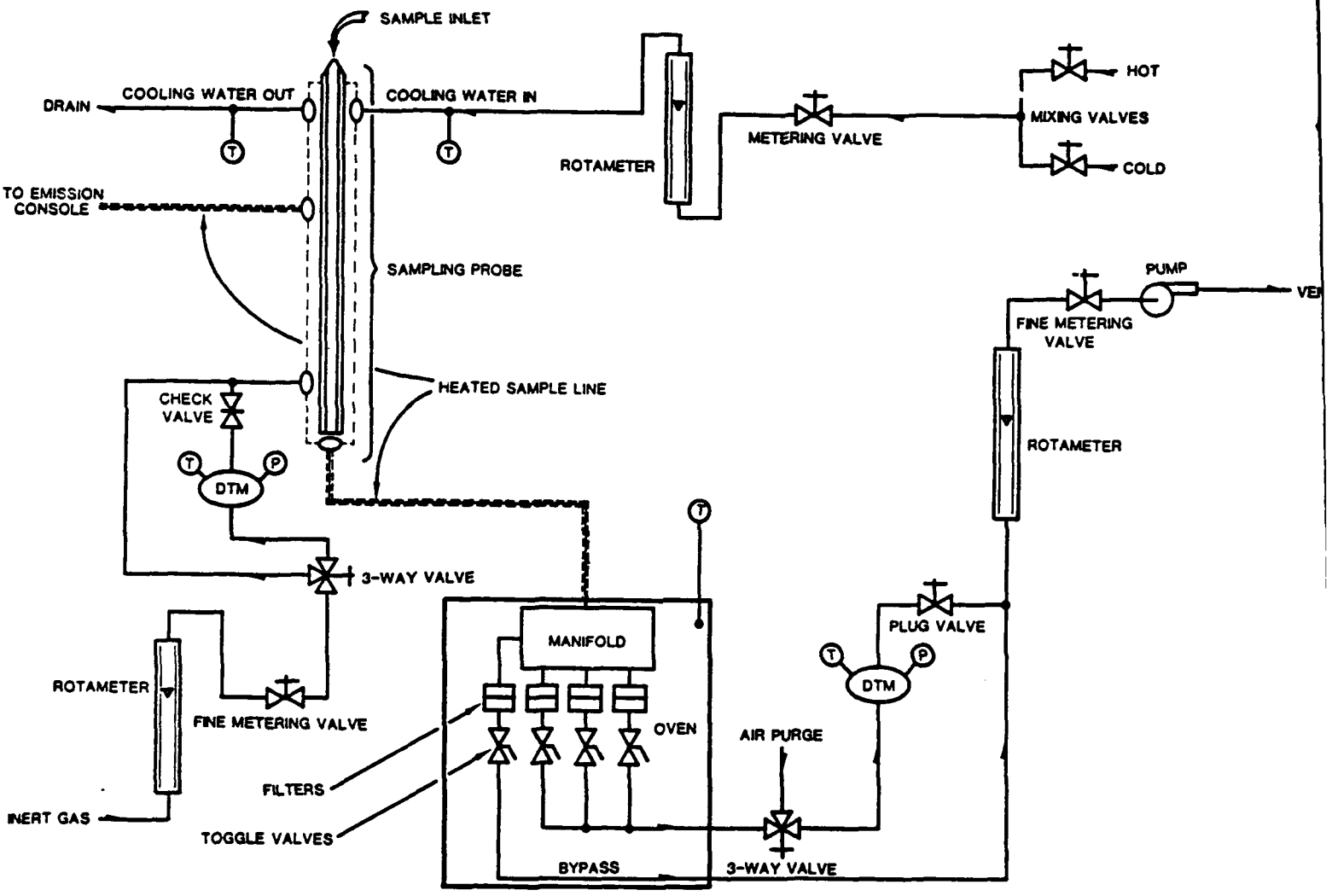

Figure 4. Extractive Probe (concluded).

designed to minimize jetting effects in the sample stream (Reference 5).

The sample system consists of a 1.2-meter (4-foot) heated (120°C [250°F]) sample line, an oven, a vacuum pump and the volumetric flow-metering equipment shown in Figure 4b. The oven, heated to 60°C (140°F), houses a manifold which directs the incoming sample stream to four separate filter holders. Selection between the bypass and three sample filters is accomplished through toggle valves located downstream of each filter. The bypass and two of the sample filters consist of 47 mm (1.85-inch) diameter Gelman microquartz fiber filters with DOP efficiencies of 99.9 percent. The remaining filter holder houses a Nuclepore membrane filter (47 mm diameter) with 0.08 μm pore size. The Gelman filters were used to collect samples for the gravimetric analyses, while the Nuclepore filters were chosen for their adaptability to scanning electron microscopy.

Isokinetic conditions are established by optically measuring with laser anemometry the axial velocity at the probe entrance and applying a gas temperature correction. Temperatures are obtained from thermocouple measurements within the flowfield.

E. THERMOCOUPLE PROBE

The temperature probe consists of a 30-gauge platinum-13 percent rhodium vs. platinum exposed junction thermocouple. The thermocouple was supported by a 1.6 mm (0.063-inch) outer diameter inconel tube, 51 mm (2 inches) long, was mounted to a 6.4 mm (0.25-inch) outer diameter inconel support to provide structural rigidity. Water cooling was provided in the larger inconel tubing to assure the structural integrity of a necessary probe bend, but only to within 42 cm (16.5 inches) of the thermocouple so as to minimize conduction losses down the length of the probe.

The probe was mounted on a three-axis positioning traverse consisting of three orthogonally oriented screw motion assemblies. With this system, the thermocouple junction could be placed within an accuracy of ±0.07 mm (±0.003-inch). The temperature was displayed on a digital thermometer (Fluke Model 2160A) having an analog output of 1.0 mV per °F.

The effects of probe perturbation on the mean values and statistics of the local aerodynamic field have been evaluated in the present combustor for a thermocouple probe of similar design (Reference 7). The variations in the mean values range from zero to a few percent, except on the centerline and in

the recirculation zone where the variation approaches 20 percent. The inference is that the mean temperature data presented here are affected by the probe perturbation to a similar extent. Parenthetically, the statistical properties (e.g., u', w', $\overline{u'w'}$), not considered in the present study, are more sensitive to probe perturbation. The data presented are not corrected for radiation loss.

F. OPTICAL SOOT PROBE

The method adopted for the point-measurement of particle size and number density of soot was scattering intensity ratioing. Figure 5a illustrates the optical configuration, a modification of that used previously (Reference 8). This earlier work utilized collection optics at 10 degrees and 5 degrees off the optical axis. The current work employed collection optics at 60 degrees and 20 degrees to reduce the smallest size of particles that could be resolved from 0.3 to 0.08 μm.

A 5-watt Model 165 Spectra-Physics argon-ion laser, operating in the multiline mode, was used as the source of light. The laser lines were separated by a dispersion prism to resolve the blue line (488.0 nm). The beam was focused to a 110 μm waist diameter using a 50 mm diameter F/5 focusing lens. The scattered intensity was detected at 60 degrees and 20 degrees which provided a particle size detection band of 0.08 μm < d < 0.38 μm. Other angles were available but 60 degrees/20 degrees provided the smallest resolvable size (0.08 μm) of those pairs available.

The scattered light was focused to two photomultiplier tubes (RCA Model 8575) having quantum efficiencies of approximately 15 percent at the 488.0 nm wavelength with pinhole aperature diameters of 200 μm. The supply voltage to the tubes was approximately 1200 volts. The output signal from the photomultiplier tubes was passed into a Spectron Development Laboratories (SDL) Model LA-1000 logarithmic amplifier which converted the negative current to a positive voltage and was scaled for +10 volts peak output when the input current was -1 mA. The amplified signals were then fed to a SDL Model RP-1001 Intensity Ratio Processor (RP). The RP registered and processed the peaks of the two signals, provided certain criteria were met. The DC voltages input from the two channels of the logarithmic amplifier were processed by an analog subtractor circuit in the RP which amplified the signal with a gain of five

(a) Optical Configuration

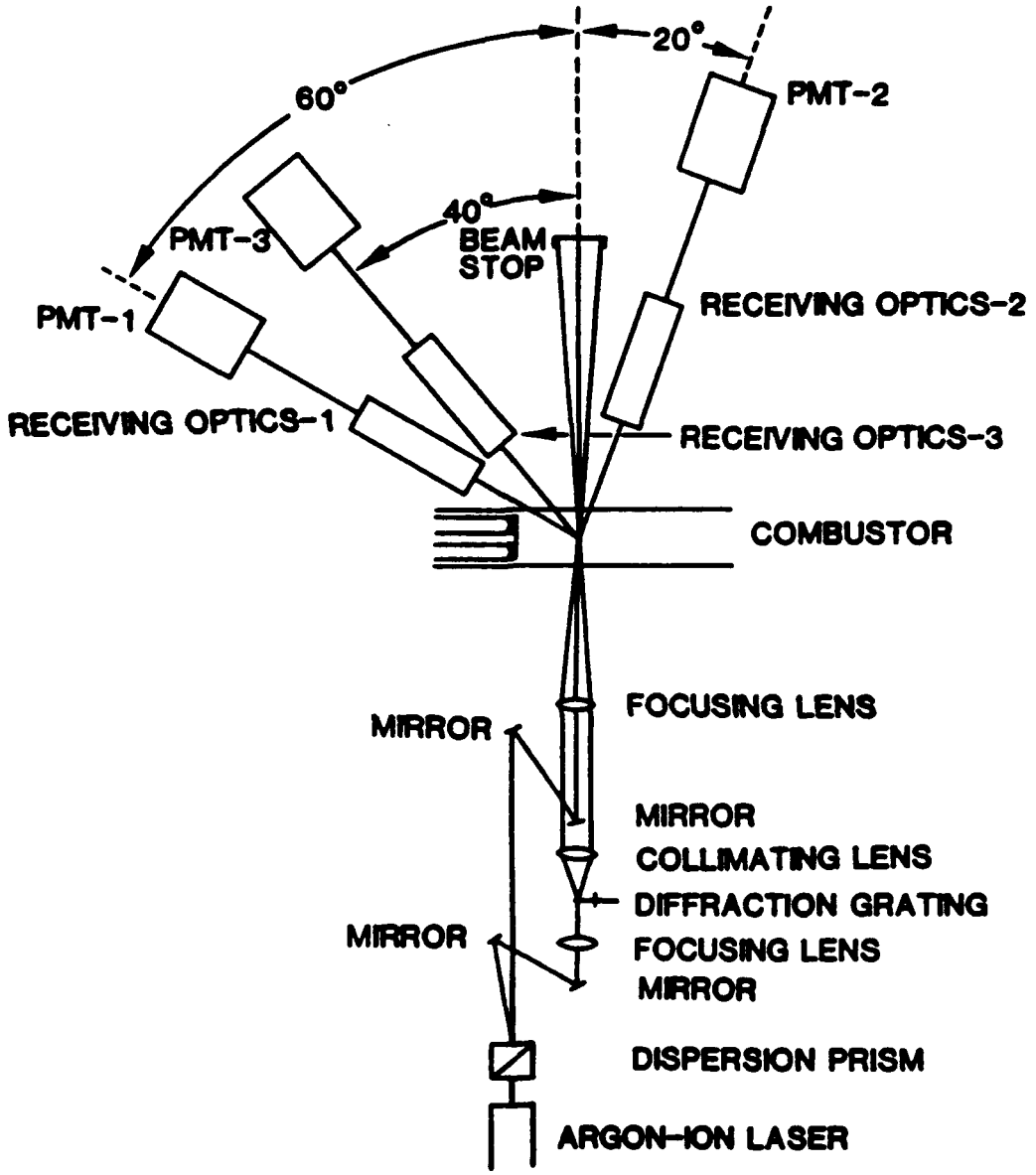

Figure 5. Optical Soot Probe and Laser Anemometer.

(b) Data Presentation

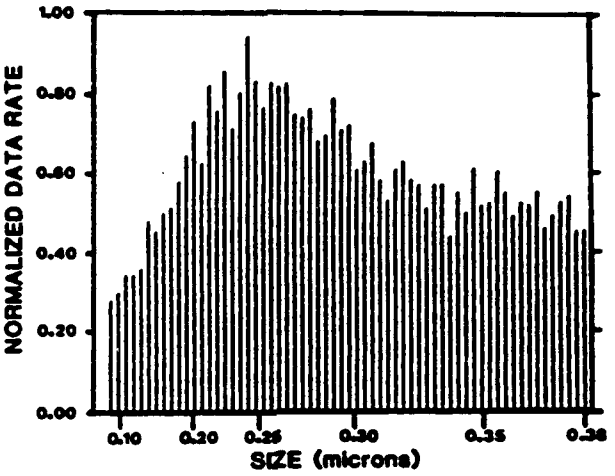

DATE: 21SEP83
SERIES: ISOTET RUN: 1006 21SEP83
COMMENT: D=DATA HV=1200/1220 LASER=1W
R/R=0.83 X/R=3.0 EQ/R=0.5 V=7.5M/S

MAX RAW COUNT = 764
TOTAL RAW COUNT = 30131
SAMPLE TIME: 11.4 SECONDS

LISTING OF RAW COUNTS

RATIO	BIN COUNT	RATIO	BIN COUNT
.946	225	.31	584
.913	239	.299	492
.881	278	.289	508
.85	279	.278	545
.82	285	.268	467
.791	387	.259	429
.763	367	.25	492
.736	405	.241	506
.71	418	.232	472
.685	472	.224	459
.661	522	.216	410
.637	594	.209	461
.615	506	.201	458
.593	670	.194	352
.572	615	.187	442
.552	696	.181	398
.532	575	.174	491
.513	652	.168	414
.495	764	.162	421
.478	672	.156	487
.461	620	.151	445
.444	669	.145	393
.429	665	.14	428
.414	669	.135	418
.399	605	.13	448
.385	597	.126	369
.371	616	.121	393
.358	549	.117	419
.345	563	.113	433
.333	634	.109	362
.321	573	.105	364

Figure 5. Optical Soot Probe and Laser Anemometer (concluded).

and converted the signal to an 8-bit binary number. The RP had a variable lower threshold voltage, allowing a measure of control over the rejection of background noise.

The binary output was fed to an Apple II microcomputer, which resolved this output into 62 bins. The size distribution was determined by the number of counts in each bin, where each bin encompassed a discrete size range (Figure 5b). The counts in each bin were then divided by the time required to collect them, resulting in a count rate (counts/second). A histogram, also shown in Figure 5b, was then generated of normalized data rate versus particle size (in microns). The normalization of this histogram was under the operator's control through the system software. The histogram could be normalized to itself (giving the bin with the highest sooting rate an intensity of 1.0), normalized to the highest sooting rate among all the histograms generated for a particular fuel, normalized to the highest sooting rate among any number of fuels or operating conditions. The results of this normalization procedure are evident in Figures 17, 18, 19, and 20.

The interpretation of the measured intensity ratio is based on the analysis of the Mie scattering properties of a homogeneous, isotropic spherical particle. Soot, a nonspherical scatterer with an index of refraction of some uncertainty, therefore requires special consideration. An evaluation of such effects, considered in an earlier study, concluded that the combined error was 20-30 percent with some broadening of the distribution (Reference 8).

Calibration of the optical system was performed routinely at the beginning of each run session using polystyrene particles of a known size (mean diameter = 0.255 μm, standard deviation = 0.9 percent). Calibrations were regularly checked at the end of each run session to verify that the optical quality of the combustor windows had not degraded. In addition, consistency in the performance of the combustor and optical system was monitored over a period of weeks by periodically repeating the isooctane/tetralin data set. After attaining thermal equilibrium, nine points in the flowfield were monitored for soot data rate and size distribution. At any given station, the variation in the peak of the size distribution of the soot never exceeded 10 percent of the nominal value at that station. The data rate was more variable. Along the outer perimeter of the combustor (e.g., r/R = 0.83), where nominal sooting rates exceeded 1500 Hz, the variation in data

rate was approximately 30 percent. At the interior stations where sooting rates were nominally below 300 Hz, the data rate varied from 47 percent to 71 percent, depending on the station, with the greater variability correlated with lower data rate. The variability of the data rates is not unreasonable at this point in the system development. Several parameters of the measurement system can influence the rate including the alignment and focusing of two optical detectors at a coincident point, and the signal processor thresholds. In addition, the condition of the twin-fluid injector had a marked effect on data rate. The specific orientation of the injector with respect to the combustor flowfield was found to change the sooting rate at specific points in the flowfield, presumably because of resulting changes in fuel distribution caused by small asymmetries in the atomized spray. The effect of nozzle configuration and performance on fuel distribution and soot production will be explored in more detail in future work.

G. LASER ANEMOMETER

The configuration of the optical soot probe incorporates a two-component Laser Anemometer (LA) system such that measurements of axial and azimuthal velocity can be made simultaneously with particle size (Figure 5a). The predominant green (514.5 nm) beam from the dispersion prism is focused onto a circular, radially etched diffraction grating where it is split into ordered pairs. The first-order pair is subsequently collimated, then focused and crossed at the probe volume. Frequency shifting, to allow the distinction between negative and positive velocities, is provided by rotating the diffraction grating. A precision motor speed control provides shift frequencies to 8 MHz. Splitting the beams in a horizontal plane results in measurement of the axial component of the velocity while a vertical split yields the azimuthal component.

The doppler bursts are collected 40 degrees off forward scatter by an EMI 9781 AB photodetector and amplified by a DISA 55L30 preamplifier. Pedestal and high frequency noise removal are accomplished with a TSI 1982 adjustable high and low pass filter. Data processing and reduction are performed by a Macrodyne series 2000 laser velocimetry electronic processor and a DEC (Digital Equipment Corporation) PDP 11/23 minicomputer, respectively.

The LA technique requires particles to scatter light while passing through the probe volume. Alumina oxide (Al_2O_3) particles are introduced following the procedure of Reference 9. All three legs of the combustor air supply (swirl dilution and nozzle atomizing streams) are seeded to yield equivalent Al_2O_3 densities, thus eliminating any stream-dependent velocity bias. Discrimination between velocity scores resulting from small droplets and the Al_2O_3 seed within the spray region of the combustor are not made. Hence, the velocity reported in the spray region includes both spray induced and swirl induced velocity components.

H. PHASE DOPPLER INTERFEROMETER

The principal measurement method used for droplet sizing and droplet velocity is phase Doppler (PD) interferometry (Figure 6). The technique determines droplet velocity by standard fringe mode laser anemometry, and establishes the droplet size by measuring the phase shift of light encoded in the spatial variation of the fringes reaching three detectors after traveling paths of different lengths through the drop. The phase shift is measured directly by the detectors, each looking at a spatially distinct portion of the collection lens. Although two detectors can provide the needed information, a third is used as a validation check and to extend the size range sensitivity.

A primary advantage of the phase Doppler technique is the capability to resolve a wide range of droplet sizes for a given optical configuration. The size range that can be measured with one optical configuration is potentially greater than 100:1. Detector gain limitations and signal-to-noise considerations restrict this potential size range to an effective window of 35:1. This window can be electronically placed anywhere within the limits imposed by the optical configuration. If the size range of the spray exceeds 35:1, data splicing from separate windows is required. A detailed description of the technique is available (Reference 10).

Different optical transmitters are used in the isothermal chamber and swirl-stabilized combustor although the manner by which the interferometric probes are formed is identical. Both are breadboarded by UCI Combustion Laboratory personnel using standard two-component laser anemometer optics. The transmitter in the isothermal chamber uses a 5 mW Melles-Griot Helium-Neon (632.8 nm) laser, whereas the transmitter used for the combustor employs the

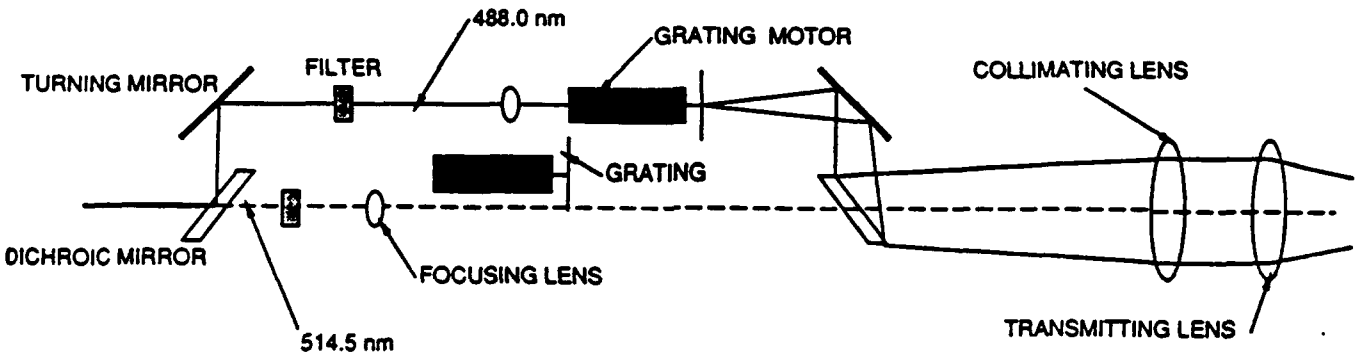

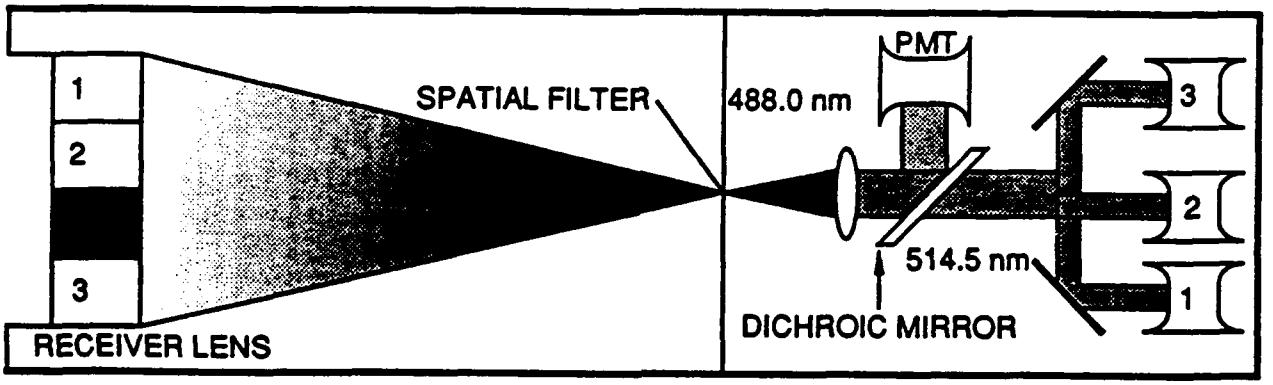

Figure 6. Phase Doppler Interferometer.

(514.5 nm) green line at a power of 400 mW from a 5W Model 165 Spectra-Physics Argon Ion laser. In each case, the laser beam is focused onto a diffraction grating where it is split into multiple modes. The two first-order beams are then collimated, focused, and crossed to form the probe volume. To allow the distinction between negative and positive velocities, frequency shifting is provided by rotating the diffraction grating. The beams are focused to a 95 μm diameter waist (to the $1/e^2$ intensity point) at the probe volume. The same receiver (Aerometrics Model 2100) and processor (Aerometrics Model 3100) are used in both experiments.

For droplet sizing purposes, the receiver is positioned 30 degrees off the beam axis. For azimuthal velocity measurements, the 30 degrees off axis position is used in the reacting case and a 7 degrees off axis position is used in the isothermal case. The narrower angle for the isothermal case is required to maintain the structural integrity of the chamber. A 50 μm by 1 mm rectangular slit serves as a spatial filter with the long axis normal to the optical axis. The photodetector voltage in the receiver and filter settings for pedestal and high frequency noise removal are menu controlled via a microcomputer (IBM AT). The computer also provides data reduction and analysis. Both size and velocity distributions are produced, as well as Sauter mean diameter (SMD).

SECTION IV
RESULTS

A. TASK 1: PROBE PERTURBATION

1. Introduction

Experimental studies that address the sooting associated with gas turbine combustors have been, to date, directed toward the **gross** soot emission and radiation from simple flames (e.g., Reference 11), well-stirred reactors (e.g., Reference 12), and production combustors (e.g., Reference 13). As the interest focuses on the mechanics of soot formation, so does the need to measure **local** properties of soot such as number density, weight concentration, and particle size distribution. Extractive probes have been and continue to be used (e.g., References 13 and 14) for these measurements. Indeed, for some measurements (e.g., morphology and composition), extractive samples are the only viable method available.

Two major questions are associated with the use of extractive probes (Reference 8):

- Representativeness of Sample. Is the extracted sample representative of the particulate at the probe entrance or do the processes of extraction, transport, and subsequent deposition of the particulate on a filter transform the morphology and number density of the soot?
- Flow Perturbation. Does the presence of the probe in the flow perturb the local conditions (e.g., temperature, aerodynamics, chemistry) and thereby, produce a condition at the probe entrance that is different from that which occurs in the absence of the probe?

In a previous study (Reference 8), both of these questions were examined for a 9.5 mm (3/8-inch) outer diameter extractive probe in a 51 mm (2-inch) swirl-stabilized combustor. The data rate of soot was measured optically at the entrance of the probe, at points radially displaced from the probe, and at a fixed point within the combustor as the extractive probe was removed in incremental steps from the fixed point. Perturbation on the data rate varied from inconsequential to substantial depending on the reference

velocity and location of the probe. In the vicinity of the recirculation zone, the perturbation on data rate was high. In the wake of the recirculation zone, perturbation was negligible at lower reference velocities (i.e., 5 m/s). At higher reference velocities (i.e., 7.5 m/s), the 9.5 mm outer diameter probe acted as a blockage in the 51 mm inner diameter duct, and the soot data rate was dramatically reduced in the presence of the probe.

In the present task, laser anemometry was employed in addition to an optical measurement of soot particulate to examine flow perturbation in a somewhat larger, 80 mm (3-inch) outer diameter swirl-stabilized combustor. The purposes were to determine where, within this larger combustor, flowfield perturbation due to the presence of an extractive probe is unacceptable, to assess the effects of anisokinetic sampling and various chemical quenching rates upon soot samples extracted from the same combustor, and to provide guidance for in-situ, extractive probe measurements within laboratory and practical swirl-stabilized combustors.

2. Experiment

a. Combustor

The combustor is described in Section III.A. For the results reported here, a high-aromatic jet fuel (Suntech Blend 3), supplied by the Naval Air Propulsion Center, was burned at an overall equivalence ratio of 0.3. The combustor was operated at atmospheric pressure and a bulk reference velocity of 7.5 m/s. Before introduction into the combustor, both swirl and dilution air were heated to 100°C. The fuel was introduced through the air-assist nozzle described in Section III.B. The injector was operated at a nozzle air-to-fuel mass ratio of 3.0 which, based on laser diffraction and laser interferometry (Reference 15) measurements, yields a bulk Sauter Mean Diameter (SMD) of less than 10 μm.

b. Extractive Probe

The extractive probe is described in Section III.D.

c. Thermocouple Probe

The thermocouple probe is described in Section III.E.

d. Optical Probe

The optical soot probe is described in Section III.F.

e. Laser Anemometer

The Laser Anemometer is described in Section III.G.

3. Results

The results are presented in three separate sections. The first consists of a presentation of the unperturbed aerodynamic, thermal, and soot fields. This is followed by a description of the perturbation of the local velocity and soot fields due to placing the probe at nine various locations (three radial at each of three axial locations) within the combustor. The results of the sample integrity task are presented in the final section.

a. Unperturbed Flowfields

The unperturbed axial and azimuthal velocity, temperature, and soot fields are presented in Figure 7. The velocity and thermal field characterizations utilize the same matrix, namely seven axial stations with ten radial locations each (all on one side of the combustor centerline) for a total of seventy points. The soot characterizations are based on a smaller matrix with eighteen points (three axial by six radial).

The size and location of two recirculation zones are evident in the axial velocity map (Figure 7a). A small on-axis region of back flow exists at $x/R = 0.25$ just off the centerline of the combustor. This small recirculation zone is induced by the hollow-cone pattern of the liquid fuel injector in the early stages of spray development, and is located within that spray region. The flame is anchored by a larger toroidal recirculation zone located at the interface separating the swirl vanes and fuel spray, between $x/R = 0.25$ and 0.75. The large positive mean axial velocities (in excess of 30 m/s) measured just off the combustor centerline at $x/R = 0.50$, and along the centerline at $x/R = 1.00$, are interpreted as the velocities of small (less than ~ 5 micrometer) droplets. These droplets are vaporized by the time they reach $x/R = 1.75$, where the measured velocities close to the centerline are approximately equal to the gas velocities measured at the downstream axial stations. The mean azimuthal velocity mapping (Figure 7b) shows anomalies (e.g. magnitudes not tending towards zero) along the centerline at the first three axial stations, which are also attributed to the presence of droplets.

Inspection of the thermal field (Figure 7c) confirms the location and size of the larger recirculation zone, and also reveals a uniform, high temperature core downstream, with a steeply decreasing radial gradient to a relatively cool outer flow. Agglomerate soot* is found only in this high temperature region (Figure 7d) with the population falling off rapidly to zero at radial locations greater than $r/R = 0.50$.

(a) Axial Velocity

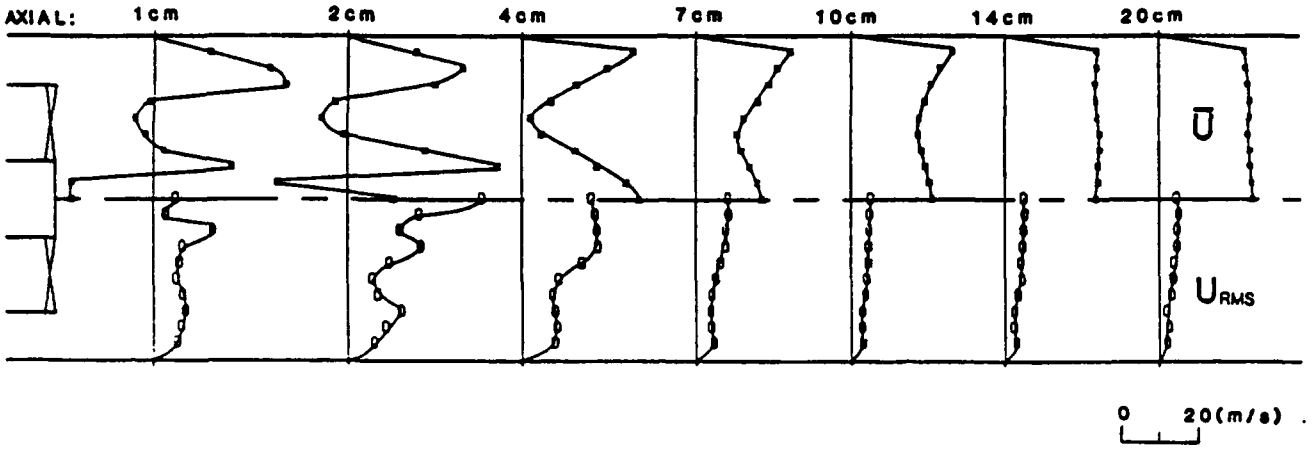

(b) Azimuthal Velocity

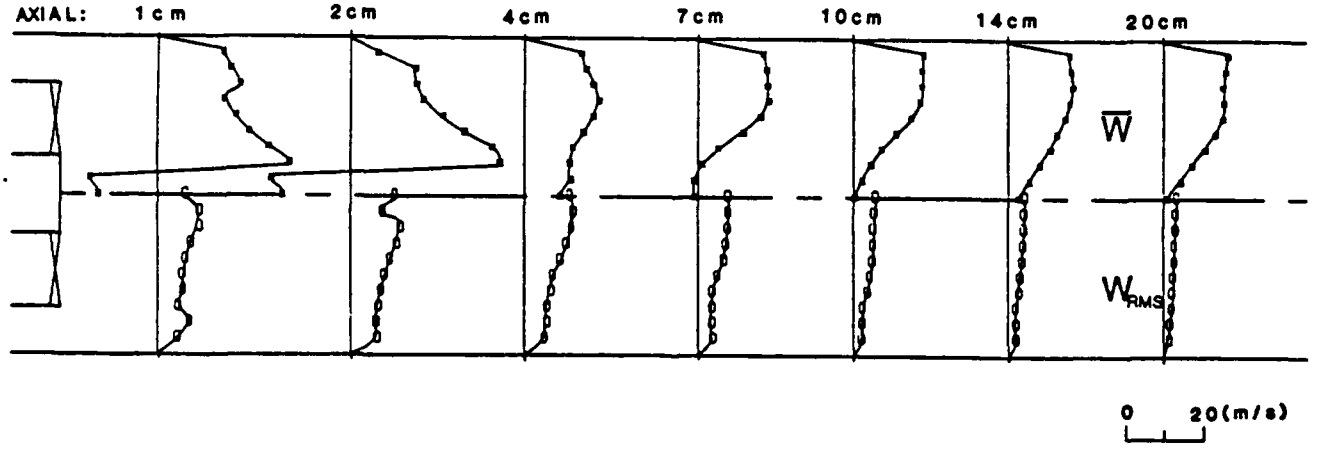

Figure 7. Task 1: Unperturbed Velocity, Temperature, and Soot Fields.

(c) Temperature

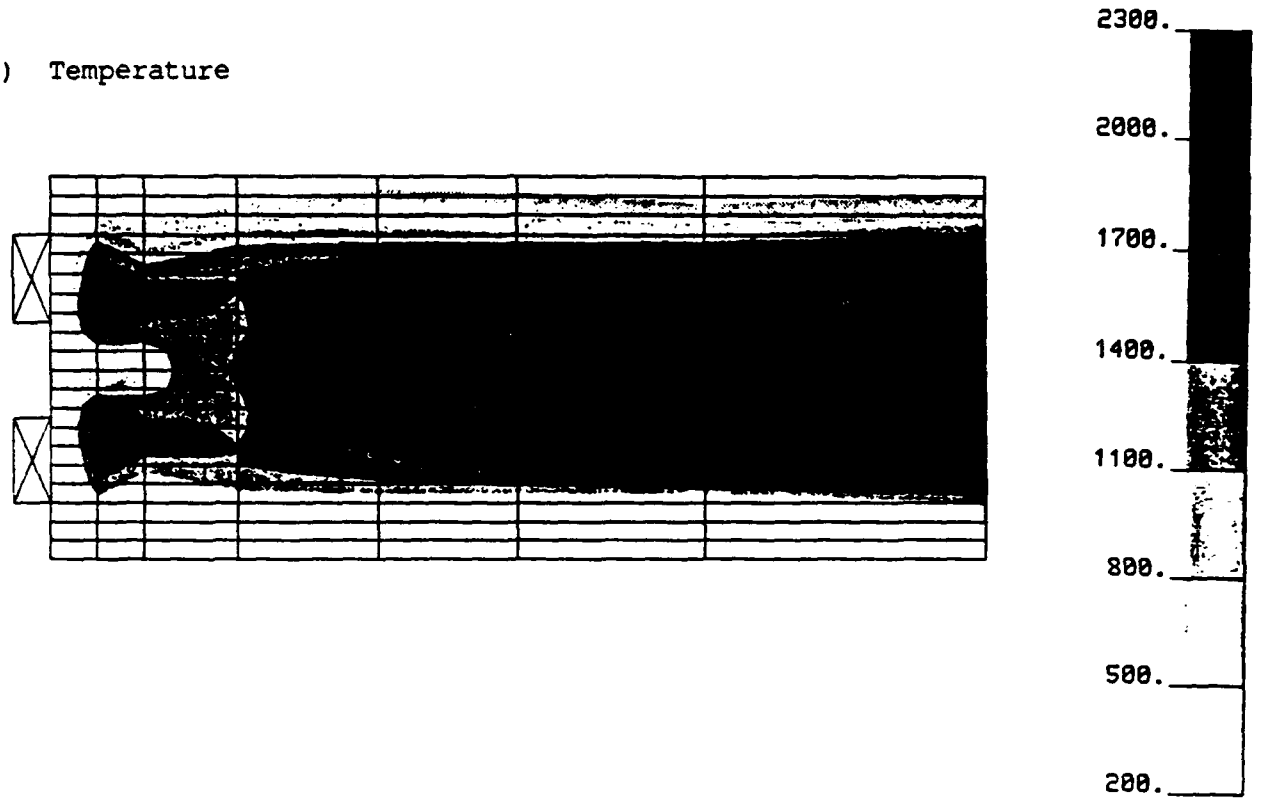

(d) Soot

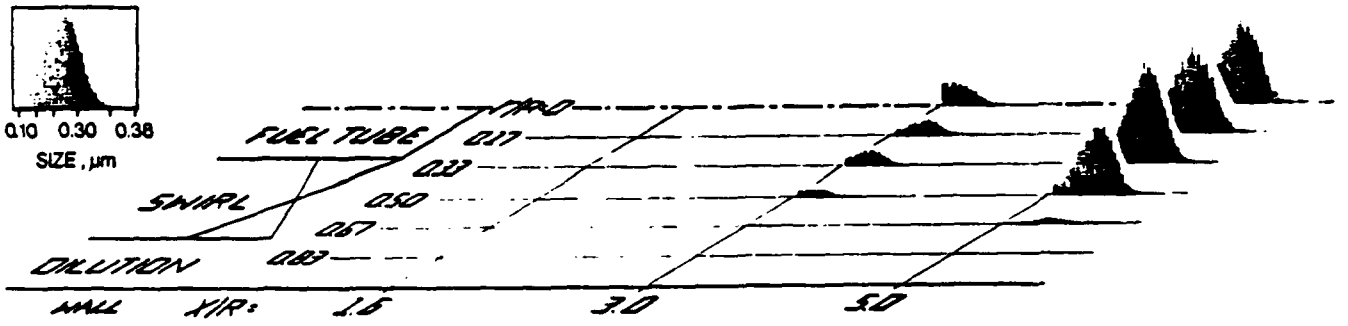

Figure 7. Task 1: Unperturbed Velocity, Temperature, and Soot Fields (concluded).

b. Probe Perturbation

The approach utilized for the assessment of the extractive probe perturbation of the velocity and soot fields encompasses two sequences of measurements. In the first, the extent of the perturbation in the radial direction is established through radial traverses of the optical probe system with and without the extractive probe in place. In the second sequence, the optics are fixed at the entrance to the extractive probe and, as the sampling probe is incrementally removed from the combustor, the conditions at the original probe position are monitored optically to assess the axial extent of the disturbance. For each sequence, measurements are made of mean and rms velocities in both the axial and azimuthal directions, as well as soot size and population.

Three axial locations were selected for the perturbation assessment ($x/R = 1.60$, 3.00, and 5.00). At each axial location, a measurement was taken at three radial locations ($r/R = 0$, 0.33, and 0.67). Thus, the perturbation is assessed for the probe placed at nine locations within the combustor; three in the near wake of the recirculation zone ($x/R = 1.60$), and six in the far wake ($x/R = 3.0$ and 5.0).

(1) Velocity Field. Figure 8 presents the results for the perturbation assessment on the mean and rms axial velocity fields. The results are reported as the difference between the perturbed ($\bar{U}$) and unperturbed ($\bar{U}_o$) velocities, normalized by the maximum unperturbed velocity measured at each of the three axial stations. This format was selected because of the substantial differences in velocity between the minimum and maximum values (especially apparent in radial traverses of the unperturbed mean azimuthal velocity, Figure 7).

The figures show a reduction of both mean and rms velocities at the location of the probe. At each axial location, the magnitude of the perturbation of the mean axial velocity (Figure 8a) increases from approximately 10 percent at the centerline to 20 percent at the sampling location closest to the combustor wall, whereas the rms velocity (Figure 8b)

---

* Previous work has shown that the range of particles resolved by the 60 degrees/20 degrees intensity ratioing technique excludes the 0.05 micrometer primary particles and encompasses the large particle "agglomerate" wing of the soot distribution (Reference 16).

(a) Radial Variation of Mean Velocity

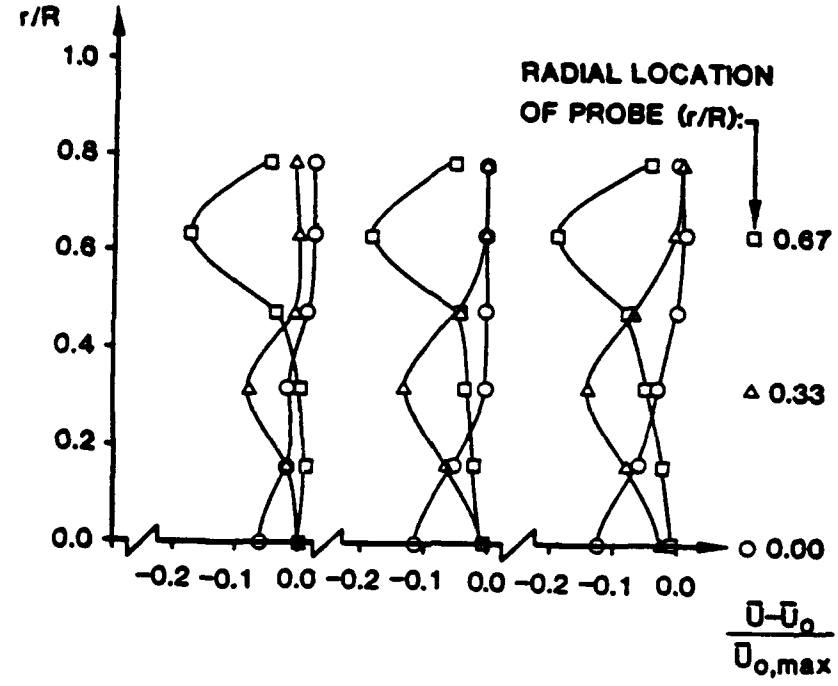

(b) Radial Variation of rms Velocity

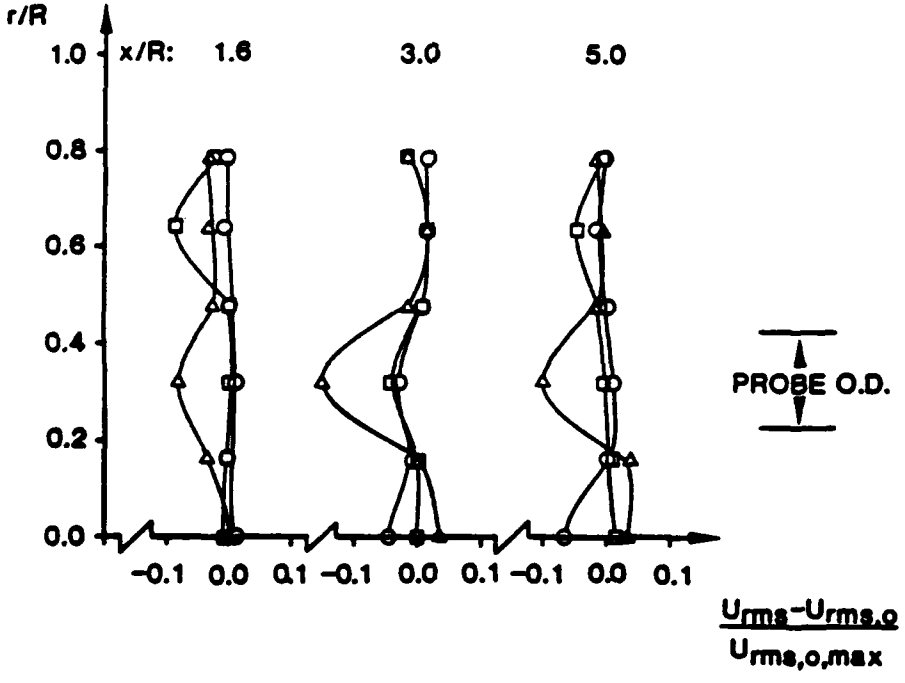

Figure 8. Task 1: Perturbed Axial Velocity Fields.

(c) Axial Variation of Mean Velocity

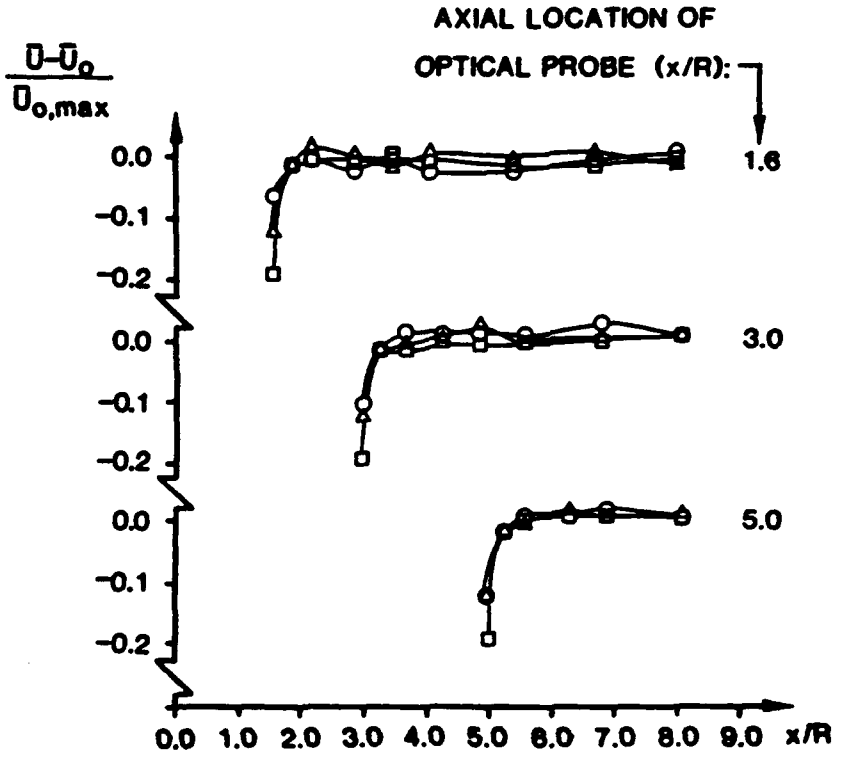

(d) Radial Variation of rms Velocity

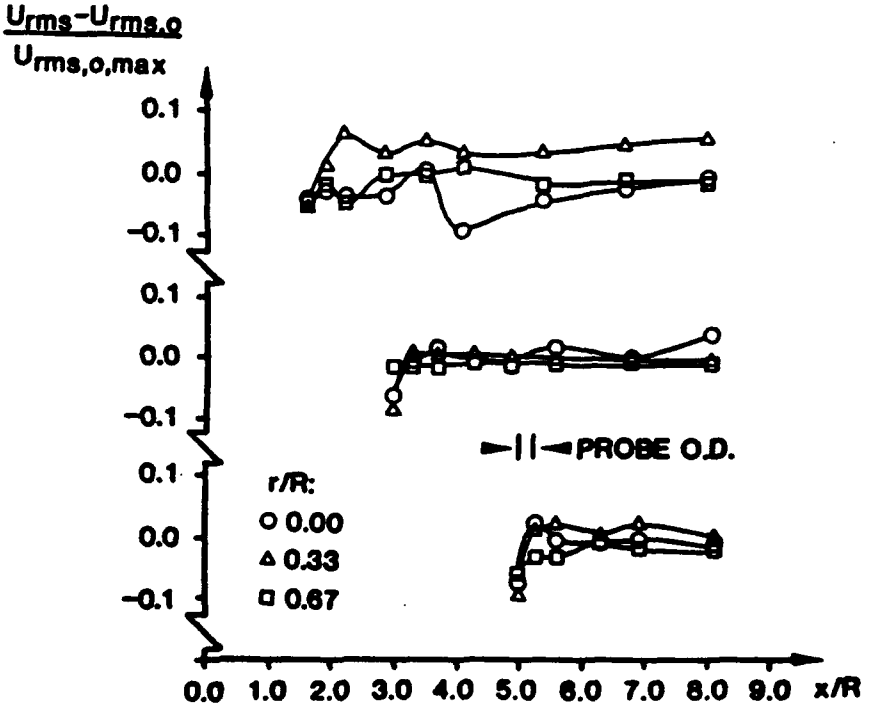

Figure 8. Task 1: Perturbed Axial Velocity Fields (concluded).

reveals significant (i.e., ≥ 10 percent) perturbation at only a few points.

The radial distance over which the extractive probe perturbs the flow increases from $r/R \cong \pm 0.15$ (one extractive probe diameter) in the near wake of the recirculation zone to a broader distance of impact of $r/R \tilde{>} \pm 0.30$ (two extractive probe diameters) at the two axial locations in the far wake of the recirculation zone. The smaller distance over which the flow is perturbed in the near wake of the recirculation zone is attributed to the local dominance of the swirler and nozzle. In the far wake, this dominance is diminished and perturbations are broadcasted, as a result, over a larger radial distance.

The results for the perturbation sequence in which the probe is incrementally removed from the combustor (Figure 8c) show clearly that the perturbation is effectively removed once the probe is separated by one (at $x/R = 1.6$) to two (at $x/R = 3.0, 5.0$) extractive probe diameters. The relative scatter in the results of the rms measurements (Figure 8d) is attributed to the collection of a number of points not sufficient to allow convergence of the data. For each velocity determination, 1000 samples are collected. This number is chosen to insure reasonable convergence while maintaining the data collection time at a manageable length.

The results of the assessment of the azimuthal velocity field perturbation due to extractive probe placement at the nine sampling locations used above are presented in Figure 9. At all three axial stations, the perturbation of the mean and rms velocities (Figures 9a and 9b) are not significant (< 5 percent), except near the combustor wall, where the mean velocity shows a consistent, but not substantial 10 percent increase. Figure 9c reveals that in all cases, the mean azimuthal velocity is slightly reduced when the probe is placed at the centerline, slightly increased at $r/R = 0.33$, and modestly increased at $r/R = 0.67$. However, the trend is not worthy of further investigation since the magnitudes of the perturbations are so small.

(2) Soot Field. The perturbation of the soot field is assessed at the same nine locations (three axial by three radial) as in the preceding velocity assessment, and the results are presented in Figure 10. Because of the substantial differences in soot data rate between the maximumvalue at the centerline and no observable soot at the wall, the results

(a) Radial Variation of Mean Velocity

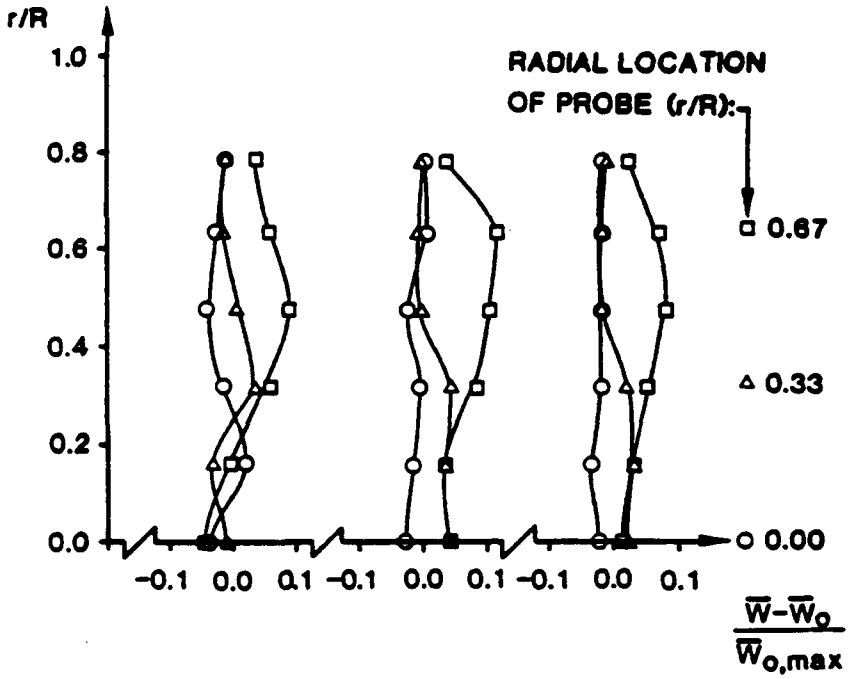

(b) Radial Variation of rms Velocity

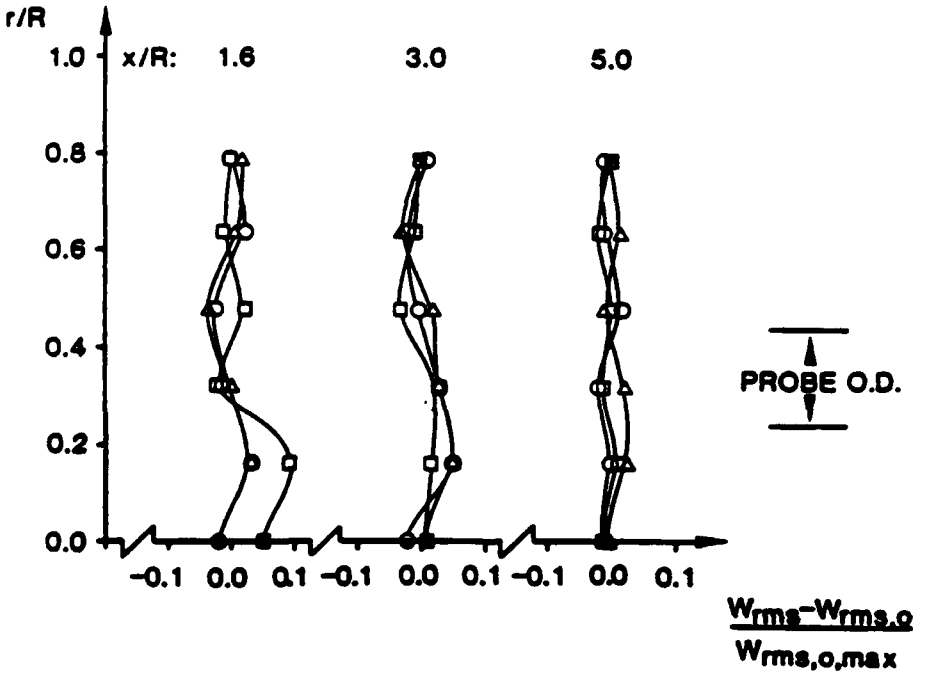

Figure 9. Task 1: Perturbed Azimuthal Velocity Fields.

(c) Axial Variation of Mean Velocity

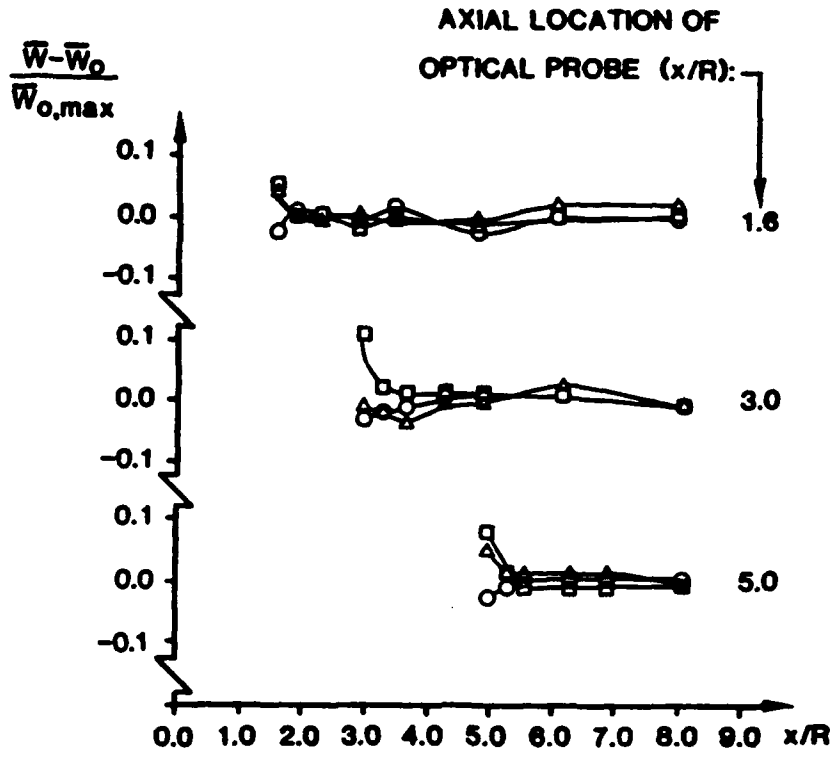

(d) Axial Variation of rms Velocity

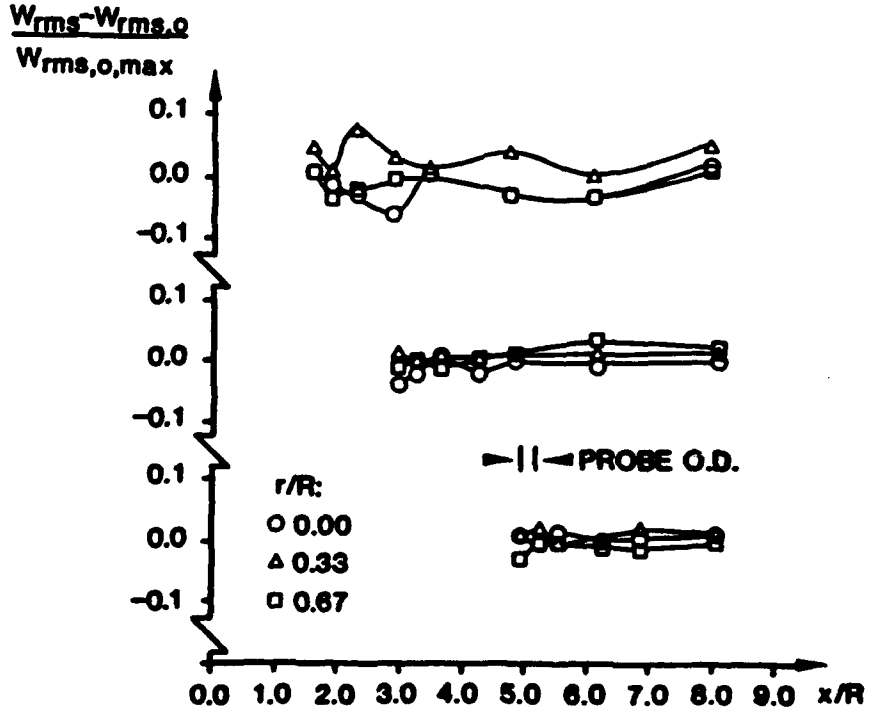

Figure 9. Task 1: Perturbed Azimuthal Velocity Fields (concluded).

(a) Radial Variation of Soot Data Rate

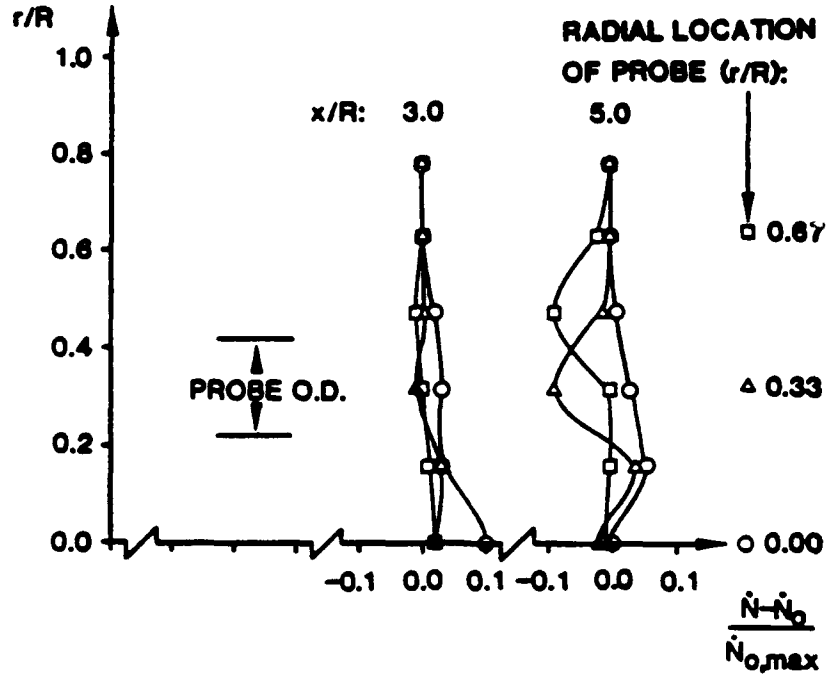

(b) Axial Variation of Soot Data Rate

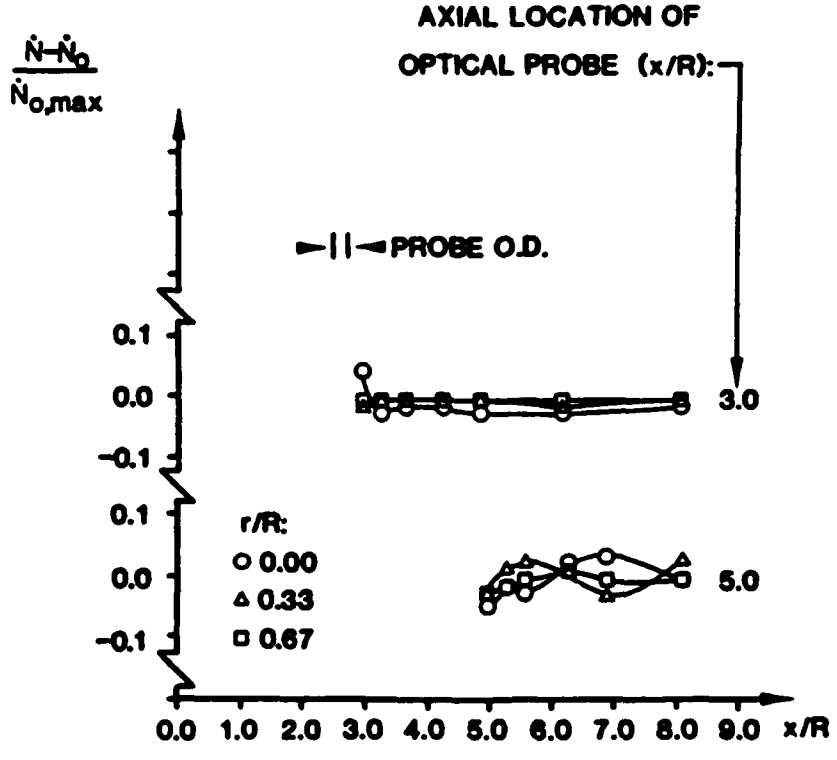

Figure 10. Task 1: Perturbed Soot Field.

(c) Centerbody Combustor

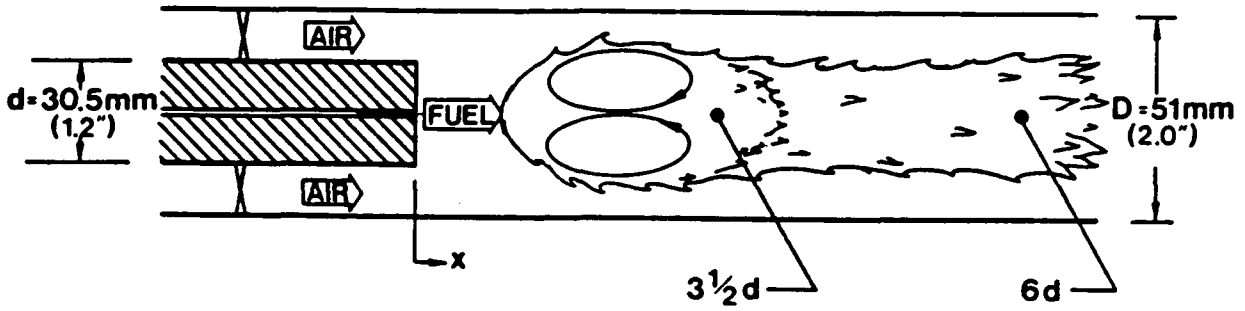

(d) Soot Size Distribution

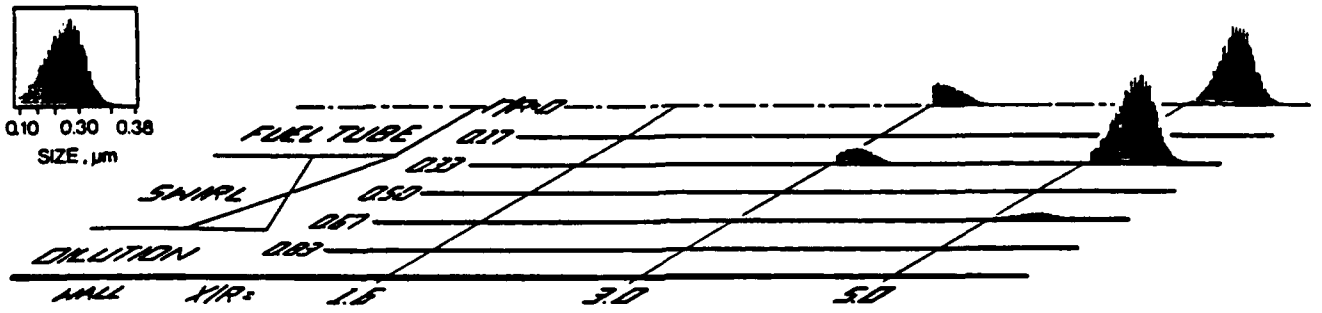

Unperturbed

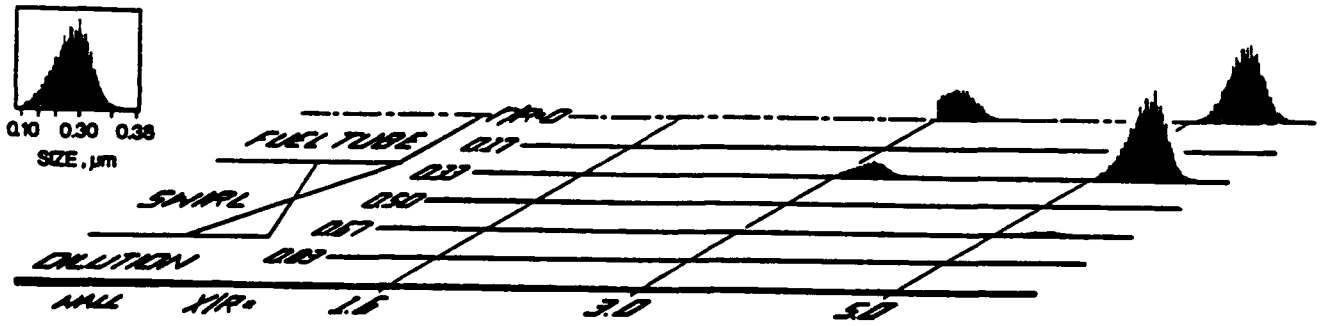

Perturbed

Figure 10. Task 1: Perturbed Soot Field (concluded).

are reported as the difference between the perturbed and unperturbed data rate, normalized by the maximum data rate measured in the combustor.

The effect of the extractive probe on data rate within the limitation of the optical size window, is negligible at all locations. This result is in contrast to the previous work (Reference 8) and is attributed to the substantial difference between the two studies in combustor size, 51 mm (2 inches) versus 80 mm (3 inches), and recirculation zone size and location. In the previous study, the combustor geometry yielded a relatively large, on-axis recirculation zone (Figure 10c) in comparison to the smaller toroidal region characteristic of the current combustor and operating conditions selected for the present study (Figure 1). An extractive probe of the same 9.5 mm (3/8-inch) outer diameter was used in both studies. Hence, the extractive probe-to-combustor diameter and area ratios were 0.190 and 0.036, respectively, in the prior study versus 0.120 and 0.014 in the present study. Second, the major perturbation in the previous study occurred with the extractive probe located within the rather voluminous recirculation zone of the swirl centerbody combustor used (x = 3-1/2d, Figure 10c).

The effect of perturbation on the mean particle size of the particle distribution within the optical window is measurable, but not substantial. As shown in Figure 10d, an increase in the size of the agglomerate peak occurs, presumably induced by the locally reduced velocity in the vicinity of the probe and associated increase in residence time, in combination with the probability of a locally reduced temperature due to the thermal sink of the probe.

Figures 10a, 10b, and 10d show that neither the soot data rate nor the soot size distribution is significantly affected by the presence of the probe, within the size window of the optical technique. However, the perturbation of the particulate falling below the size window is still an open question. The limitations of the optical system in this region are assessed in detail in Reference 17. However, a substantial impact on the smaller particulate is not expected because (1) the mean size is well below the 5- micrometer cutoff seen in Reference 18, above which particle concentrations can be significantly biased by aerodynamic forces; and (2) Figure 10d does not reveal a significant change in the agglomerate peak, which indicates that the smaller particles are not significantly agglomerating under the perturbed condition.

c. Sample Integrity

The results of the sample integrity study are divided into two subsections. The first reports on the sample integrity effects due to variations in the total sample flow rate, while the second reports on effects due to variations in the inert gas flow rate. Both are conducted at a single location within the combustor: $x/R = 5.0$, $r/R = 0.67$.

(1) Sample Rate Study. To assess the effect of nonisokinetic sampling conditions, the optical probe volume is placed as close as possible to the extractive probe inlet (approximately 2 mm directly upstream), and the size distribution and population of the soot entering the probe are monitored optically as the sampling rate is varied from no flow to twice isokinetic (the maximum value attainable by the current sampling system). The results are presented in Figure 11.

Variations of the sample rate between 0.5 isokinetic and 1.5 isokinetic show no effect upon either soot size distribution or data rate (population) within the optical size window. Increasing the sample rate to twice isokinetic still yields no effect upon the size distribution. This is due to the size of the soot falling below the 5-micrometer cutoff (Reference 18) at which anisokinetic sampling fails to segregate smaller particles from relatively larger ones. However, the overall soot population may be biased in this region, as evidenced by the 10 percent increase in the measured data rate (Figure 11e).

Decreasing the sample rate to zero induces a shift in the size distribution to the larger end and reduces the data rate 7 percent, consistent with anisokinetic theory; namely, lower flowrates promote a radial convection of smaller particles away from the sampling volume. The shift in size distribution is attributed to imposing a change upon the local flowfield such that streamlines are not allowed to enter the probe. Under these conditions, the streamline distortion immediately upstream of the probe inlet is much more drastic than that for the twice isokinetic case, leading to a measurable impact upon the size distribution, 2mm upstream of the probe entrance.

Once again, the limitations of the optical technique must be considered when interpreting the above results. The data show no significant impact on the soot population within the optical size window (excluding the unrealistic no-flow case). However, the optical system does

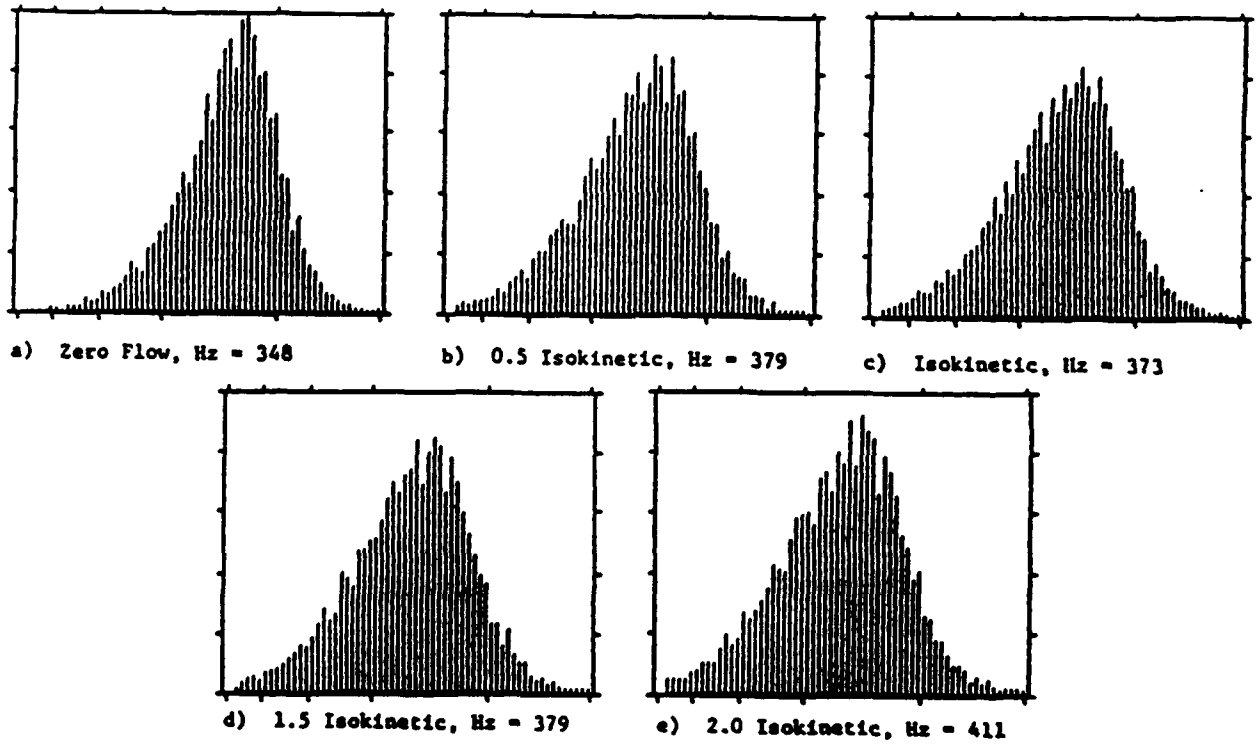

Figure 11. Task 1: Effect of Anisokinetic Sampling.

not detect a majority of the smaller particulate, and thus the extent of the perturbation in this area is not determined experimentally. A perturbation of the smaller particulate is not likely though, due to the generally accepted 5 micron cutoff.

(2) Dilution Rate Study. Scanning electron micrographs of samples collected with various nitrogen injection rates are examined to assess the effect of sample cooling rate upon soot morphology. Probe inert gas to sample ratios are varied from 0.0 to 1.6, and the resulting micrographs are presented in Figure 12.

Inspection of the results reveal that nitrogen injection has no visible effect on the morphology of the sample.* This is again in direct contrast with the results found in Reference 8, where substantial morphological changes were induced by varying the nitrogen dilution rate. The contrast is attributed to differences in combustor conditions (geometry, fuel, equivalence ratio, etc.) which, in the current study, combine to yield a sooting condition at the probe inlet which is sufficiently quenched by the convective action of the cooling water thus rendering the dilution quench unnecessary. In the previous study, the probe inlet section was also water cooled but the combustor conditions yielded a reactive chemical and thermal environment at the probe entrance which could not adequately be quenched by convection. In this case, inert gas injection was allowed to play a role in the particle quenching process, and the morphology was vulnerable to change in accordance with the level of dilution quench.

Although all samples destined for SEM analysis are collected on membrane filters with a 0.08-micrometer pore size, the pores in Figure 12a are substantially larger than those seen in the subsequent figures. In this case, the sample temperature has exceeded the working temperature limit of the filter material (285°F) and the pores are distorted (enlarged) due to the excessive heat. Since the probe cooling water, heated sample line, and oven temperatures are held constant throughout the inert gas injection study (i.e. nitrogen dilution rate is the only variable), the distortion of the pores attests

* The apparent decrease in population is caused by an increasing sample dilution due to the nitrogen injection.

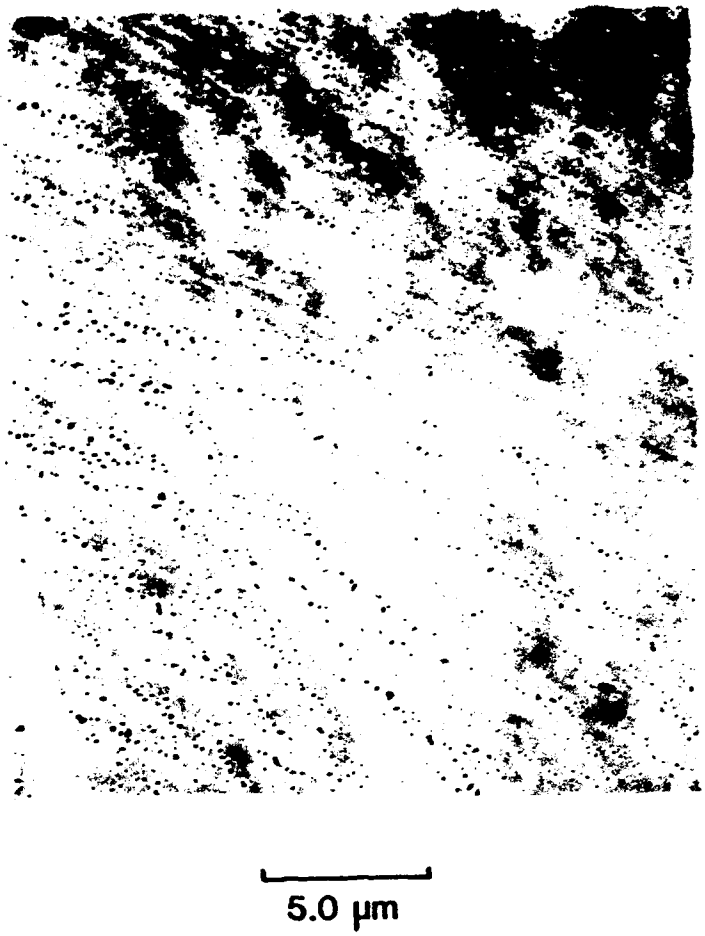

(a) N_2/Sample = 0.0
(4000 x)

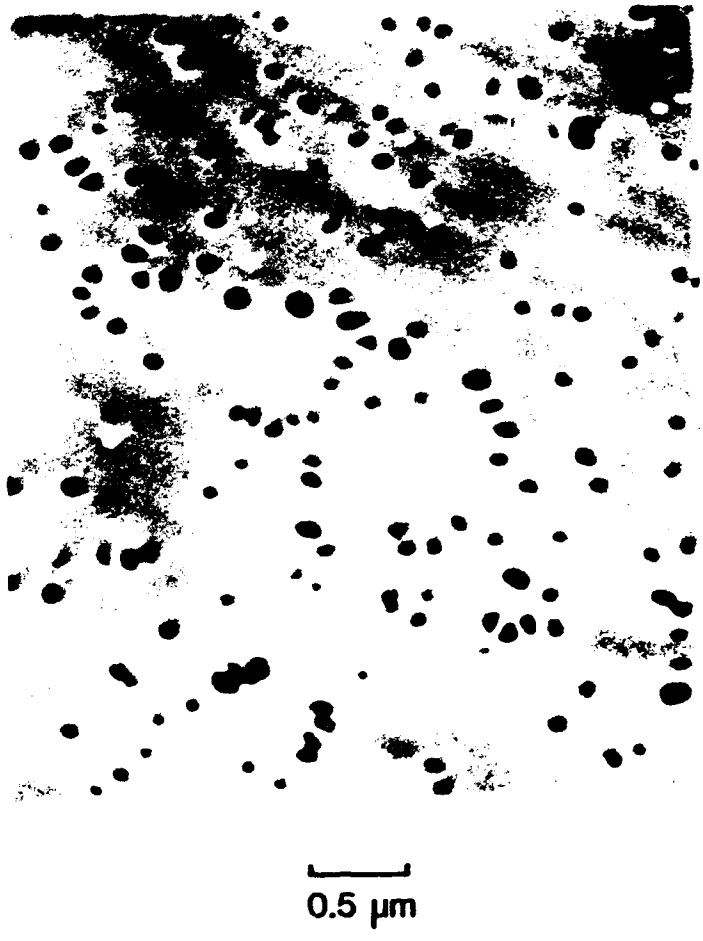

(b) N_2/Sample = 0.0
(20,000 x)

Figure 12. Task 1: Effect of Sample Dilution Rate.

(c) N_2/Sample = 0.4
(4000 x)

5.0 µm

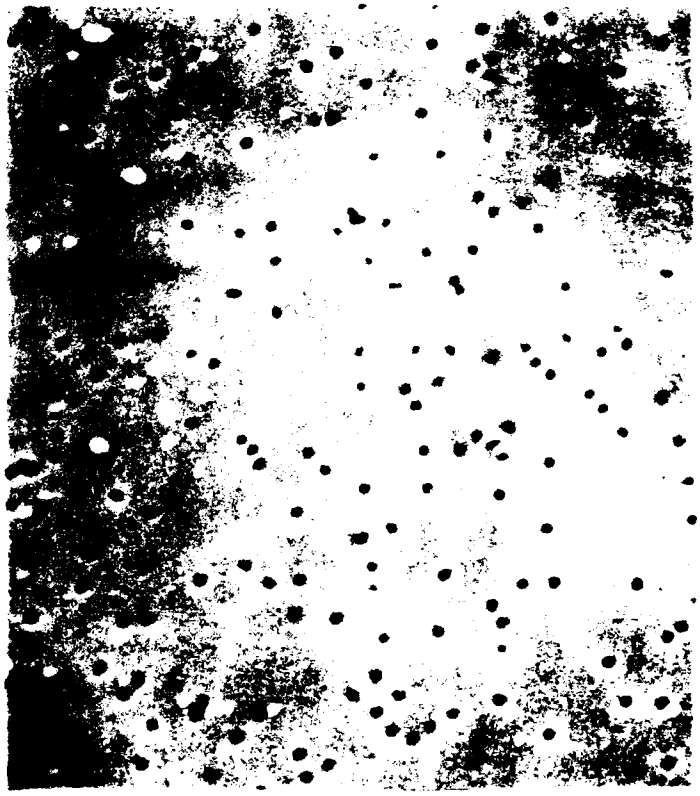

(d) N_2/Sample = 0.4
(20,000 x)

0.5 µm

Figure 12. Task 1: Effect of Sample Dilution Rate (continued).

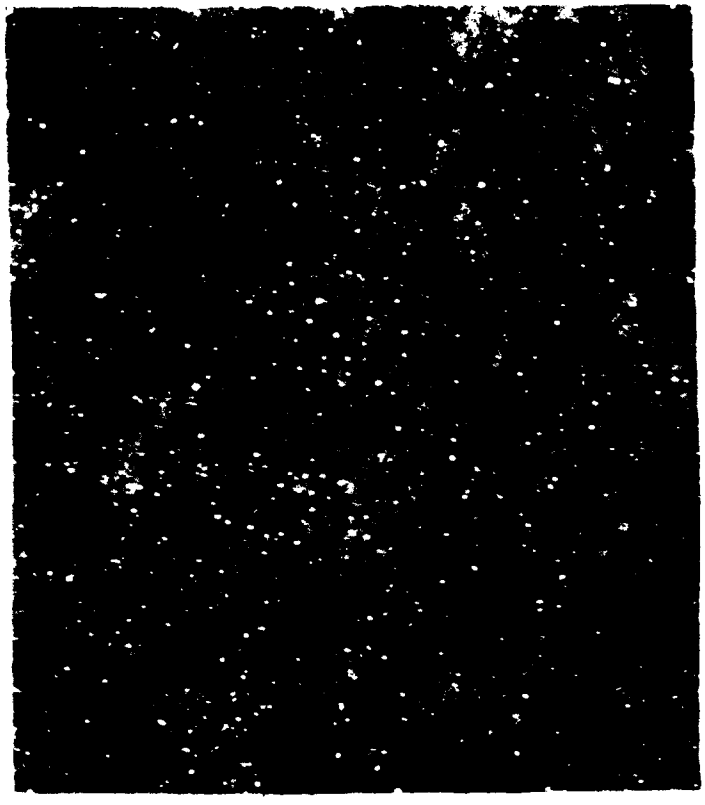

(e) N_2/Sample = 0.8
(4000 x)

5.0 μm

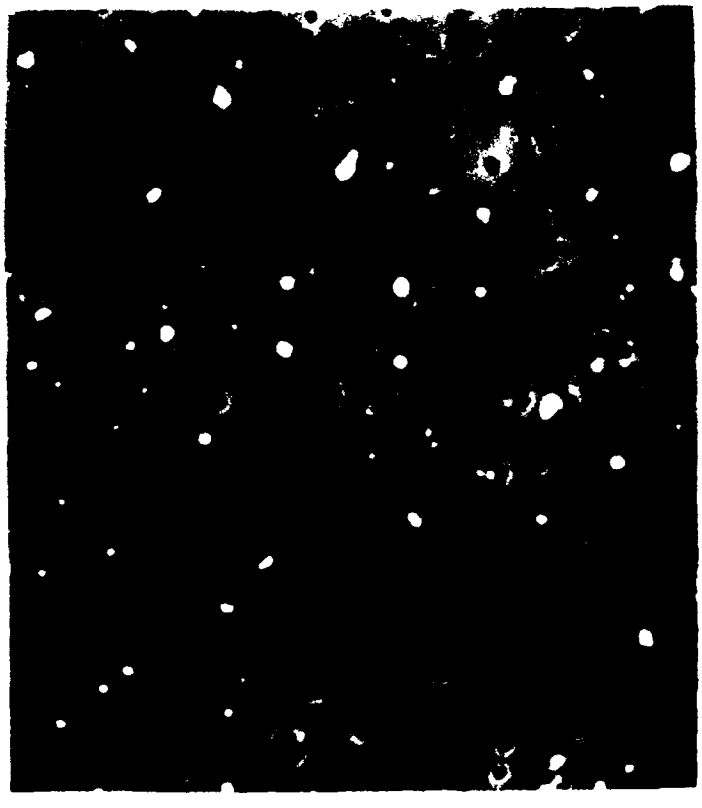

(f) N_2/Sample = 0.8
(20,000 x)

0.5 μm

Figure 12. Task 1: Effect of Sample Dilution Rate (continued).

(g) N_2/Sample = 1.2
(4000 x)

5.0 μm

(h) N_2/Sample = 1.2
(20,000 x)

0.5 μm

Figure 12. Task 1: Effect of Sample Dilution Rate (continued).

(i) N_2/Sample = 1.6
(4000 x)

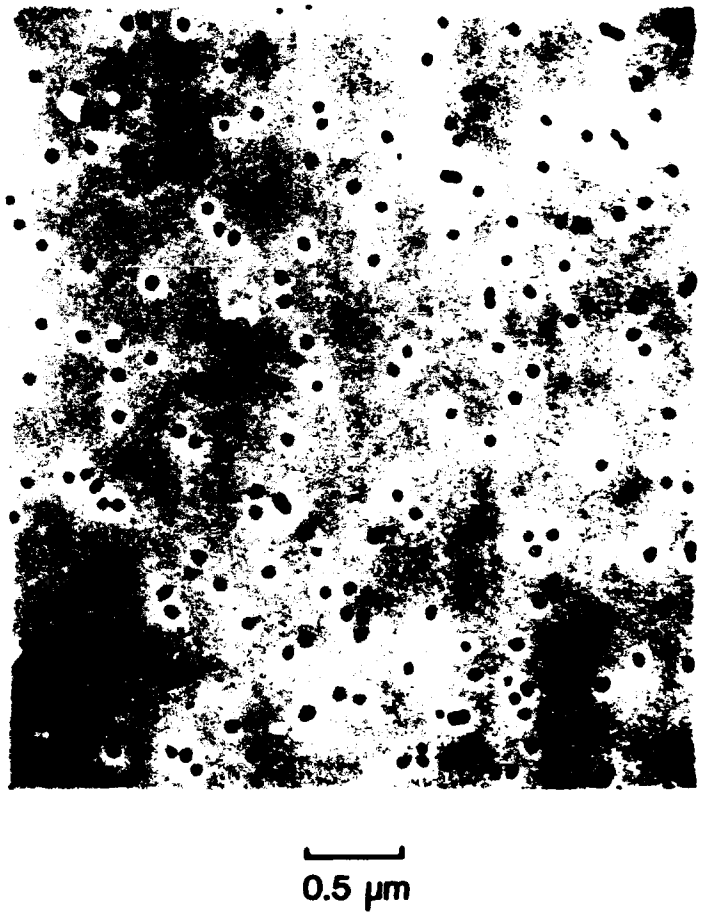

(j) N_2/Sample = 1.6
(20,000 x)

Figure 12. Task 1: Effect of Sample Dilution Rate (concluded).

to the effectiveness of sample cooling by inert gas injection. An extreme case of filter distortion is shown in Figure 13, in which the vast majority of pores are closed. This "melting" of the filter surface occurred during an exploratory run in which the temperature of the heated sample line was set at 300°F.

The morphology of the agglomerated soot in Figure 13 demonstrates another result of the sample integrity study; namely, the effect of static charge. Long agglomerate chains of the primary soot particles are formed under these "charged" conditions. This morphology is distinctly different than the compact agglomerate structure seen in Figure 12. Two cases in which static charge had a noticeable effect upon the sample are presented in Figure 13b. The first shows a morphology typical of that seen before initiation of steps to alleviate the charge, while the second illustrates an extreme case of charging with a chain structure approaching 30 micrometers in length. A thorough inspection of the sampling system revealed that the extractive probe was charged. Placing an ammeter between ground and the probe (with no cooling water flow) showed the probe to be uncharged. A similar test was conducted on the water entering the probe and showed that the water also carried no charge. However, when the water exiting the probe was measured, the ammeter showed a current of approximately 10 μA flowing into the water. Therefore, the charge was being generated by the water moving through the cooling circuit of the probe. Grounding the probe and all electrically conductive hardware through which the sample passes eliminates the effect of static electricity, and results in the morphology typical of Figure 12.

4. Conclusions

As a result of this study, the following conclusions are made:

a. Optical diagnostics provide a resource for assessing the perturbation of an extractive probe in an aerodynamically complex flow.

b. Perturbations of an extractive probe on the velocity and soot fields are combustor and operating condition specific, and depend on the sampling location.

(a) Effect of Temperature, N_2/Sample = 0.00

Figure 13. Task 1: Effect to Temperature and Static Charge.

(b) Normal Charging

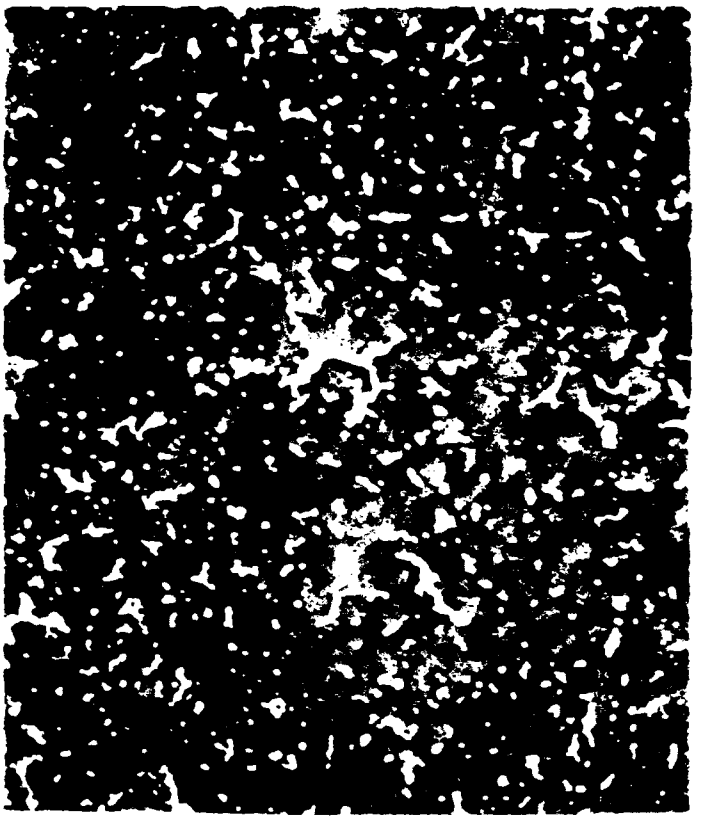

(c) Heavy Charging

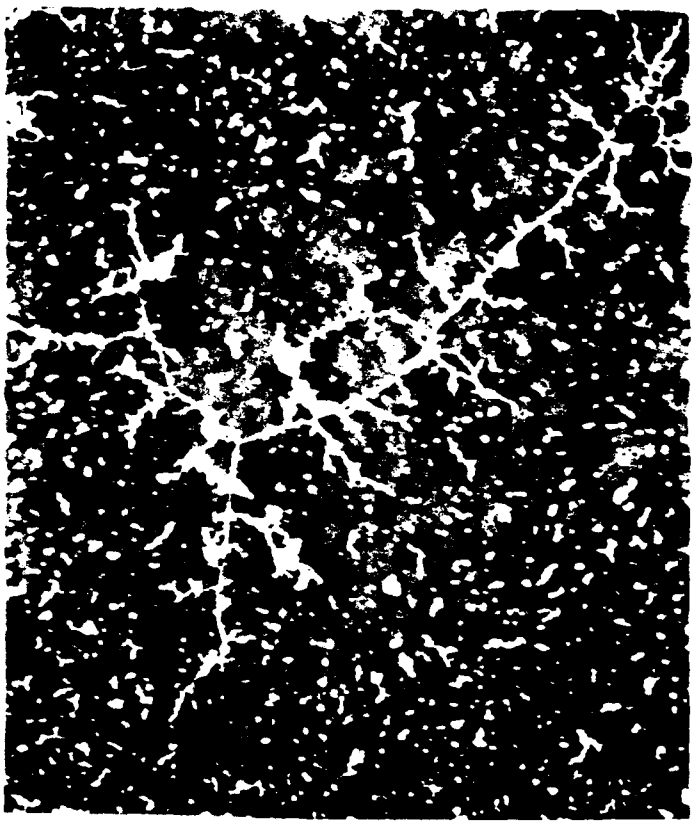

Figure 13. Task 1: Effect to Temperature and Static Charge (concluded).

c. For the combustor and operating condition assessed in the present study:

- The mean and rms velocity was reduced 10 to 20 percent in the immediate vicinity of the probe.
- Neither the soot data rate nor the soot size distribution was significantly affected within the size window of the current optical technique.
- Variations in total sampling and inert gas dilution rates yielded insignificant impacts on soot number density and morphology.
- An electrically charged probe can significantly affect soot morphology, resulting in substantial particle agglomeration during the sample transport process.

B. TASK 2: PARAMETRIC SENSITIVITY

1. Introduction

Fuel flexibility is a viable and realistic approach to assure adequate availability of aviation fuel through this century. To achieve this position, the relationship of fuel properties and composition to combustion hardware performance and durability must be identified more precisely. Such information is necessary if fuel specifications are to be successfully relaxed to a level that both maintains the required performance of the combustion system (and other subsystems) and permits the desired latitude in the portion of hydrocarbon resources (petroleum, oil shale, coal, tar sands, etc.) that can be used to produce aviation fuel. These potential changes in fuel processing and fuel source make future fuel composition effects on gas turbines a primary consideration and concern.

Currently, the specification limit on aromatics for aviation fuel is a maximum of 20 percent (Jet A) or 25 percent (JP-4, JP-5, JP-8) by volume. The limit is set to preclude a series of combustion related problems associated with the production of soot, examples of which include increased flame radiation, deposit of carbonaceous material, and emission of particles. Radiation and deposition influence hardware durability and performance, while the emission of visible particles

results in aesthetic and tactical problems. The aromatic content is of special interest because a relaxed specification for aromatics could ease the demand for hydrogen addition in the refining of low hydrogen resources. An upper limit of 35 percent aromatics has been discussed (Reference 19).

To accommodate an increased fuel aromaticity, the production of soot from combustors operating on relaxed-specification fuels must be reduced. Toward this end, experimental evidence is needed with respect to the effects that fuel properties, fuel-additive properties, and combustor operating conditions have on soot formation and burnout. Of particular interest are the mass emission, size distribution, and composition of the soot particulate. Extractive probe measurements have been used in the past to derive this set of information (e.g., References 6, 20, 21) but, as addressed in the previous section, backmixing in complex flows can exacerbate and widely distribute perturbations introduced by the presence of a physical probe, caution must be exercised in the use of such methods. This may include limiting the measurements to the combustor exit-plane, far downstream of the recirculation zone. Such a limit substantially restricts the information available. Excluded is the spatial distribution of local soot size and soot number density in the near wake of the recirculation zone and within the recirculation zone itself. Such measurements must be nonintrusive and therefore rely on optical techniques. Although optical techniques have been successfully employed to measure soot in relatively simple flows (flat flames and diffusion flames), applications to complex flows are limited (e.g., References 8 and 22).

In a past study (Reference 22) we addressed the application of a nonintrusive, optical probe to a complex flow where the principal objective was to evaluate the performance of large angle intensity ratioing for optically measuring the local soot size and soot number density in the reaction zones of a complex flow. Isooctane and blends of isooctane with pure hydrocarbons of varying aromaticity were introduced prevaporized. In the present study, the objectives were to (1) introduce the fuels as liquid sprays and add to the fuels tested a shale-derived JP-8, and (2) conduct an assessment of the impact of key parameters (fuel molecular structure, atomization quality, injection state) on the spatial distribution of soot in a swirl-stabilized combustor.

2. Experiment

a. Approach

The approach was to optically measure the spatial distribution of local soot size and number density in a model laboratory complex flow combustor. Radial profiles were measured at three axial locations for a shale-derived JP-8, isooctane, and three fuel blends introduced through a twin-fluid atomizer. The three fuel blends were mixed to yield the same ASTM smoke point as the JP-8 in order to assess the effect of fuel molecular structure on soot yield in a complex flow. The effect of atomization quality was addressed for the shale-derived JP-8, and a parametric variation was conducted on one fuel blend to assess the effect of injection state (prevaporized versus liquid fuel injection) on soot yield.

b. Combustor

The axisymmetric can combustor (ASCC) is described in Section III.A. Fuel was introduced through the twin-fluid injector described as well in Section III.B. Sauter Mean Diameter (SMD) was measured using a Malvern ST2200 laser diffraction instrument as a function of nozzle air-to-fuel mass ratio. The data are presented in Figure 14. Although the values of SMD approach the limit of resolution for the Malvern as nozzle air-to-fuel ratio is increased, the trend toward enhanced atomization quality is clearly evident. The intensity ratioing results of the present work were obtained for an air-to-fuel mass ratio of 3.0. For the shale-derived JP-8, data were also obtained at air-to-fuel ratios of 2.5 and 3.5 to assess the effect of this parameter on soot size and spatial distribution. A cone-annular nozzle was used for the one fuel blend introduced in a prevaporized state. The combustor was operated at atmospheric pressure.

c. Fuels

A shale-derived JP-8 and four liquid fuels of varying molecular structure representative of compounds found in petroleum, shale, and coal derived fuels were used in this study. Isooctane (2,2,4-trimethylpentane) served as the base fuel as it represents a major component of JP-8 and serves as the reference fuel in the ASTM smoke point test. The three remaining fuels consisted of mixtures of isooctane with one of three compounds with varying degrees of saturation and ring number (Figure 15) -- toluene, tetralin (1,2,3,4-tetrahydronaphthalene), or 1-methylnaphthalene.

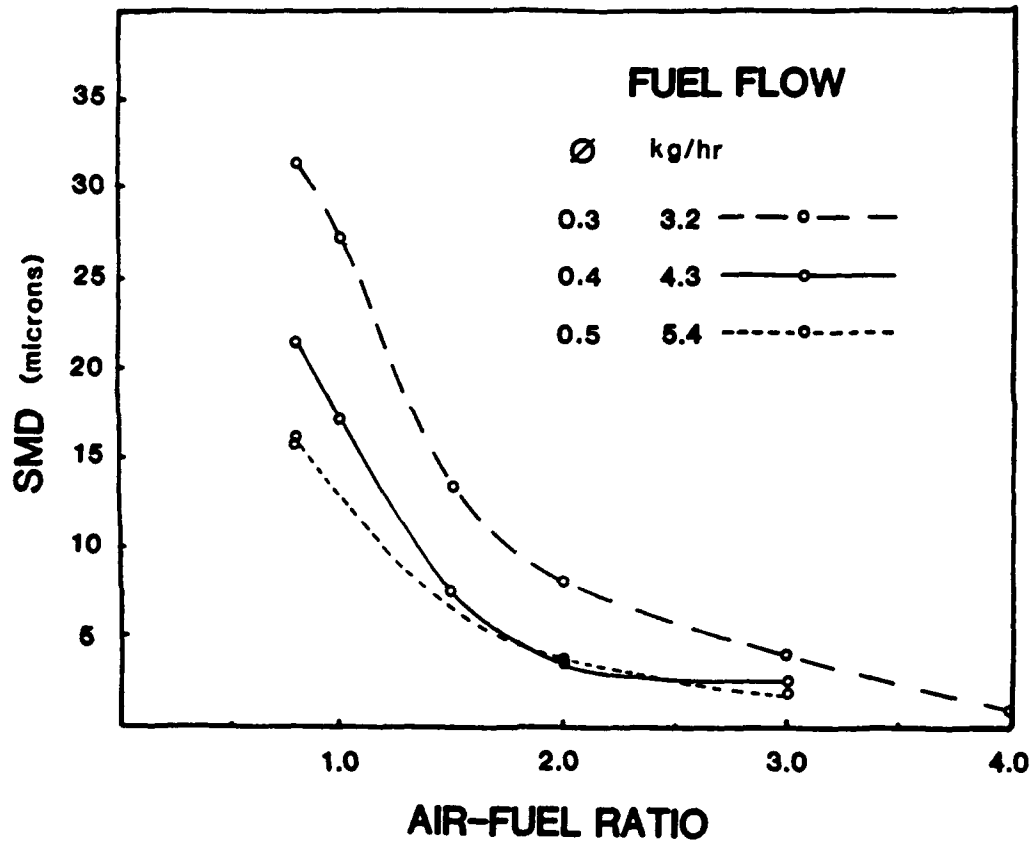

Figure 14. Task 2: Nozzle Characterization.

ISOOCTANE $(CH_3)_2CHCH_2C(CH_3)_3$

TOLUENE 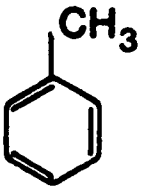

TETRALIN 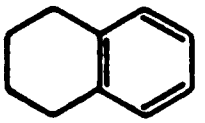

1-METHYLNAPHTHALENE 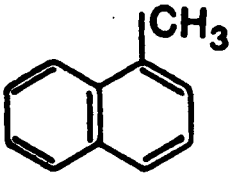

Figure 15. Task 2: Fuel Molecular Structure.

The amount of hydrocarbon blended with the isooctane was selected to yield the same ASTM smoke point as that obtained for the JP-8 stock. The amount of each compound blended with isooctane was determined by first preparing a curve of smoke point vs. volume percent isooctane (Figure 16). Table 1 summarizes the composition and the actual smoke point found for each blend. The smoke points, while not identical, are equivalent within the achievable accuracy of the smoke point test (± 1mm) shown by the error bands in Figure 16.

TABLE 1. TASK 2: FUEL SUMMARY

Fuel[a]	Smoke point, mm[b]	Hydrogen, wt. %
Isooctane	43.0	15.79
JP-8	23.0	13.89[c]
Blend 1 21% Toluene/79% Isooctane	24.0	14.02
Blend 2 8% Tetralin/92% Isooctane	25.3	15.06
Blend 3 5% 1-Methylnaphthalene/ 95% Isooctane	22.2	15.16

[a] Blend composition stated in volume percent
[b] Distance above base of burner in mm at which sooting first occurs
[c] Wright Patterson AFB
Source: Reference 6

d. Optical System

The optical system is described in Section III.F.

e. Velocity

Velocity measurements were made using a two-color laser anemometry (LA) system described in Reference 23. Streamlines were calculated from velocity and temperature measurements at ten radial locations at each of six axial stations. Velocity data were biased in the recirculation region by

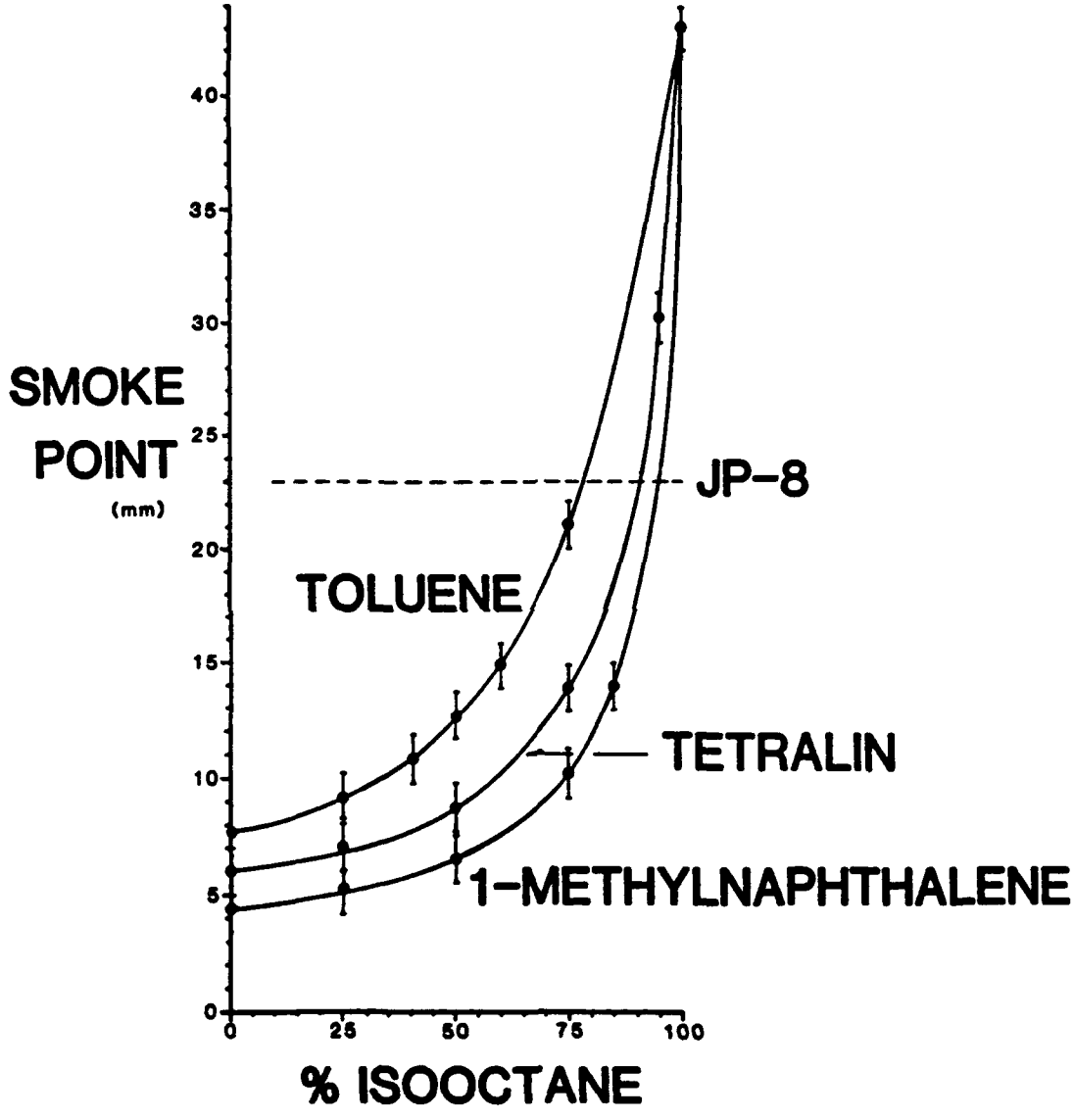

Figure 16. Task 2: ASTM Smoke Point.

the spray-atomized fuel droplets and, as a result, the streamline structure in the recirculation zone was established using the temperature data and velocity data obtained from gaseous propane injection, as well as the current velocity set.

f. Temperature

The temperature probe is described in Section III.E.

g. Test Matrix

The test matrix for the present study is presented in Table 2. Tests were conducted at overall equivalence ratios of 0.3 and 0.5, except for the JP-8, which was tested only at 0.3. (At equivalence ratios greater than 0.3, a portion of the atomized JP-8 was found to penetrate the recirculation zone and impinge on the walls of the combustor). The nominal air-to-fuel rate for the nozzle was 3.0 for the JP-8, isooctane, and three blends. The nozzle air was in addition to the main air (swirl plus dilution) and corresponded to 10 and 6 percent of the main air at ϕ = 0.5 and ϕ = 0.3, respectively. Although not optimum for each individual case, an air-to-fuel ratio of 3.0 was selected as the operating condition which provided the most satisfactory performance (highest stability) for the group of fuels tested. The effect of atomization quality was demonstrated for the shale-derived JP-8. The combustor was operated at a reference velocity of 7.5 m/s.

3. Results

The results are presented in two groups. The performance and utility of the optical system for in-situ, nonintrusive measurements of soot size and number density are first evaluated. Second, the effects of fuel molecular structure, fuel loading, nozzle performance, and injection state on the spatial variation of soot size and number density within the combustor are assessed.

a. Data Presentation

An example of the data provided by the optical system is shown in Figure 5b for the tetralin blend at ϕ = 0.5. The histogram represents the distribution of intensity ratio for 30131 validated samples. The total data rate for this case (2643 Hz) is the number of validated samples (30131) divided by the total sample time (11.4 seconds) and represents the sum of the bin data rates for each of the 62 bins comprising the histogram. The

total data rate for each sampling location for this case and for all fuels and conditions tested is listed in Table 3.

TABLE 2. TASK 2: TEST MATRIX

Fuel[a]	Overall Equivalence Ratio ϕ	Nozzle Air-to-Fuel Ratio	Injection State	Figure
Isooctane	0.3, 0.5	3.0	Liquid	18
JP-8	0.3	2.5,3.0,3.5	Liquid	19
Blend 1 - 21% Toluene/ 79% Isooctane	0.3, 0.5	3.0	Liquid	18
Blend 2 - 8% Tetralin/ 92% Isooctane	0.3, 0.5	3.0	Liquid	18
	0.3, 0.5	NA[b]	Prevap.	18,20
Blend 3 - 5% 1-Methylnaphthalene/ 95% Isooctane	0.3, 0.5	3.0	Liquid	17,18

[a] Blend composition stated as volume percent
[b] NA = Not Applicable

The utility of a point measurement is the ability to map the combustor for soot size and number density. An example of such a mapping is presented in Figure 17 for the 1-methylnaphthalene blend at $\phi = 0.5$. Radial profiles of optically-measured soot size and number density are presented at three axial locations within the combustor. The locations of peak soot concentration for the 1-methylnaphthalene blend can be identified ($x/R = 1.6$; $r/R = 0.83$), and the reduction of soot downstream is clearly evident.

The effects of fuel molecular structure, nozzle performance, and injection state on the soot field are presented in Figures 18, 19, and 20, respectively. In Figure 17, as well as in Figures 18, 19, and 20, radial and axial locations are nondimensionalized to the combustor radius ($R = 40$ mm). All the histograms in Figures 17, 18, and 19 represent results obtained with the fuels injected as liquids and are, as a result, normalized as a group to

TABLE 3. TASK 2: DATA RATE (Hz)

Fuel	Equivalence ratio ϕ	Location							Injection state
		Axial x/R	Radial r/R						
			0	0 17	0.33	0.50	0.67	0.83	
Isooctane	0.5	1.6	57	70	66	61	109	247	liquid
		3.0	0	0	0	0	7	26	
		5.0	0	0	0	0	0	1	
Blend 1	0.5	1.6	30	72	122	204	406	581	liquid
21% toluene/		3.0	0	0	1	6	65	296	
79% isooctane		5.0	0	0	0	4	59	419	
Blend 2	0.5	1.6	236	305	389	700	1521	1982	liquid
8% tetralin/		3.0	1	6	61	444	1775	2643	
92% isooctane		5.0	0	1	3	9	98	1746	
Blend 3	0.5	1.6	260	346	450	770	1482	1612	liquid
5% 1-methylnaphthalene/		3.0	0	5	61	429	1532	1991	
95% isooctane		5.0	0	1	2	6	90	1399	
JP-8	0.3	1.6	26	25	24	22	24	21	liquid
(A/F = 3.0)		3.0	22	22	20	14	12	19	
		5.0	105	134	122	25	10	15	
JP-8	0.3	1.6	45	46	53	61	42	20	liquid
(A/F = 2.5)		3.0	425	330	311	166	29	28	
		5.0	1812	1686	1211	470	88	20	
JP-8	0.3	1.6	13	10	11	35	236	372	liquid
(A/F = 3.5)		3.0	11	11	10	12	56	269	
		5.0	6	8	10	24	92	191	
Blend 2	0.5	1.6	1505	1221	874	468	142	103	pre-
8% tetralin/		3.0	1054	775	928	373	143	244	vaporized
92% isooctane		5.0	183	394	1761	934	861	3373	
Blend 2	0.3	1.6	1120	980	857	603	239	239	pre-
8% tetralin/		3.0	313	345	887	416	282	488	vaporized
92% isooctane		5.0	284	677	2364	1023	1914	3816	
Blend 2	0.5	2.3	1200	1590	1347	1175	1631	2236	pre-
8% tetralin/		3.7	1269	1293	1717	2104	2361	2708	vaporized
92% isooctane		5.0	1164	1081	1291	1686	2032	2405	(weak swirl)

Figure 17. Task 2: Isooctane/1-Methylnaphthalene (ϕ = 0.5).

(a) isooctane

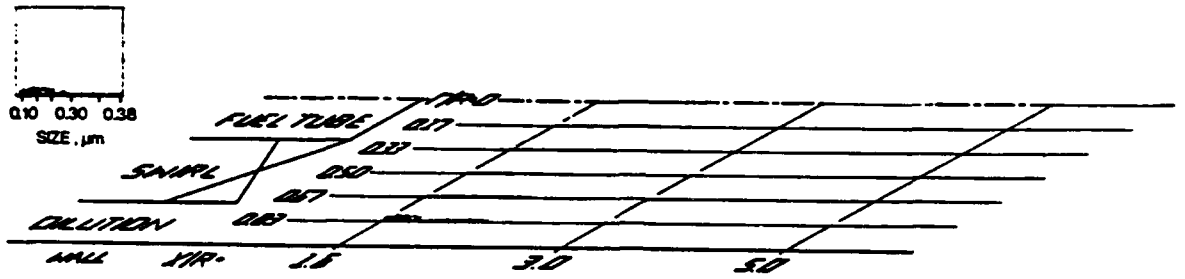

(b) isooctane/toluene

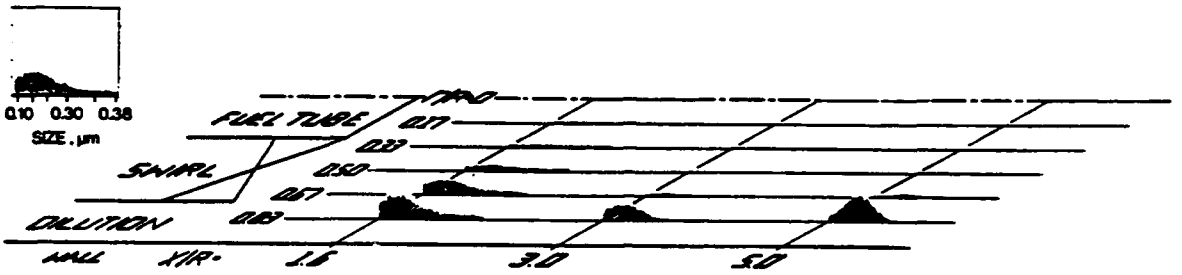

(c) isooctane/tetralin

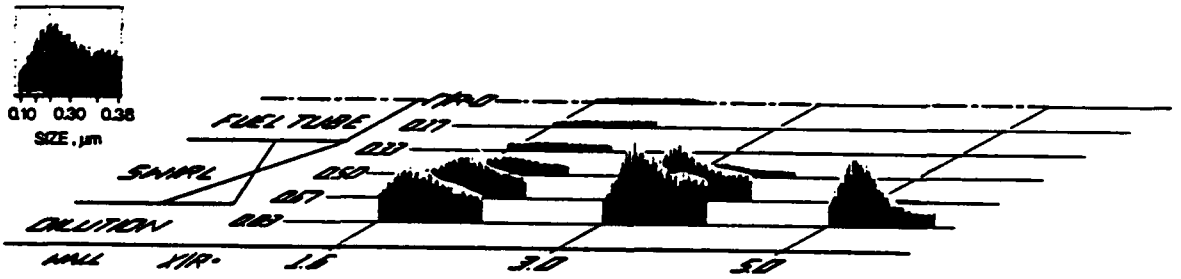

(d) isooctane/1-methlnaphthalene

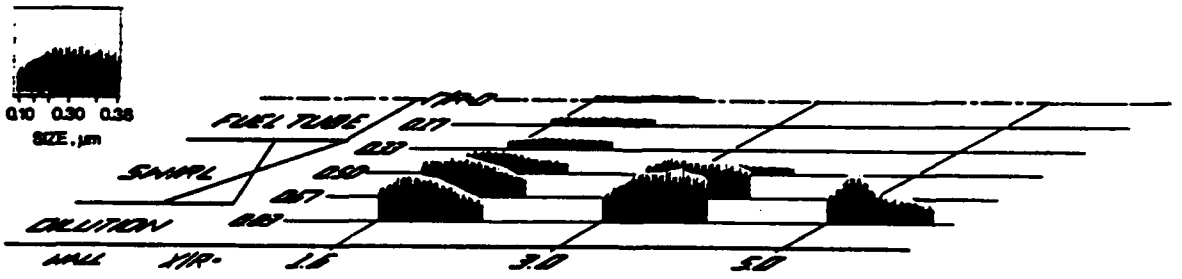

Figure 18. Task 2: Fuel Molecular Structure (ϕ = 0.5).

(a) A/F = 3.0

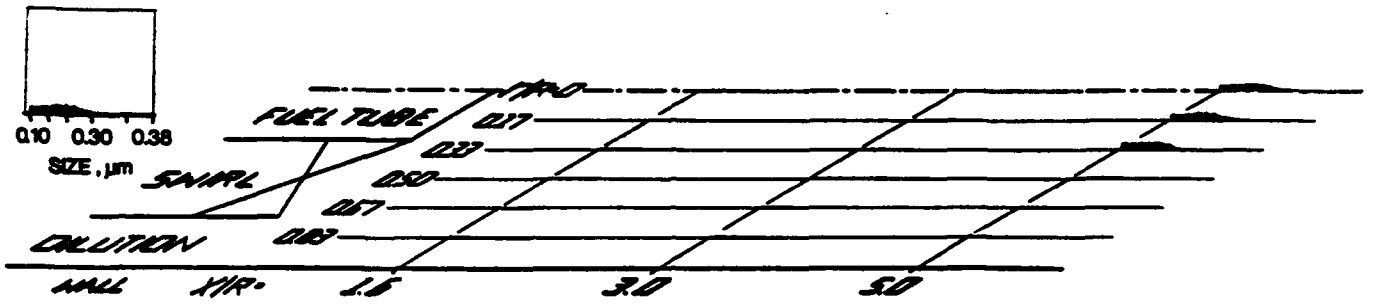

(b) A/F = 2.5

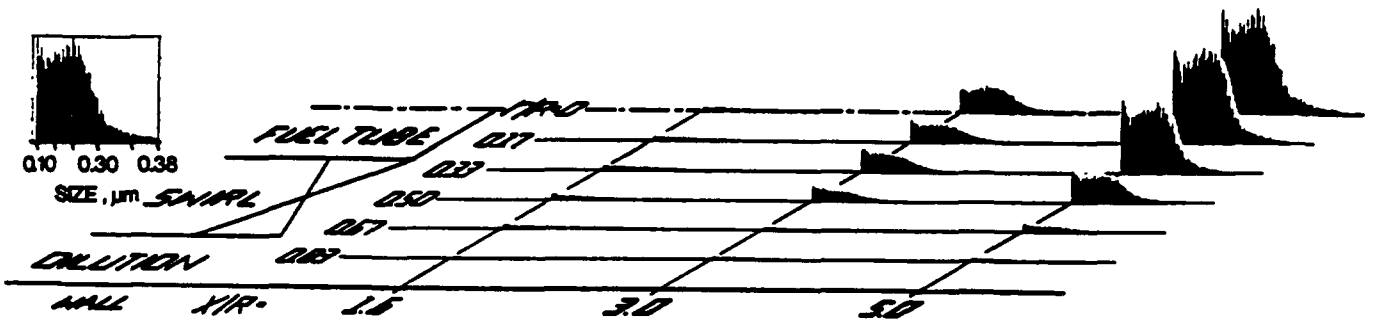

(c) A/F = 3.5

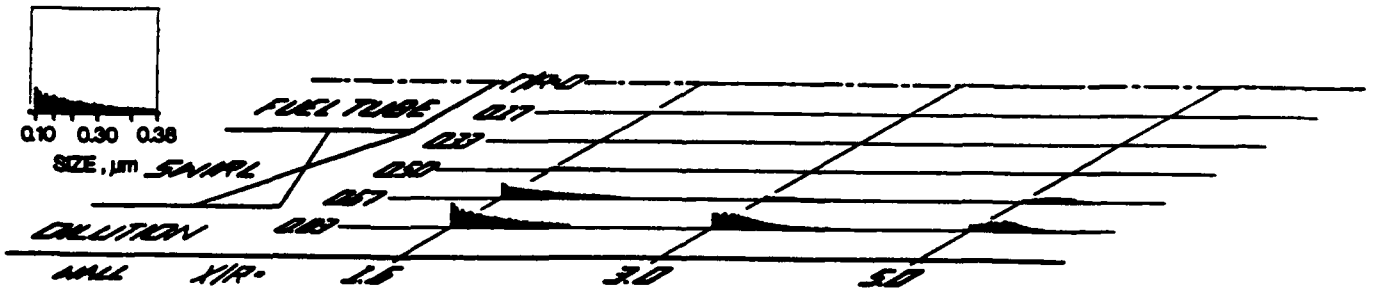

Figure 19. Task 2: Nozzle Performance (JP-8, ϕ = 0.3).

(a) prevaporized injection, ϕ = 0.5

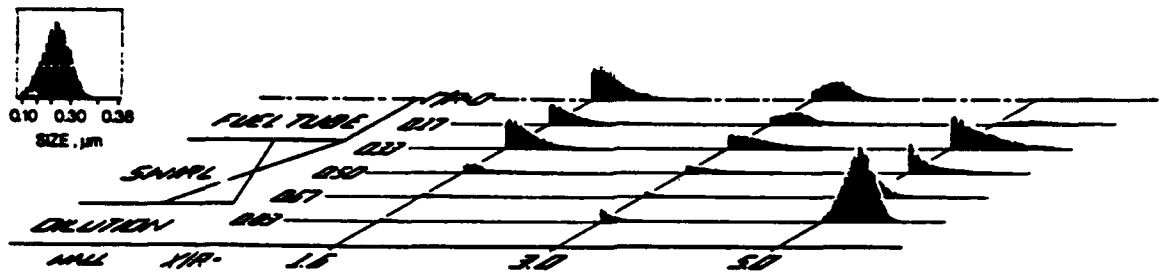

(b) prevaporized injection, ϕ = 0.3

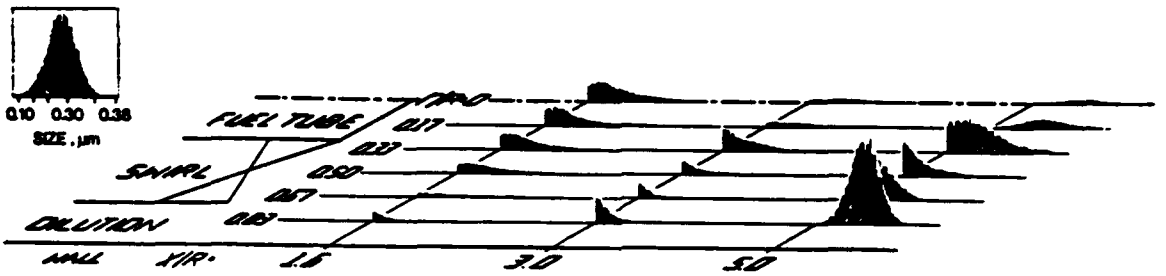

(c) liquid injection, ϕ = 0.5

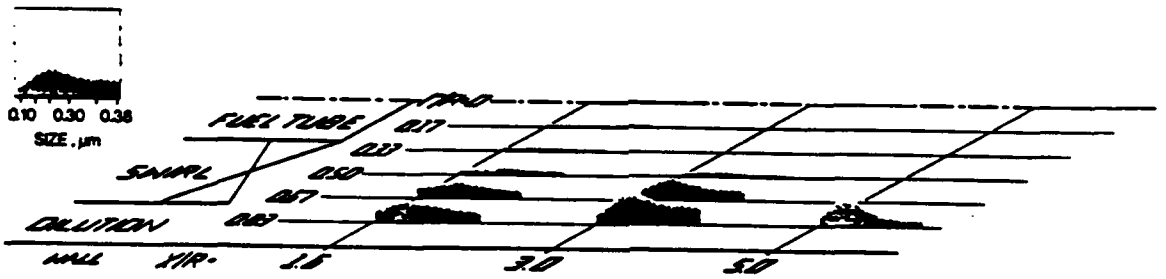

(d) prevaporized injection, diminished swirl intensity, ϕ = 0.5

Figure 20. Task 2: Injection State (Isooctane/Tetralin).

the peak bin data rate in the set (JP-8, Figure 19b). In Figure 20, the state of fuel injection is varied. Hence, these histograms are normalized to the peak bin data rate in this set (prevaporized isooctane/tetralin, Figure 20b). To assist in comparing the histograms in each three-dimensional plot and within each set of results, the histogram with the peak bin data rate in the field is reproduced and dimensioned in the upper left corner of each plot. Because the peak bin data rate in Figure 17, for example, is normalized to the peak bin data rate of JP-8 in Figure 19b, the height of the histogram in the upper left corner of Figure 17 is less than unity.

b. Evaluation

An example of the uncorrected and "probe-volume" corrected data provided by the optical system is shown in Figure 21 for the base fuel (isooctane/tetralin blend) at $\phi = 0.5$. The histogram represents the distribution of intensity ratio for 30131 validated samples. The total data rate for this case (2643 Hz) is the number of validated samples (30131) divided by the total sample time (11.4 seconds) and represents the sum of the bin data rates for each of the 62 bins comprising the histogram. The total data rate for each sampling location for this case and for all fuels and conditions tested is listed in Table 3.

To validate the optical system, the optical probe was positioned at the entrance of the extractive probe described in Section III.D. The extractive probe was located at an axial location ($x/R = 5.0$) and radial location ($r/R = 0.83$) well displaced from the centerline where flow perturbation is minimized. A scanning electron microscopy analysis of the extracted sample was compared to the optical data.

The morphology of the soot (Figure 22) is spherical particles (~ 0.05 μm) and agglomerates of the spherical particles (~0.1 to 0.4 μm) which is consistent with the morphology and size observed in other combustor studies (e.g., References 6, 8, 22, 24, and 25). An example of the size distribution derived from a scanning electron micrograph (SEM) of the extracted sample is compared to the optical measurement in Figure 22b. The range of particle sizes resolved by the 60 degrees/20 degrees intensity ratioing techniques: (1) is at the large particle end of the SEM distribution, (2) encompasses the agglomerates, and (3) excludes the primary particles. In terms of mass density, the optical data reflect approximately 70 percent of the SEM distribution. The difference is attributed primarily to

(a) uncorrected

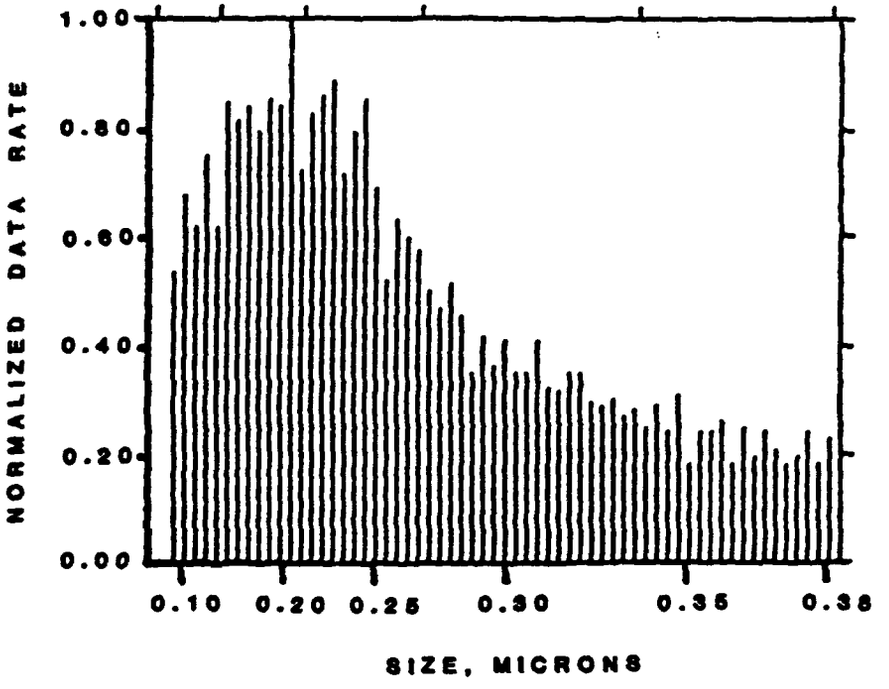

(b) corrected

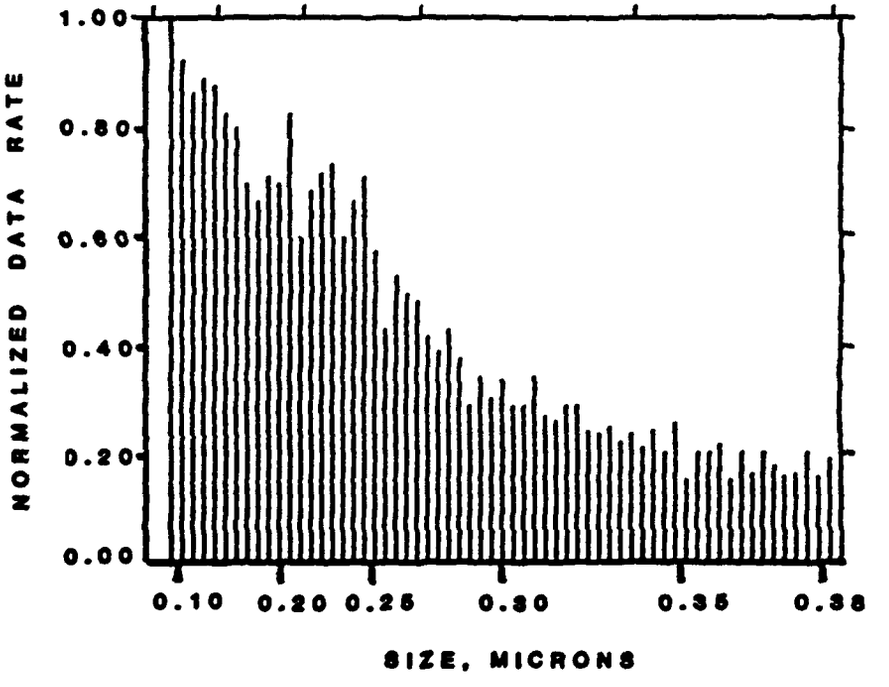

Figure 21. Task 2: Representative Optical Soot Data (Isooctane/Tetralin, ϕ = 0.5).

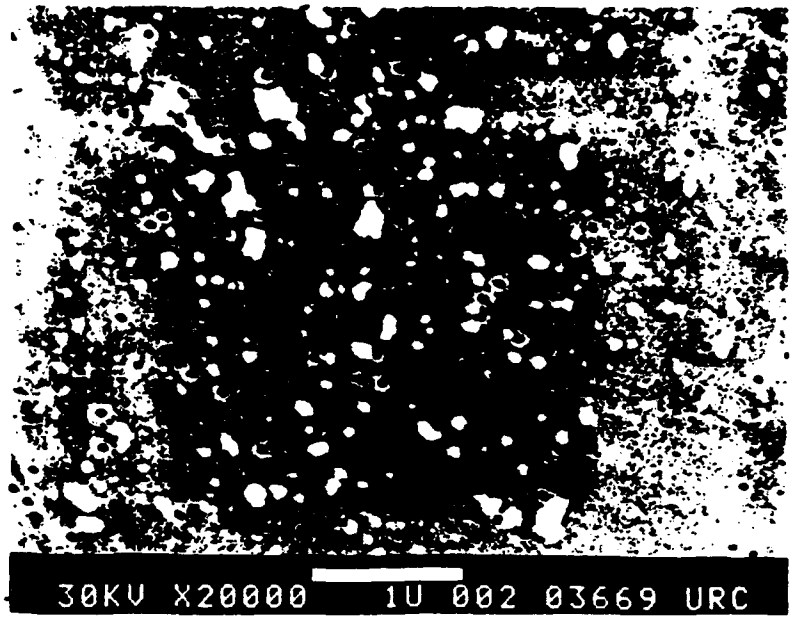

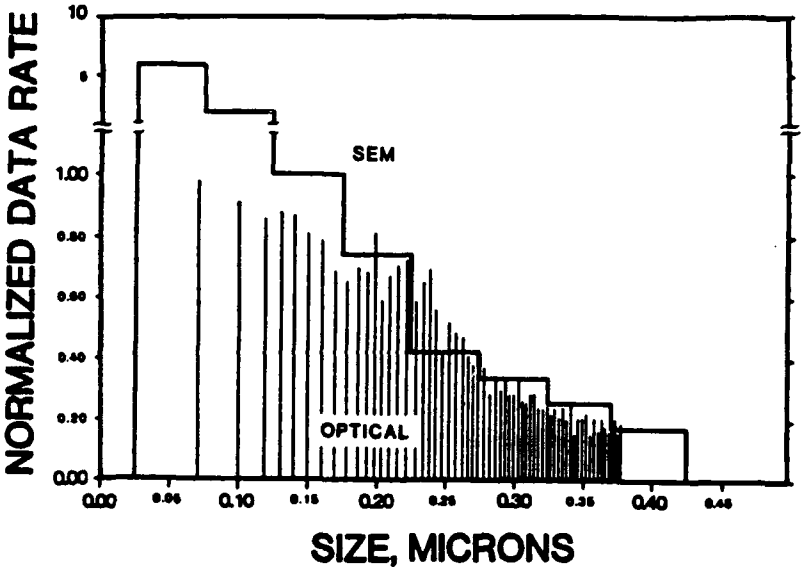

Figure 22. Task 2: SEM Validation.

the upper limit (~0.4 μm) on the optical window which filters the large (relatively heavy) particle wing of the distribution. In addition, the small (relatively light) primary particles are excluded from measurement. The validation logic of the software invalidates some scores such as those that occur from multiparticle scattering.

The aerodynamic and temperature fields are presented in Figure 23. The recirculation zone extends one duct diameter downstream and consists,for this combination of swirl strength and nozzle condition, of a double vortex surrounding a positive velocity on the centerline. The thermal map shows a uniform, high-temperature core with a radially diverging steep gradient to a relatively cool, outer flow.

At x/R = 1.6, the agglomerate population measured by the optical probe is low and uniformly distributed at the three interior radial positions (r/R = 0.0, 0.17, 0.33) that are aligned with the relatively high temperature, well-mixed recirculation zone of the combustor. The agglomerate population at the three outer radial stations (r/R = 0.50, 0.67, 0.83) increases as the temperature drops and the residence time increases. The population reaches the maximum in this data set at the exterior radial station at the second axial location (x/R = 3.0). The soot in the core of the combustor has been essentially burned out (Table 3). At the third axial station (x/R = 5.0), the soot is burned out as the temperature increases radially inward. At the r/R = 0.83 station, the temperature is not yet sufficient to completely burn out the soot, but the large particle wing of the soot particulate is noticeably reduced, as well as a significant (though less substantial) reduction of the small particle wing. The extent to which this may be attributed to burnout and/or a reorientation of the soot structure is not yet established.

The oxidation of soot in regions of elevated temperature is consistent with the hypothesis that, in premixed flames, the oxidative attack on soot increases faster than pyrolysis as the temperature is raised (Reference 11). Whether the present burner behaves as a premixed system is, at present, a point only of conjecture. Although the burner, in fact, comprises a myriad of diffusion-limited and premixed parcels, the combination of the intense fuel/air mixing, fine atomization, and the efficient distribution of fuel provided by the air-assist nozzle is conducive to the promotion of an overall premixed behavior. (The burner can be driven to a

(a) Soot Field

(b) Aerodynamic and Temperature Field

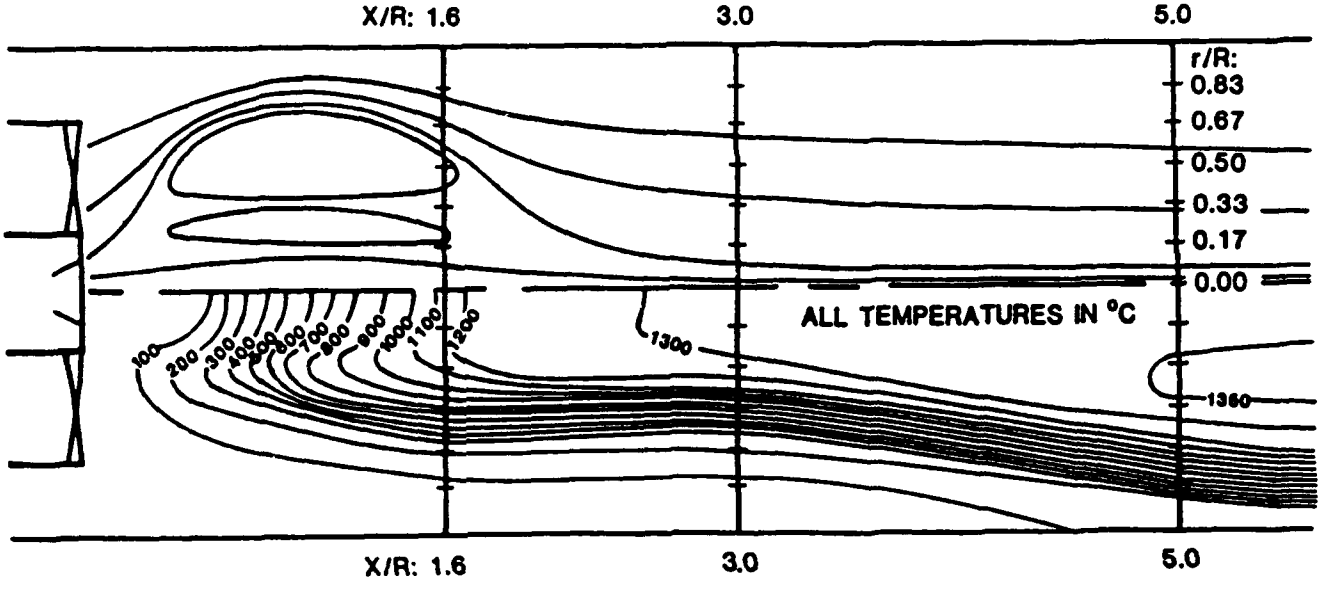

Figure 23. Spatial Maps of Velocity, Temperature, and Soot.

diffusion-type character by a reduction in the atomizing air-to-fuel ratio which results in larger droplets and a collapse of a portion of the fuel onto the centerline to form a fuel-rich combustor core (References 16 and 26).

c. Parametric Assessment

(1) Fuel Molecular Structure. The results for the effect of fuel molecular structure on soot size and number density are presented in Figure 18 for isooctane and the three blends (79 percent isooctane/21 percent toluene; 92 percent isooctane/8 percent tetralin; 95 percent isooctane/5 percent 1-methylnaphthalene) prepared to yield the same smoke point as a JP-8 stock. The data are normalized to the peak bin data rate observed for JP-8 at an air-to-fuel ratio = 2.5, ϕ = 0.3 (Figure 19b). The total data rates for each location are tabulated in Table 3.

It is first noteworthy to compare the results for the isooctane blends (Figures 18b, c, d) with the results for the pure isooctane (Figure 18a). The data rates for the blends are higher than the data rates observed for the pure isooctane. Hence, the addition of ring compounds (as small as 5 percent by volume in the case of 1-methylnaphthalene) has a substantial impact on the soot produced.

For the isooctane and all three blends, soot is observed at all radial stations at the x/R = 1.6 axial station, but only at the outer radial stations at x/R = 3.0 and 5.0. This is attributed to (1) the intersection of the x/R = 1.6 axial station with the recirculation zone, the outer boundary of which extends to approximately 80 mm (x/R = 2.0), and (2) the injection of the fuel into the outer boundary ("shear layer") of the recirculation zone. Note that the data rate is of the same magnitude for radial stations within the recirculation zone (0 < r/R < 0.50) which is consistent with the presence of a zone of strong backmixing.

The peak data rate for the isooctane and fuel blends occurs at the outer radial positions, coincident with the injection of fuel into the shear layer. Downstream of the recirculation zone (x/R = 3.0, 5.0), the soot particles are transported radially outward as a consequence of the strong swirl.

The data rate for isooctane drops dramatically at the two downstream locations and, at x/R = 5.0, the soot particulate is completely burned out. The addition of ring compounds, by contrast, not only results in more soot produced, but shows evidence of only marginal burn out.

The distribution of soot particulate has both similarities and significant differences in this data set. The distributions are similar in the relatively uniform distribution in the recirculation zone. The flatness of the distribution reflects an early stage of particulate formation prior to the onset of agglomerate growth. Evidence for the agglomerate growth is reflected in distributions measured at locations displaced from the recirculation zone, namely at $x/R = 1.6$ ($0.67 \leq r/R \leq 0.83$), $x/R = 3.0$, and $x/R = 5.0$. The distribution differs as to where within the combustor the agglomerate begins to build. The buildup of the agglomerate peak occurs further away from the recirculation zone as the molecular complexity of the ring compound increases. This reflects the longer time for fuel pyrolysis and/or longer time for polymerization as the fuel complexity increases.

Data were also obtained at a reduced fuel loading ($\phi = 0.3$) for the isooctane and three fuel blends. Virtually no soot particulate was detected by the optical probe at any of the eighteen sampling points within the combustor (e.g., total data rates were less than 1 Hz). In direct contrast, the total data rates for the shale-derived JP-8 at $\phi = 0.3$ were not insignificant (Table 3, Figure 19a). It is also noteworthy that the highest sooting rate occurs at the centerline for the JP-8. This is attributed to the probable collapse of a portion of the fuel jet onto the centerline at this lower nozzle fuel flow rate. Such a collapse has been detected with two-color anemometry (Reference 2) and the subsequent centerline formation of soot has been verified with hi-speed video recordings.

Finally, the fuel blends, mixed to the same smoke point as the shale-derived JP-8, produced different soot yields (area weighted soot flux) at the last axial plane sampled ($x/R = 5.0$, Figures 18b,c,d). The double-ring tetralin and 1-methylnaphthalene blends both yielded a higher soot level than the single-ring toluene blend. The tetralin blend yielded the highest production of the three. At $\phi = 0.3$ the JP-8 yielded significant soot whereas the blends yielded no soot at this lower equivalence ratio.

(2) Nozzle Performance. To assess the effect of nozzle performance, the nozzle air-to-fuel (A/F) ratio for one fuel, the JP-8, was varied from the nominal value of 3.0 by changing the air flowrate at a constant fuel flowrate corresponding to $\phi = 0.3$ (Figure 19). At a degraded level of performance (A/F = 2.5), the soot production went up markedly (Figure

19b). This demonstrates the importance of nozzle performance in dictating sooting levels. As further evidence for this, note that the spatial distribution of soot for A/F = 3.5 (Figure 19c) is different from that measured for A/F = 3.0 and 2.5 (Figures 19a, b), and similar to the spatial distributions measured for the blends at ϕ = 0.5, A/F = 3.0 (Figures 18b, c, d). This is attributed to a higher fuel momentum associated with the higher A/F (in the case of the JP-8 at ϕ = 0.3) and higher fuel flow rate (in the case of the blends at A/F = 3.0), thereby preventing collapse of fuel onto the centerline.

(3) Prevaporization. One blend (92 percent isooctane/8 percent tetralin) was injected prevaporized through a cone-annular nozzle (see Figure 1) to assess the sooting propensity when evaporation of injected droplets are not a factor in the injection and subsequent fuel/air contacting. The results are shown in Figure 20 for ϕ = 0.5 (Figure 20a) and ϕ = 0.3 (Figure 20b). (The tetralin blend injected in the liquid state at ϕ = 0.5 is shown in Figure 37c and is normalized to Figure 20b for comparison). The soot yield was greater for the prevaporized fuel and soot was present at all points measured in the combustor. This is consistent with previous results (Reference 22) shown in Figure 20d, where the swirl was not as intense. This difference in sooting behavior is attributed to the different fuel distribution in the recirculation zone resulting from (1) the state of the fuel when injected, and (2) the nozzle. Fuel injected as a vapor enhances the early mixing with the air, and rapidly breaks down the jet penetration. The resulting flame reflects a fuel rich, diffusion type core that extends out of the combustor, giving enhanced sooting levels at the interior radial positions along the entire length of the duct. In contrast, fuel injected as liquid droplets can direct the fuel into the outer boundary of the swirl-induced recirculation zone (the shear layer) resulting in enhanced processing of the fuel within the recirculation zone. This decreases the diffusion type character of the flame, reduces the soot produced, and limits the presence of soot to the outer portion of the combustor.

4. Summary and Conclusions

An optical system based on large-angle intensity ratioing has been used to measure soot particulate in an aerodynamically complex flowfield representative of a practical turbine combustor. The utility of such a

diagnostic tool is the provision of detailed mapping to identify the regions of soot formation and burnout. To demonstrate the utility and applicability of the technique, parametric variation on fuel molecular structure, fuel loading, nozzle performance, and injection state was performed. The results are summarized in the following list of observations and conclusions:

a. Summary of Observations

(1) Blends of ring compounds in isooctane (as little as 5% 1-methylnaphthalene) produced substantially more soot than the isooctane alone.

(2) Blends mixed to the same smoke point as a shale-derived JP-8 and injected as liquid sprays yielded less soot than the JP-8 and varied among the blends in the yield of soot with the multiring tetralin and 1-methylnaphthalene blends producing substantially more soot than the single-ring toluene blend.

(3) The soot yield for the prevaporized blend was higher than for the fuel injected as a liquid. Whereas soot was virtually absent in the core of the combustor for the blends injected as liquids, the soot was spatially distributed more evenly throughout the combustor for the blend injected prevaporized. This is attributed to the reduced momentum of the prevaporized fuel jet and subsequent collapse of a portion of the fuel onto the centerline.

(4) Although the shale-derived JP-8 yielded more soot than the blends mixed to the same smoke point, an increased nozzle air-to-fuel ratio substantially reduced the soot produced and indicates that nozzle performance and combustor aerodynamics can be tailored to reduce the soot yield to approximately that of the blends. Nozzle air-to-fuel ratio not only changed the soot yield but also changed the spatial distribution of soot. At low air-to-fuel ratios, both the fuel jet momentum and atomization quality is degraded, a portion of the fuel collapses onto the centerline, and soot is produced in the core of the combustor. At

high air-to-fuel ratios, the fuel is injected and processed in the shear layer of the recirculation zone.

b. Conclusions

(1) The spatial distribution of soot, as well as the soot yield in a complex flow combustor, is a function of not only fuel molecular structure and fuel loading, but of flow aerodynamics and pattern of fuel injection. This result points to (1) the importance of aerodynamics and nozzle performance, alone and in combination, in controlling the amount of soot produced, and (2) the requirement for spatially resolved, nonintrusive optical measurements to guide combustor design, nozzle design, and fuel property specifications for future fuels.

(2) To unravel and delineate the coupling between the aerodynamics and nozzle performance, and to assume that the results of nonintrusive optical measurements in aerodynamically complex flows are of quantitative as well as qualitative value,

- Optical techniques must be pursued to extend the resolvable size to encompass sizes at or about 0.05 μm.
- Spatially resolved measurements of the velocity and temperature must be acquired to facilitate interpretation of the soot field data.

C. TASK 3: FUEL SIMULATION

1. Introduction

Practical distillate aviation fuels are chemically complex, often containing more than 300 compounds. Few species exceed 1 percent in volume. The composition varies, as well, as a function of refinery, crude oil source, season, and year. As a result, it is difficult to control the consistency in fuel composition required for the purposes of research.

The use of a surrogate blend comprised of pure hydrocarbons to simulate a practical fuel has the advantage of allowing the fuel composition to be accurately controlled and monitored. Areas of research where compositional control is essential include the acquisition of data for the development and verification of numerical codes for combustor design, and studies of the effects of composition on the sooting behavior of fuels.

The present paper reports in-flame measurements of velocity and temperature acquired in a swirl-stabilized, spray-atomized model laboratory combustor. A practical fuel (a petroleum derived JP-4) and a surrogate blend of 14 pure hydrocarbons prepared to simulate the distillation and compositional characteristics of the practical fuel serve as the fuels for this study. The aerodynamic and thermal fields for each fuel are established via laser anemometry and thermocouple measurements, respectively.

In addition, isothermal spray field characterizations of the surrogate and practical fuel are performed to further assess the ability of the surrogate to represent the petroleum JP-4. A high aromatic petroleum JP-5 fuel, which matches neither the distillation curve nor the compound class composition of the petroleum JP-4, is characterized as well to: (1) support the use of distillation curves in surrogate development and (2) determine the extent to which a significant change in fuel properties affects the atomization in the isothermal chamber, and the velocity and temperature fields in the laboratory combustor.

2. Approach

The approach was to: (1) establish a rationale for the preparation of the surrogate fuel, (2) blend the surrogate following the adopted rationale, (3) compare the physical and chemical properties of the blended surrogate and the parent, petroleum derived JP-4, and finally, (4) evaluate the atomization and combustion performance of the two fuels against each other and against other fuels of disparate properties.

3. Fuel Preparation

The present study employs a surrogate fuel consisting of 14 pure hydrocarbons blended to match the distillation curve and compound class composition of the petroleum derived JP-4. Table 4 lists the individual components of the surrogate in order of increasing boiling point, along with

their volume percent and chemical formula. The individual components of the surrogate were of high purity (≥ 99 percent).

TABLE 4. TASK 3: SURROGATE COMPOSITION

Surrogate JP-4 Component	Boiling Point °C	Volume Percent	Chemical Formula
1. n-Hexane	69	5.5	C_6H_{14}
2. Cyclohexane	81	8.0	C_6H_{12}
3. n-Heptane	98	8.0	C_7H_{16}
4. Methylcyclohexane	101	8.0	C_7H_{14}
5. Toluene	111	8.0	C_8H_8
6. n-Octane	126	8.0	C_8H_{18}
7. n-Noane	151	10.0	C_9H_{20}
8. Cyclooctane	151	8.0	C_8H_{16}
9. n-Decane	174	10.0	$C_{10}H_{22}$
10. Decalin	190	5.0	$C_{10}H_{18}$
11. Tetralin	207	1.0	$C_{10}H_{12}$
12. n-Dodecane	216	10.0	$C_{12}H_{26}$
13. 1-Methylnaphthalene	241	0.5	$C_{11}H_{10}$
14. n-Tetradecane	253	10.0	$C_{14}H_{30}$
		100.0%	

Figure 24 presents distillation curves (ASTM method D86) for both the petroleum JP-4 and the surrogate, as well as the cumulative boiling point (b.p.) curve for the surrogate. The cumulative b.p. curve represents the cumulative volume percent boiling at or below a particular temperature. As such, it is equivalent to a "perfect" distillation performed with an infinite number of theoretical plates. Although the surrogate was formulated to

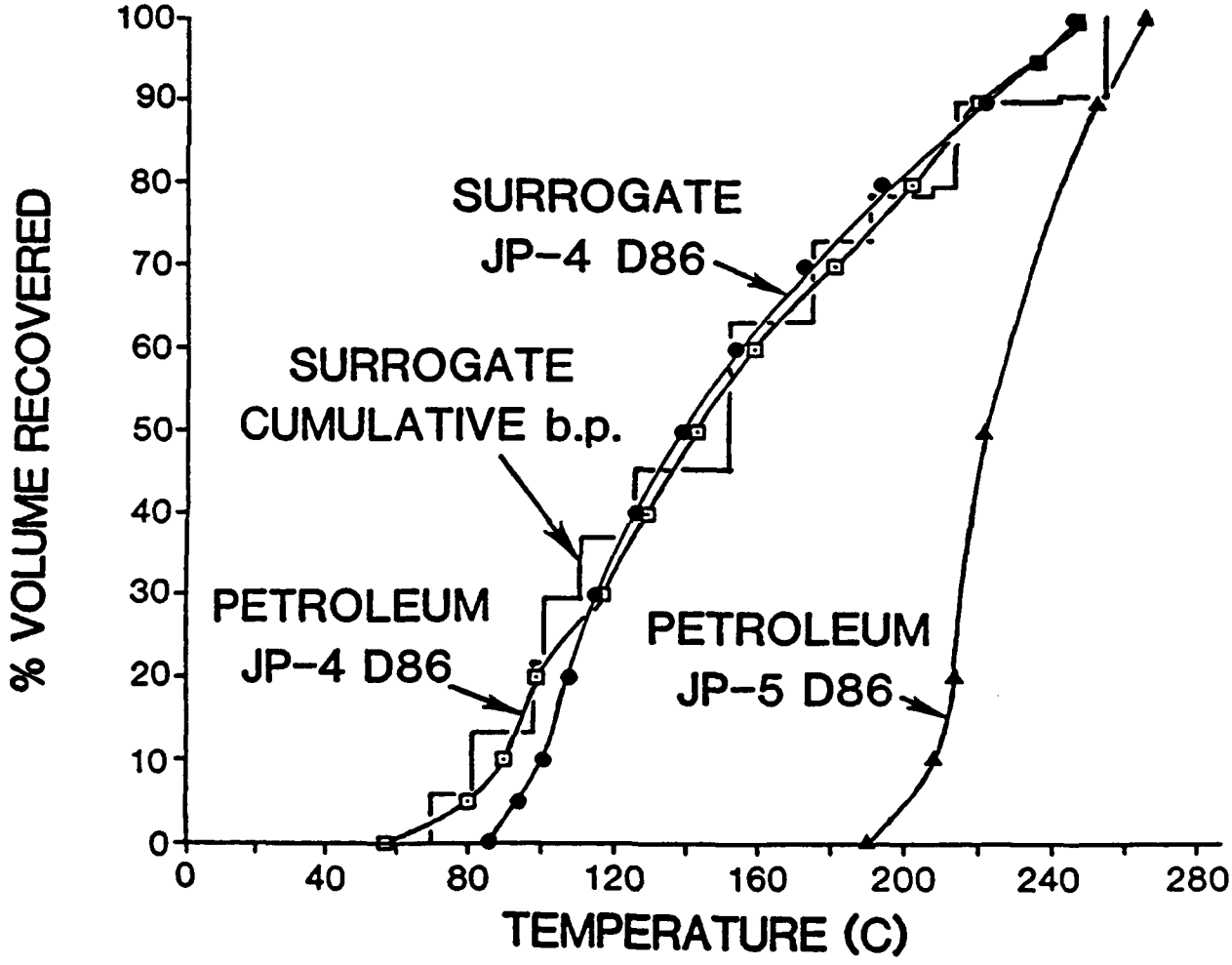

Figure 24. Task 3: Distillation and Cumulative Boiling Point Curves.

produce a cumulative b.p. curve that matched the D86 distillation curve of the petroleum JP-4, the actual D86 for the surrogate shows it to begin boiling approximately 25°C higher than the petroleum JP-4. (Note the curve quickly aligns with the petroleum JP-4 curve and matches it closely to the final boiling point.) The slight delay in the initial boiling point of the surrogate relative to the petroleum JP-4 indicates the necessity of slightly overestimating the concentration of the most volatile (lowest boiling) fraction of the surrogate relative to the petroleum JP-4 (i.e., for the D86 curves to coincide, the surrogate components must be chosen to displace the cumulative boiling point curve toward lower temperatures by approximately 25°C relative to the petroleum JP-4).

A summary of compound class composition for both fuels and a breakdown of the individual chemical components of the surrogate by compound class is presented in Table 5. (Note that the class composition of the surrogate matches that of the petroleum JP-4 to within less than 0.5 percent for each class.) Gas chromatograms are presented for both the petroleum JP-4 (Figure 25a) and the surrogate JP-4 (Figure 25b) to show the inherent chemical complexity of the petroleum JP-4 relative to the surrogate. The paraffins, which comprise over 60 percent of the petroleum JP-4, are represented in the surrogate by normal paraffins from hexane to tetradecane. Whereas the gas chromatographic analysis reveals the individual normal paraffins in the petroleum JP-4 to increase in concentration from C_2 to C_8 and then decrease with increasing molecular weight, the normal paraffins in the surrogate are chosen to increase in concentration to C_9, and stay constant at 10 vol % from C_9 to C_{14}, to allow the surrogate to match both the distillation curve and the paraffin class volume percent of the petroleum JP-4. Note that the surrogate gas chromatogram shows the decalin (chosen to model the dicycloparaffin class) to be comprised of an approximately equimolar mixture of *cis*- and *trans*-decalin, (whose boiling points differ by 9°C), resulting in a chromatogram with 15 individual peaks.

The monocycloparaffin class composition of the surrogate is composed of equal volume percent fractions of C_6, C_7, and C_8 monocyclic compounds. These were chosen to both match the distillation curve of the petroleum JP-4 and to keep fuel costs at a reasonable level. Monocyclic compounds with higher carbon numbers were found to be prohibitively expensive.

(a) Petroleum JP-4

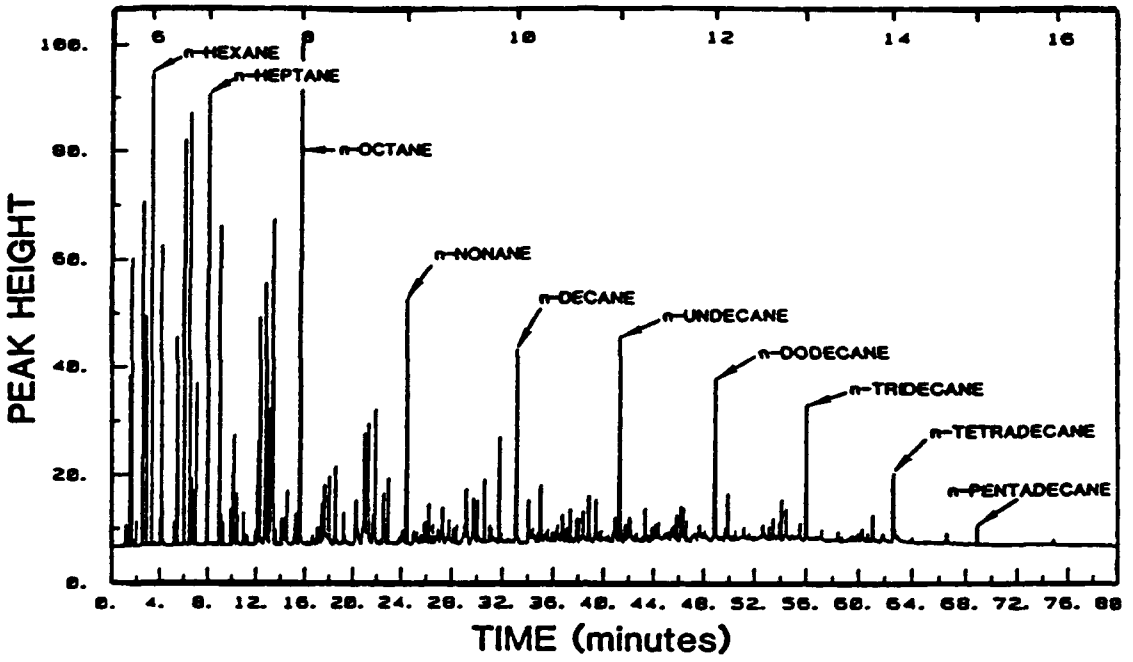

(b) Surrogate JP-4

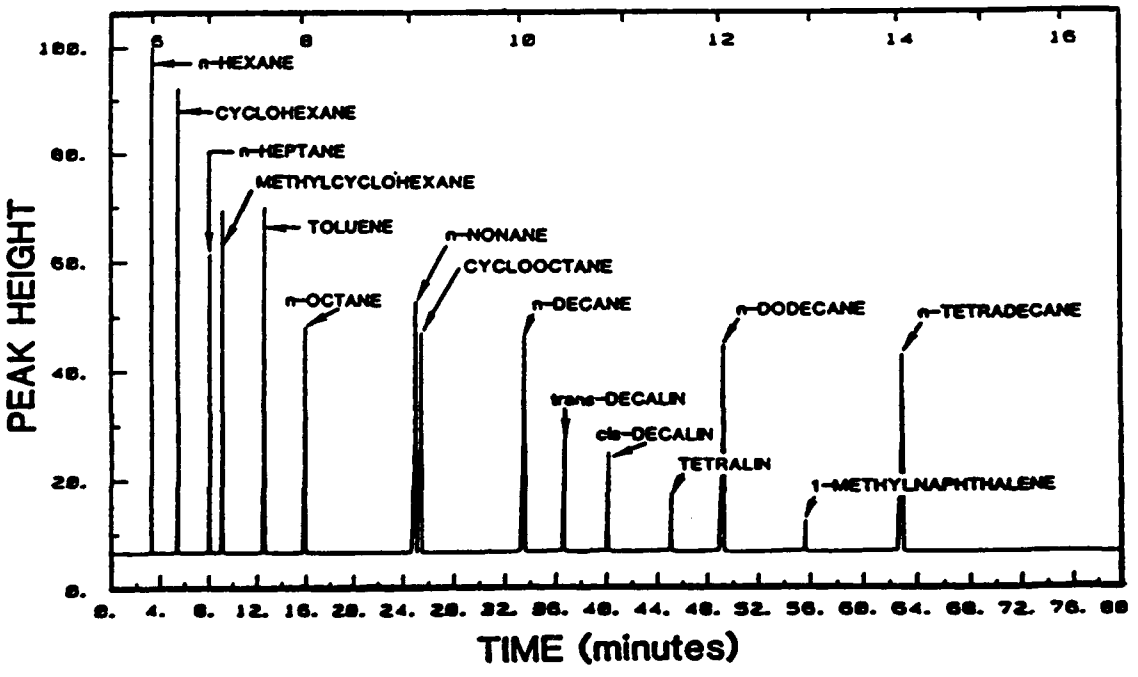

Figure 25. Task 3: Gas Chromatograms.

TABLE 5. TASK 3: FUEL COMPOSITION BY COMPOUND CLASS

Compound Class	Petroleum JP-4 Volume Percent	Surrogate JP-4 Volume Percent	Surrogate Components
Paraffins	61.2	61.5	n-Hexane n-Heptane n-Octane n-Nonane n-Decane n-Dodecane n-Tetradecane
Monocycloparaffins	24.2	24.0	Cyclohexane Methylcyclo-hexane Cyclooctane
Dicyloparaffins	4.9	5.0	Decalin
Alkylbenzenes	8.2	8.0	Toluene
Indans and Tetralins	1.1	1.0	Tetralin
Indenes and Dihydronaphthalenes	-	-	-
Naphthalenes	0.4	0.5	1-Methyl-naphthalene
TOTAL PARAFFINS	90.3	90.5	
TOTAL AROMATICS	9.7 100.0%	9.5 100.0%	

The remaining compound classes are represented in the surrogate fuel by a single compound in each class, chosen as representative of that class, with the exception of the indene/dihydronaphthalene class, for which no compounds were detected in the petroleum JP-4.

The physical properties of the resulting surrogate fuel, as well as those of the petroleum JP-4 practical fuel are listed in Table 6. The properties of the surrogate and petroleum JP-4 compare favorably with the exception of the smoke point and viscosity. The higher smoke point of the surrogate indicates that the surrogate does not have the same propensity to soot as the petroleum JP-4. The higher viscosity could result in differences in atomization quality.

In addition to the JP-4 and its surrogate, a high aromatic petroleum JP-5 was chosen for parallel comparison . Its properties are also included in Table 6. The extent to which the surrogate formulation protocol produces a surrogate fuel which effectively reproduces the performance characteristics of the parent can be demonstrated by comparing these fuels to a fuel of purposefully disparate chemical and physical properties. For example, compared to the surrogate and petroleum JP-4, the JP-5 has (1) a distillation curve of much higher initial boiling point and much narrower

TABLE 6. TASK 3: FUEL PROPERTIES

	Petroleum JP-4	Surrogate JP-4	High Aromatic JP-5
Equivalent Chemical Formula	not determined	$C_{8.35}H_{16.8}$[e]	$C_{11.6}H_{21.1}$[e]
Equivalent Molecular Weight (g/mole)	not determined	117.2[e]	161[h]
Vol. % Aromatics	9.7[a]	9.5[e]	22.7[f]
Specific Gravity (@20°C)	0.757[g]	0.761[g]	0.832[f]
Viscosity (@ 38°C) (centistokes)	0.786[a] 0.789[b]	0.894[b]	1.50[f]
Surface Tension (dynes/cm)	25.7[c]	26.4[c]	not determined
Hydrogen Weight Percent	14.5[a]	14.7[e]	13.5[f]
Smoke Point (mm)	25.0[a] 24.3[d]	46.0[d]	21.0[f]
Heat of Combustion (MJ/kg)	43.6[a]	43.9[e]	42.9[f]

a. Letter from William Harrison, 2LT, USAF, Fuels Branch, Division, Air Force Wright Aeronautical Laboratories Patterson AFB, Ohio, dated 13 August 1981.
b. ASTM Method D445, UNOCAL Research Center Analysis.
c. ASTM Method D971, UNOCAL Research Center Analysis.
d. ASTM Method D1322, UCICL Analysis.
e. Calculated.
f. Letter from Anthony Klarman, Naval Air Propulsion Center Jersey, dated 1 May 1985.
g. ASTM Method D1298, UNOCAL Research Center Analysis.
h. Private communications from Dr. Dennis Hardy, Naval Research Laboratory, Washington, D.C., March, 1987.

boiling point range (see Figure 24), (2) a much higher aromatic content (22.7 vol percent vs. 9.5 vol percent), (3) a significantly lower hydrogen wt percent (13.5 percent vs. 14.5 percent), and (4) a higher specific gravity and viscosity.

4. Experiment

a. Isothermal Flow

(1) Chamber. The isothermal spray characterization chamber is described in Section III.C.

(2) Phase Doppler Interferometer. The Phase Doppler interferometer is described in Section III.H. This task focused on the comparison of data rate, SMD, and mean azimuthal droplet velocity in the isothermal chamber and combustor.

b. Reacting Flow

(1) Combustor. The combustor is described in Section III.A. For the results reported here, the fuels were burned at an overall equivalence ratio of 0.3, corresponding to a primary zone equivalence ratio of approximately 0.8 with the current combustor geometry. The combustor was operated at atmospheric pressure and a bulk reference velocity of 7.5 m/s. The ratio of swirl air to dilution air is 1.5 by mass. Prior to introduction into the combustor, both swirl and dilution air were heated to 100°C. The nozzle, described in Section III.B, was operated under reacting conditions at a nominal air-to-fuel mass ratio of 3.0.

(2) Laser Anemometer. The two-component laser anemometer is described in Section III.G.

(3) Thermocouple Probe. The temperature probe is described in Section III.E.

5. Results

a. Isothermal Spray Chamber Comparison

The mean droplet velocity and temporal SMD profiles are presented in Figure 26. The data are presented for one axial station, 9 cm from the nozzle. This location was selected to facilitate the interferometric based measurement, since the nozzle operating conditions selected for this study result in an extremely dense spray

(a) Petroleum JP-4 and Surrogate JP-4

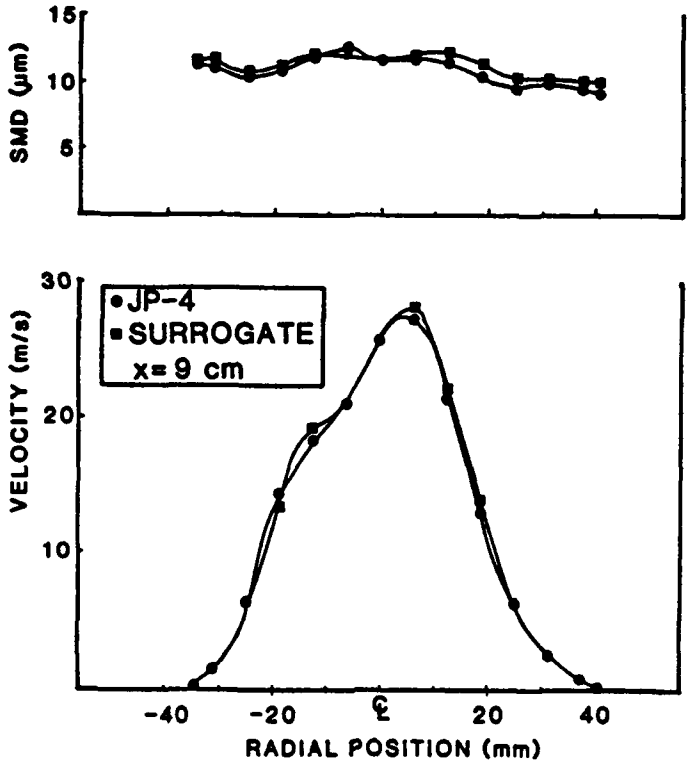

(b) Petroleum JP-4 and Petroleum JP-5

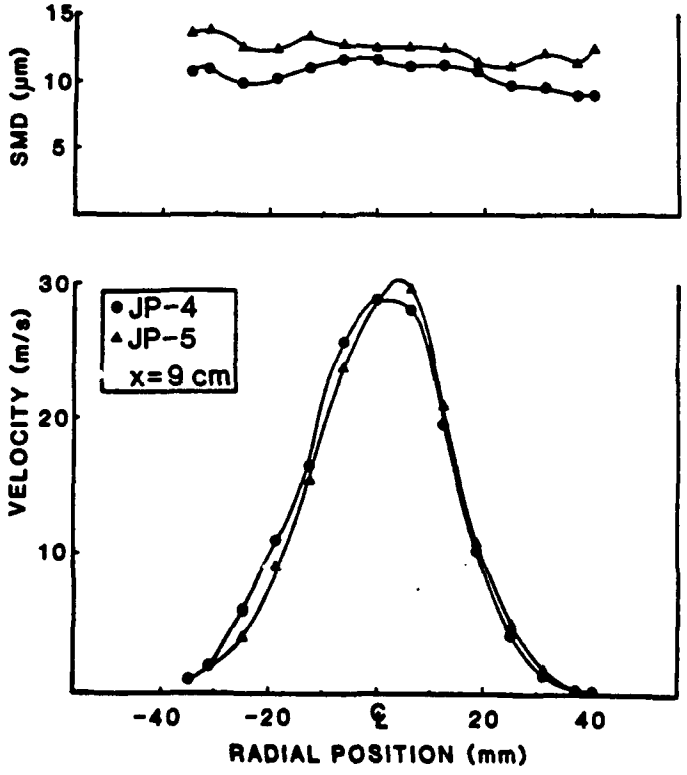

Figure 26. Task 3: Isothermal Comparison.

field which limits this measurement technique to locations well separated from the nozzle exit.

A comparison of droplet size provided by phase Doppler interferometry is shown in Figure 26a for both the petroleum and surrogate JP-4. The temporal-SMD profiles indicate that both fuels maintain very similar SMD values at all points in the spray field. The consistency in size across the spray suggests that the spray field is well-mixed at this axial location. Also shown in Figure 26a are the mean velocity profiles for both fuels, which are shown to be the same. The skewed profile is attributed to a slight nozzle asymmetry observed and documented in Reference 26.

A comparison of droplet size for the petroleum JP-4 and JP-5 is presented in Figure 26b. The temporal-SMD profiles again indicate a well-mixed spray field for both fuels. Although the air-assist nozzle used in the present study is relatively insensitive to fuel property variations in the range evaluated (Reference 15), the values of SMD for the JP-5 are consistently larger by approximately 30 percent.

The mean velocity profiles, shown also in Figure 26b for both fuels, are again the same. Note that the asymmetry present in Figure 26a is not evident. The nozzle is rotated in this case from the data of Figure 26a, with the result that the nozzle generates a slightly different velocity profile than that of Figure 26a.

b. Combustor Comparison

Results are presented first for the aerodynamic fields, followed by the thermal fields.

(1) Aerodynamic Fields. The mean axial velocity fields for the petroleum JP-4, surrogate JP-4, and JP-5 are presented in Figure 27. Also presented in Figure 27 is the aerodynamic field for isoctane, a high-purity compound of relatively high volatility (b.p. = 99.2°C). Isoctane is included here for comparison to verify the effects of fuel volatility discussed below.

With the exception of the axial station at x/R=1.00, the mean axial velocity profiles for all four fuels are remarkably similar. The velocity field for each fuel clearly shows the presence of an off-axis, toroidal recirculation zone at x/R=0.30,

(a) Petroleum JP-4

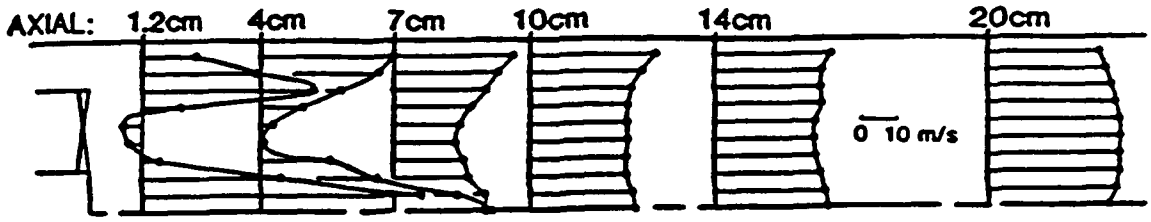

(b) Surrogate JP-4

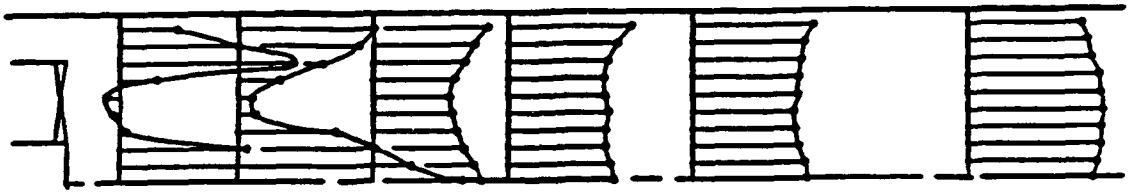

(c) Petroleum JP-5

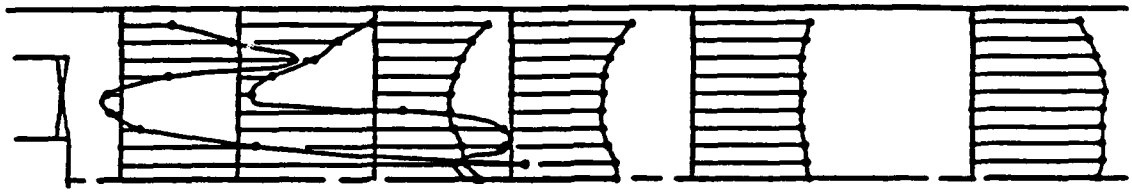

(d) Isooctane

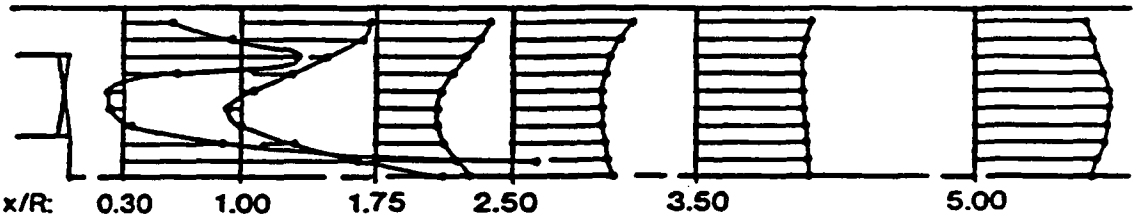

Figure 27. Task 3: Mean Axial Velocity Fields.

positioned directly downstream of the swirl vanes. At x/R=1.75, and at axial locations further downstream, the mean velocity profiles are again remarkably similar among the four fuels. Data are not presented at the core radial locations at the axial station at x/R=0.30 due to the very high spray density which precluded, at these locations, the measurement of axial velocity.

At x/R=1.00, the mean axial velocity profiles show significant differences among the isoctane, petroleum JP-4, and JP-5 fuels. The dramatic increase in mean axial velocity just off the centerline is evident as fuel volatility decreases from isoctane to petroleum JP-4 to JP-5. Whereas the isoctane profile shows clear evidence of the downstream end of the aerodynamic recirculation zone, the JP-5 profile shows positive mean axial velocities in excess of 60 m/s, with the petroleum JP-4 profile falling between. These trends are interpreted as showing the increasing influence of spray droplets on the mean axial velocity as fuel volatility is decreased. This scenario is supported by visual observations of laser beam brightness, which correlate with the number and size of droplets present in the LDA beams. However, since the processing instrumentation used on the LA system cannot distinguish between alumina seeding and fuel droplets, the measured mean velocity profiles can be significantly influenced by the presence of high velocity droplets, as is the case here for the petroleum JP-4 and JP-5. The velocity shoulder on the petroleum JP-4 profile (the location of spray droplet influence) was a persistent result which was consistently measured in 6 different experiments performed over 9 days.

The mean axial velocity profiles of petroleum JP-4 and surrogate JP-4 at x/R=1.00 are plotted in Figure 28 for comparison. It is immediately clear that the mean axial velocity profile of the surrogate is an excellent match for the petroleum JP-4 profile, and is significantly different from either the isoctane or JP-5.

(2) Thermal Fields. The thermal fields for the petroleum JP-4, surrogate JP-4, and JP-5 are presented in Figure 29. Inspection of the thermal field for petroleum JP-4 (Figure 29a) confirms the location and size of the off axis, toroidal recirculation zone, and

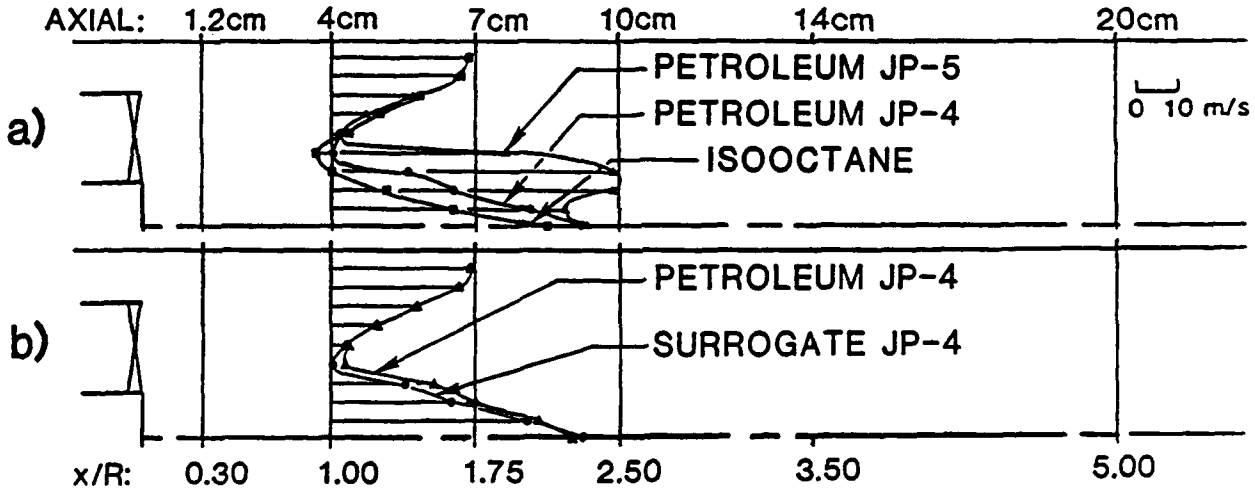

Figure 28. Task 3: Mean Axial Velocity Profiles at x/R = 1.0.

(a) Petroleum JP-4

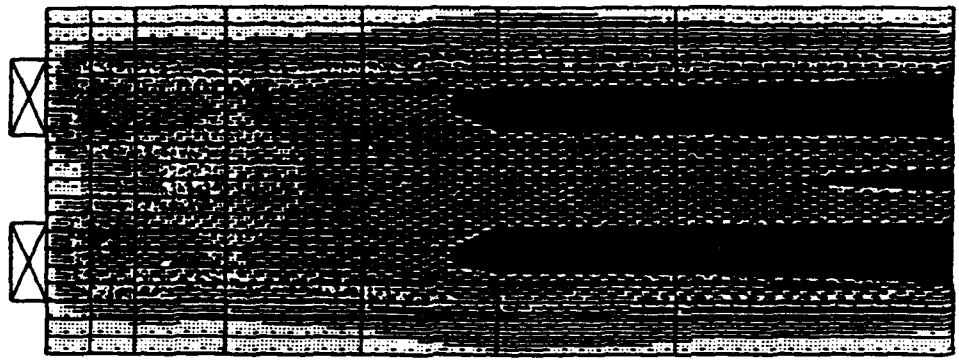

(b) Surrogate JP-4

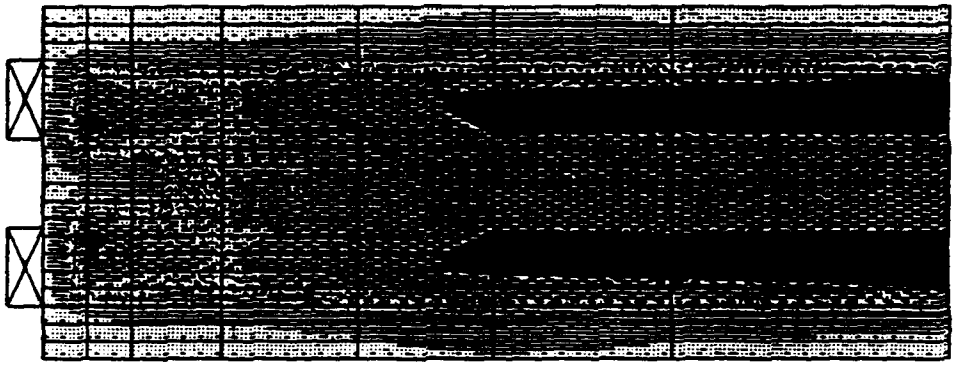

(c) Petroleum JP-5

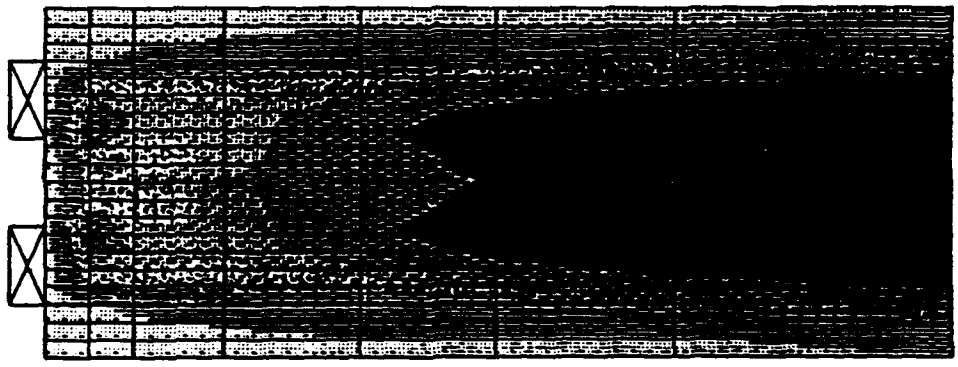

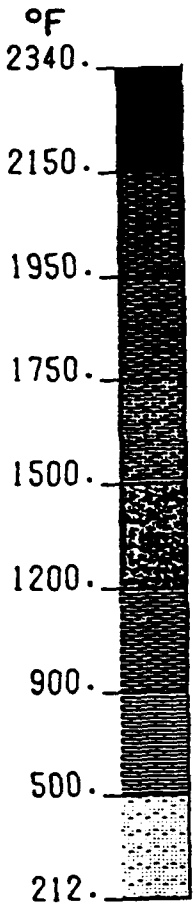

Figure 29. Task 3: Thermal Fields.

also reveals a uniform, high temperature core downstream, with a steeply decreasing radial gradient to a relatively cool outer flow. Figure 29b shows the surrogate temperature field within the combustor to be virtually identical for the JP-4 surrogate.

The thermal field for the fuel with disparate properties, JP-5 (Figure 29c), is indeed distinct from both the petroleum and surrogate JP-4. First, the region near the nozzle exit depicts a more pronounced hollow cone, which indicates maintenance of the cone at distances further from the nozzle than either the petroleum or surrogate JP-4. This is consistent with the higher number densities of droplets encountered during measurements of velocity at x/R=1.00. Second, the overall temperature is higher in the core region of the combustor for the JP-5.

6. Summary and Conclusions

In-flame measurements of velocity and temperature have been acquired in a swirl-stabilized, spray-atomized model laboratory combustor to assess the suitability of utilizing a surrogate multicomponent blend of pure hydrocarbons to simulate the combustion performance of a practical jet fuel. The surrogate is established by matching the distillation curve and compound class composition of a petroleum derived JP-4. The resulting velocity and thermal fields of the surrogate match very closely those of the petroleum JP-4, yet are easily distinguished from those belonging to JP-5, a fuel of disparate properties. Hence, the surrogate provides a suitable baseline fuel of controlled composition and manageable complexity from which to explore fuel property and chemical composition effects upon gas turbine combustion.

D. TASK 4: FUEL ATOMIZATION

1. Introduction

The performance of spray combustion systems is dependent upon the atomization quality of the spray and the spatial distribution of fuel (References 16 and 27). Little is currently known about the interactions between a fuel nozzle spray and the aerodynamic and thermal

environment of a combustion system. Because of the hostile environment and limited optical access of combustors, the characterization of sprays is presently performed in isothermal spray chambers (References 4 and 28) usually in the absence of the strong aerodynamic and elevated thermal environment into which a spray is injected in practical systems.

The objective of this task was to characterize a liquid spray in both an isothermal spray chamber and in a swirl-stabilized combustor under the same nozzle operating conditions. The overall goal was to assess the extent to which isothermal characterization relates to in-situ combustor nozzle performance.

2. Approach

The approach was to measure drop size and drop velocity using phase Doppler interferometry, first in an isothermal spray chamber, and second in a swirl-stabilized model combustor. As a check of consistency, and to acquire spray drop size using an industrial standard, laser diffraction (Malvern) measurements were made as well in the isothermal chamber. To explain the differences between the two environments, spatially-resolved velocity maps were obtained in the combustor with two-component laser anemometry, and a temperature map was established with a thermocouple probe.

3. Experiment

a. Atomizer

The atomizer is described in Section III.B. For the present task, the same atomizer was operated in both the isothermal chamber and combustor at a liquid mass flow rate of 3.27 kg/hr of JP-4 and an atomizing air-to-liquid mass ratio of 1.5.

b. Isothermal Chamber

The isothermal chamber is described in Section III.C.

c. Combustor

The swirl-stabilized combustor is described in Section III.A. The atomizer was plumbed to a fuel/air delivery tube which was identical to that in the isothermal chamber. For the results reported here, the combustor was operated at atmospheric pressure, a bulk reference velocity of 7.5 m/s, and an overall equivalence ratio of

0.3. Both swirl and dilution were heated to 100°C before introduction into the combustor.

The environment into which the fuel was injected was characterized by laser anemometry measurements of the aerodynamic field and thermocouple probe measurements of the temperature (thermal) field. The details of these methods are provided in Reference 29. The results are presented in Figure 30. The presence of a recirculation zone is evident in the aerodynamic field at the 1 and 2 cm axial stations. This zone is established by the interaction of the fuel spray and surrounding aerodynamic swirl. The strength of the fuel spray momentum is sufficient in the present case to preclude the formation of an on-axis recirculation zone. The thermal field exhibits peak temperatures exceeding 1200°C. Note the relatively high temperatures (900 - 1100°C) located in the aerodynamically defined recirculation zone. These data confirm the location and size of the primary recirculation zone, and also reveal a relatively cool region (300 - 500°C) in the immediate vicinity of the atomizer and along the core of the combustor.

d. Diagnostics

The phase Doppler (PD) interferometer, described in Section III.H, was used to measure droplet size and droplet velocity. Special considerations were required in the two environments in which measurements were made: isothermal and reacting.

(1) Isothermal Chamber. In the chamber, the transmitter optics are configured to give fringe spacings of 8.8 μm. With this configuration, a droplet-sizing window is provided with ranges varying from 1.2-to-42 μm to 4.7-to-166 μm.

To verify the phase Doppler measurements, droplet size data are also acquired in the isothermal chamber using laser diffraction, a technique generally accepted in industry for the line-of-sight ensemble measurement of spray SMD. A commercial instrument is employed (Malvern Model ST2200) with an optical path in the same plane but directed 90° from that of the radial point measurements. The diffraction data are processed using both a two-parameter Rosin Rammler (RR) and a fifteen-parameter Model Independent (MI) algorithm.

(a) Swirl-Stabilized Combustor

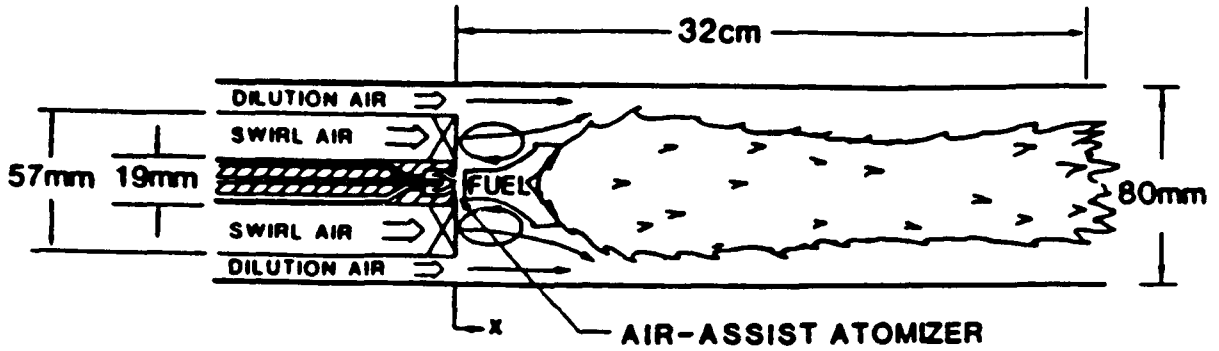

(b) Aerodynamic and Thermal Fields

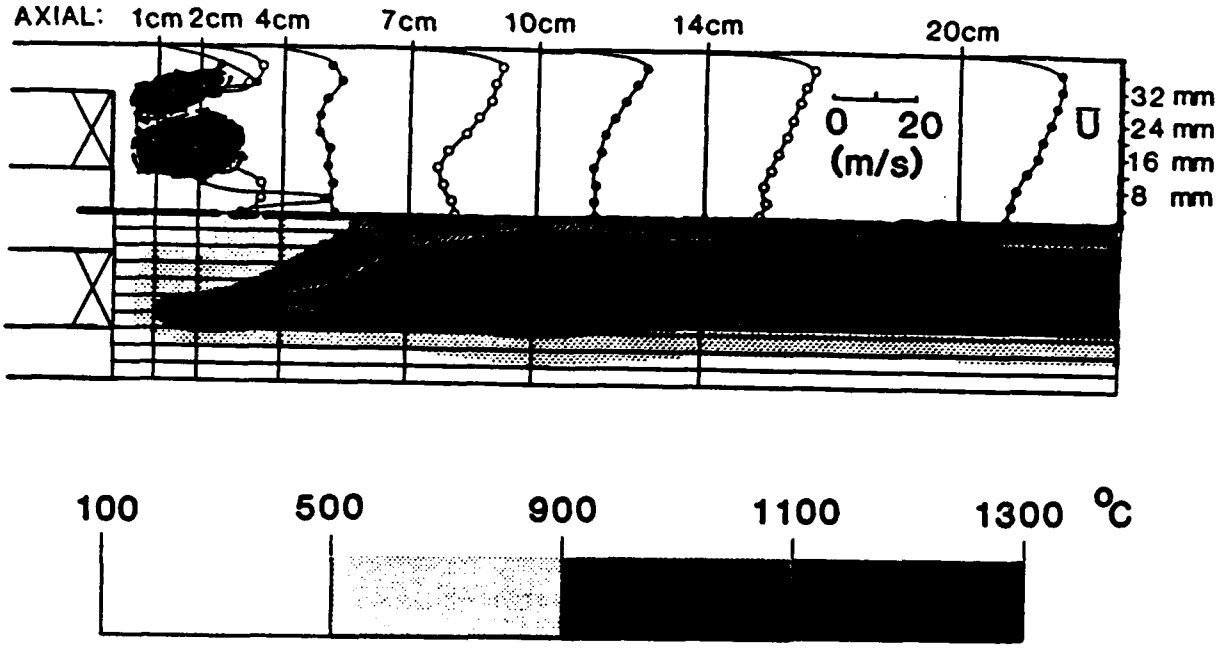

Figure 30. Task 4: Swirl-Stabilized Combustor Velocity and Thermal Fields.

The diffraction-based measurements of SMD represent a value deduced from a "snapshot" of the spray at an instant in time. Such a measurement can be biased. For example, if small droplets are moving slower than the large droplets, the SMD will encompass proportionately more small droplets and yield a size distribution biased to the small droplets. This value of SMD is termed a "spatial-SMD." In contrast, the PD makes a continuous point measurement of single droplet realizations. A value of SMD derived in this fashion is termed a "temporal-SMD." However, because the PD acquires data in size-velocity pairs, a spatial-SMD can be calculated to compares the line-of-sight diffraction-based (spatial) measurements to the point interferometric (temporal) measurements. To this end, a data reduction protocol has been developed for the PD data to (1) generate spatial-SMD in addition to temporal-SMD, and to (2) integrate the PD point measurements across the spray to produce a comparable line-of-sight "composite SMD" (Reference 31).

(2) Swirl-Stabilized Combustor. The optical configuration used for PD measurements in the swirl-stabilized combustor provides droplet sizing windows with ranges varying from 1.3-to-45.5 μm to 5.17-to-181 μm. The fringe spacing is 7.9 μm. Measurements are acquired in the absence of LA seeding to allow for the unambiguous discrimination of droplet velocity and size.

With increasing experience and the results from comparative tests in spray chambers, the verification of the PD technique (including the delineation of the limits of applicability) in isothermal sprays is progressing with satisfactory results (Reference 4). Properly applied, PD data acquired in an isothermal spray chamber can be quantitatively used for modeling and other forms of analyses with increasing confidence. The application of PD to reacting flows, in contrast, is new and data acquired under such conditions must be interpreted with caution. The specific questions divide into two categories. First, with respect to the technique itself:

- What are the characteristics of the processor data rate transfer; what is the effect of this transfer function on SMD and velocity?
- What are the response limitations of the technique, if any, to the imposition of frequency shift?

With respect to the reacting environment:

- What is the effect of variations in gas-phase index of refraction induced by thermal gradients?
- What is the effect of variation in droplet index of refraction imposed by selective evaporation of a practical fuel?
- What further limits on sensitivity are imposed by increased noise due to flame luminosity?

These and other questions remain subjects of active inquiry. The present measurements of droplet size and droplet velocity measured in the combustor are based on the protocol developed in exploratory tests. As such, the accuracy is not yet established, but experience to date suggests the uncertainty associated with the droplet size and droplet velocity data presented here are conservatively within ±30 percent.

4. Results

Photographs of the spray in the two environments are presented in Figure 31. The cone angles in both cases are visually identical, approximately 45-degree full angle. Otherwise, the spray in both cases is visually different. First, the axial extent of the spray is greater in the isothermal spray chamber. Second, the number density is higher in the isothermal case. Third, a hollow-cone shape is discernible in the combustion case. Hence, from the photographic documentation alone, the performance of the spray in the two environments is clearly different. To quantify these differences, laser diffraction and laser interferometry were applied to characterize the spray.

The first results presented are the comparison of diffraction based and interferometric based ensemble SMD. These results are followed by the results for the phase Doppler measurements of droplet data rate, droplet size, and droplet velocity in both the isothermal chamber and the swirl-stabilized combustor. At the conclusion of the section, the interferometric results are discussed relative to the performance of the spray in the swirl-stabilized combustor.

a. Comparative Measurements

The ensemble SMD data determined by laser diffraction are compared in Figure 32, to the composite SMD data produced by the phase Doppler. The data at 25.0 cm shows that, at a Malvern measured obscuration of

Figure 31. Task 4: Spray Photography.

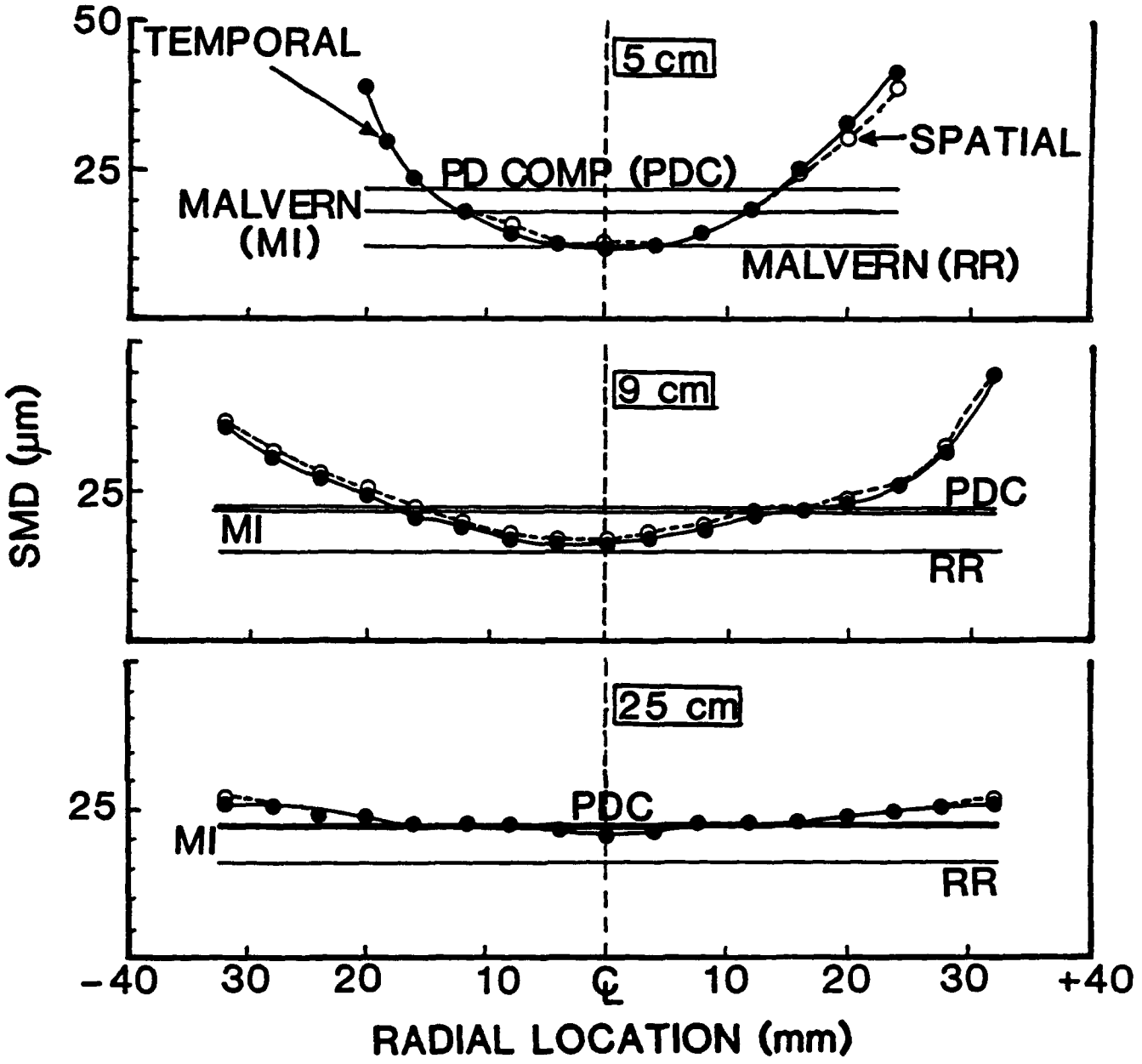

Figure 32. Task 4: SMD Measurements by Laser Diffraction and Laser Interferometry.

41 percent, the phase Doppler composite (PDC) spatial-SMD and MI spatial-SMD both yield a value of 22 μm. At 9.0 cm and an obscuration of 52 percent, a similar correspondence results. At 5.0 cm and an obscuration of 58 percent, both Malvern models fall short of the PD composite. This is consistent with findings that, for obscurations greater than 50 percent, multidroplet scattering becomes significant with the net effect of biasing the diffraction measured SMD to lower values (Reference 30). For this spray, the 15-parameter MI model compares consistently better to the PD composite than the two-parameter RR model (Reference 4). The difference between the spatial- and temporal-SMD at each radial point in the spray is also shown in Figure 32. The difference is small in the present case because, by 5 cm from the atomizer, all droplet sizes present in the spray have assumed the dilute phase flow velocity.

Two important findings result from these comparative measurements. First, in regions of this practical spray field where neither instrument is limited, the correspondence is excellent. Second, in regions of this spray that are of primary interest to the present work (i.e., close to the nozzle), the phase Doppler technique provides the ability to make quantitative measurements whereas the diffraction technique becomes limited by obscuration.

b. Laser Interferometric Results

A characterization of the spray using phase Doppler interferometry is presented in Figures 33-36 for both the isothermal chamber and swirl-stabilized combustor. Measurements made in 1 cm increments are presented from 2 cm (the first axial location at which ligaments did not affect the PD measurements) to 5 cm (the last axial location at which the droplet data rate in the combustor exceeds 25 Hz, a value arbitrarily selected to represent the boundary of the spray). At each axial location, data were acquired radially at 4 mm increments. Results for both droplet SMD and mean azimuthal velocity are reported at locations where the data rate exceeds 25 Hz.

(1) Data Rate. The radial profiles of data rate are presented in Figure 33a. Dashed lines are used in the regions where the data rate exceeds 4000 Hz as the PD processor rolls off data rates above this value. Hence, in the isothermal case, the peak data rate is higher than that reported and the precise shape of the data rate profile cannot be established

(a) Radial Profiles for Isothermal (Cold) and Combustor (Hot)

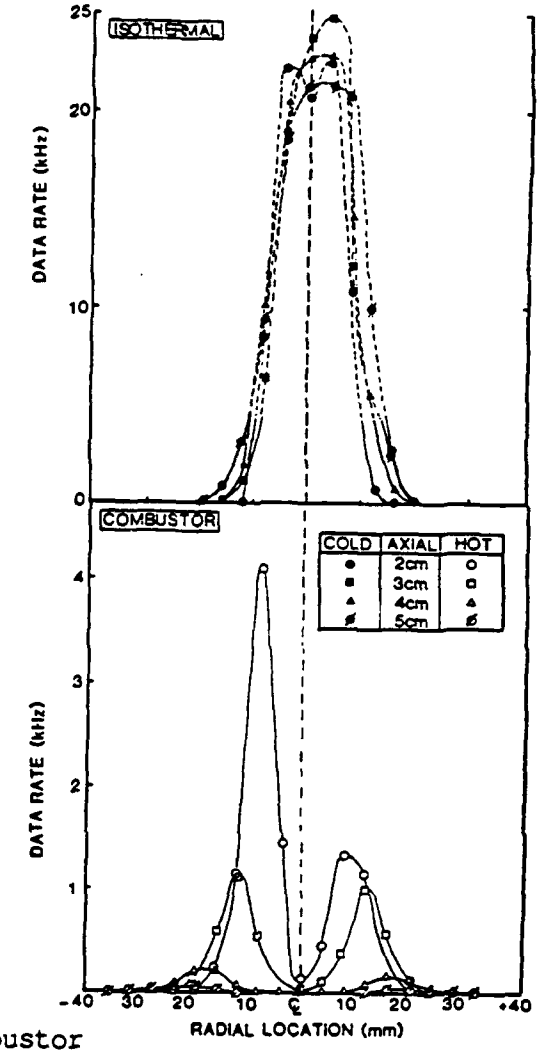

(b) Isopleths for Combustor

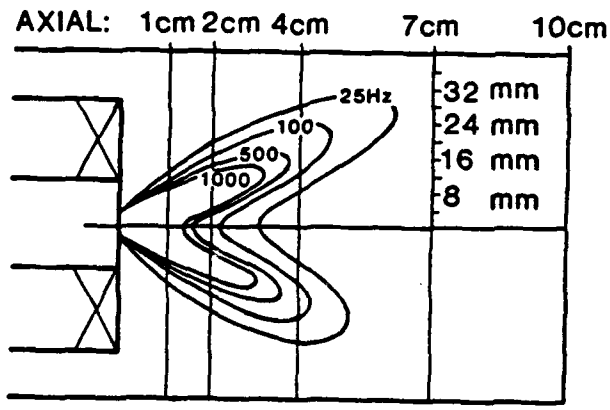

Figure 33. Task 4: Laser Interferometric Results - Data Rate

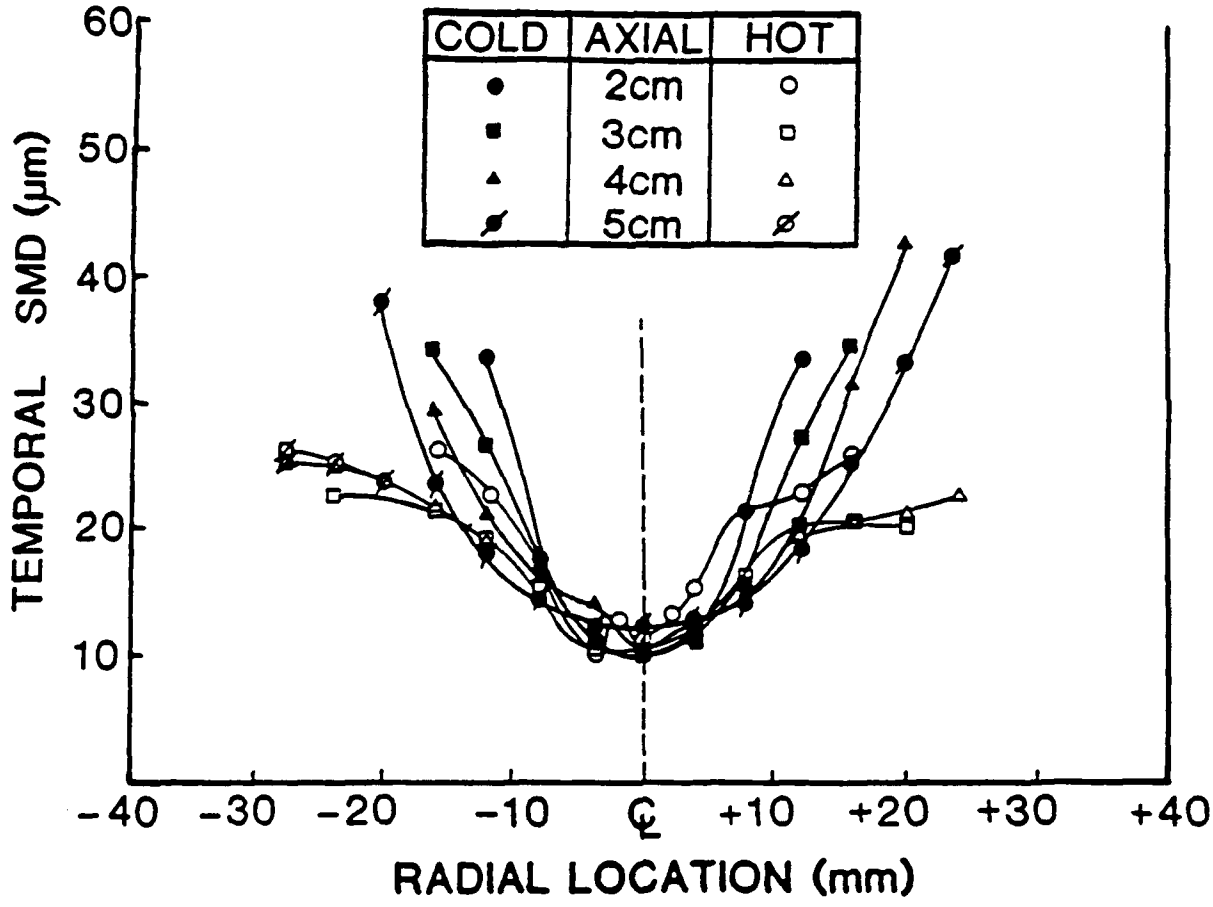

Figure 34. Task 4: Laser Interferometric Results - Temporal-SMD for Isothermal (Cold) and Combustor (Hot).

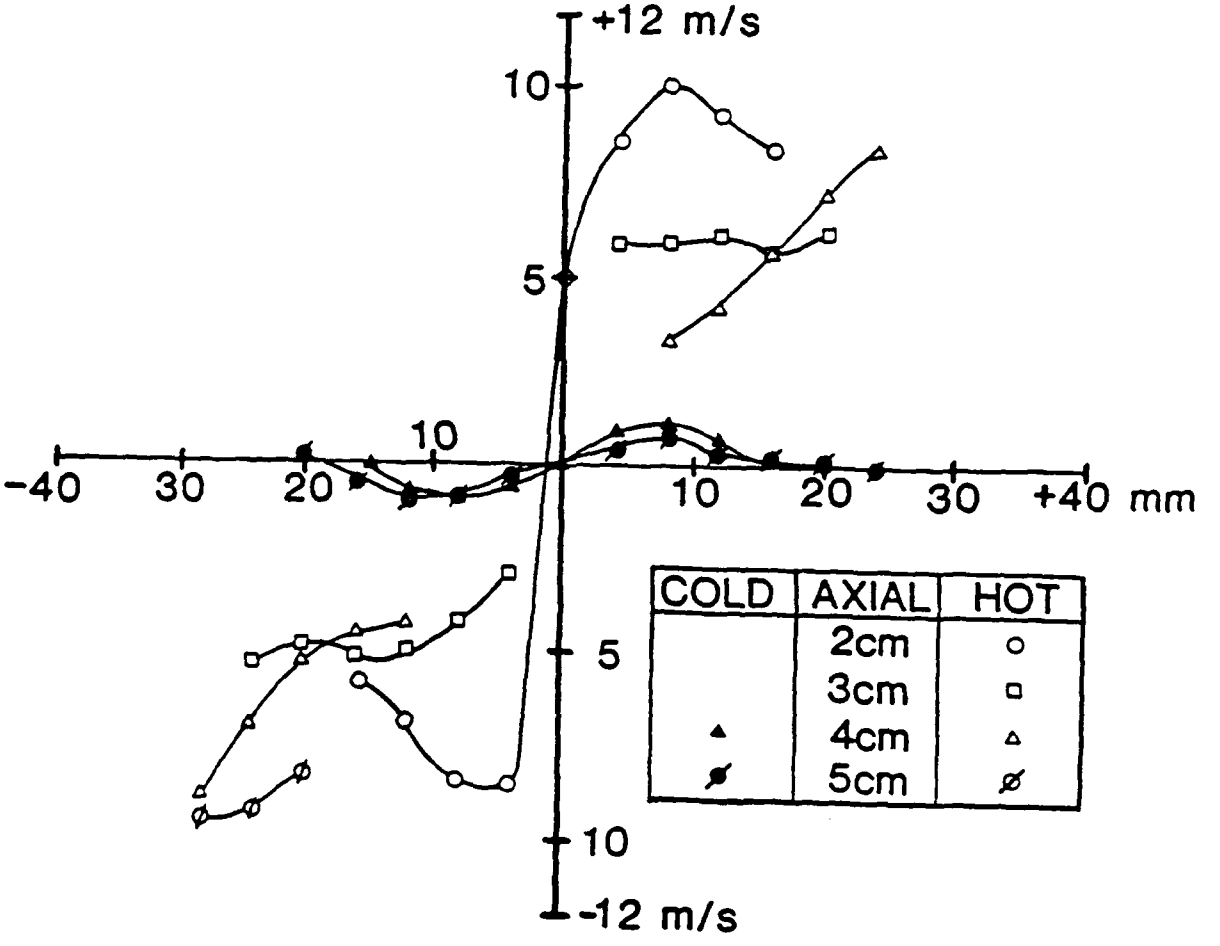

Figure 35. Task 4: Laser Interferometric Results - Azimuthal Velocity.

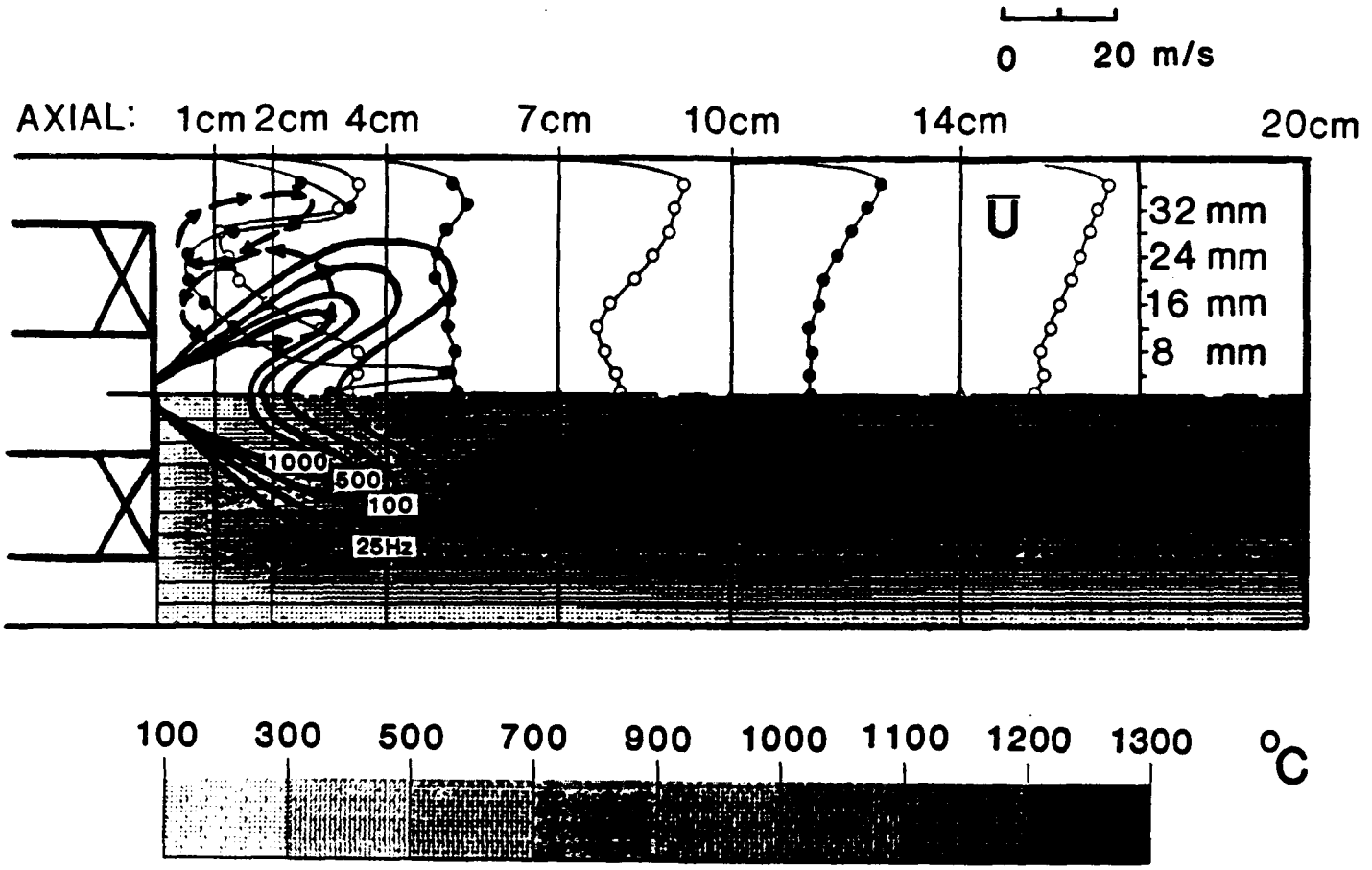

Figure 36. Task 4: Relationship of Spray Field to Combustor Environment.

above 4000 Hz. Clearly, however, the isothermal data rate is at least an order of magnitude higher in most regions of the spray compared to the combustor case. These data also suggest that, in the isothermal chamber, the initial hollow cone nature of this spray collapses within two centimeters of the nozzle to a solid cone spray.

The data rate profiles in the combustor indicate that droplets are not present in the core of the spray at 4 and 5 cm. Hence, the hollow cone nature of the spray is preserved in this environment. Visual observations of beam scattering through the spray confirm this structure. The data rate profiles in the combustor also indicate an increased angle of injection (~ 60 degrees compared to ~ 45 degrees in the isothermal chamber). This difference is again confirmed by visual observations of beam scattering through the spray. This result is in apparent contradiction to the injection angles derived from the photographs (Figure 31) where the angle appears to be the same in both environments. The explanation for these contrasting results rests with the number density associated with those droplets that extend beyond the 45 degrees cone angle in the combustor environment. The number density is clearly too low to be photographically recorded in this region.

The 2 cm profile in the combustor reveals a mass flow asymmetry. The asymmetry, attributed to the discrete fuel jets within the air-assist circuit (Reference 31) is further illustrated by the data rate isopleths presented in Figure 33b.

(2) Temporal-SMD. Measurements of temporal-SMD are presented in Figure 34. In general, the data show the extent to which the spray SMD is symmetric about the centerline in both environments. In both cases, the temporal-SMD increases radially outward. In the isothermal case the increase is greater approaching 4-to-1. The extent of the radial spread is significantly greater in the case of the combustor, as noted above.

(3) Azimuthal Velocity. Azimuthal mean velocity data ($\bar{w}$, Figure 35) are selected for presentation in order to characterize: (1) the effect of the two nozzle swirlers, and (2) the added influence of the aerodynamic swirler in the combustor. (Note that, for the optical configuration required for the measurement of azimuthal velocity, PD measurements were not possible at axial positions of 2 and 3 cm in the isothermal chamber due to high number density. In the combustor, the number density was not a limiting factor at these axial positions.) The azimuthal

velocities for the isothermal case (1) do not exceed 1.25 m/s, and (2) are reasonably symmetric about the centerline. The profiles for the combustor case also reflect a general symmetry of droplet azimuthal velocities about the geometric centerline of the combustor. However, the azimuthal velocities are higher in the combustor by almost an order of magnitude due to the strong swirl field imposed by the combustor swirler. (LDA measurements of the dilute phase indicate azimuthal velocities of 5 to 10 m/s in the region of the spray field.)

(4) Relationship of Spray Field to Combustor Environment. The data acquired in the combustor are significantly different from those acquired in the isothermal chamber. The explanations for these differences can be deduced by the superposition of the droplet data rate isopleths (Figure 33b) on the thermal and aerodynamic fields of the combustor (Figure 30b). The result is presented in Figure 36. (Note that the data rate isopleths from the lower half plane of Figure 33b have been mirror-imaged in Figure 36 and represent, as a result, an apparent symmetry that does not in fact exist.) the size and location of the recirculation zones, inferred from the axial velocity measurements, are shown as regions bounded by arrows.

The outer portion of the spray field is seen to traverse the interior recirculation zone. The data rate drops rapidly as the spray is directed outward and droplets traverse the steep thermal gradient toward higher temperatures. The relatively wider spray (Figure 33a) and lower SMD (Figure 34) of the spray in the combustor is attributed to the outward radial momentum imparted to the spray by the interior recirculation zone and elevated azimuthal velocities. The small droplets are preferentially accelerated outward and, hence, the SMD is lower. This preferential acceleration is confirmed by the size-velocity correlations deduced from the PD measurements in the combustor. The rapid evaporation in the reacting environment further enhances the reduction in SMD.

Figure 36 also suggests the sequential path by which the combustor is stabilized. First, small droplets, along with fuel vapor, are entrained from the spray field into the inner recirculation zone and reacted with air captured by the outer recirculation zone. This reaction region corresponds in locale to the high temperature region indicated by the thermal field. Second, combustion intermediates and products are transported back into the spray field by the interior recirculation zone, leading to the

rapid evaporation (and hence, lower data rate) observed in the combustor environment. Finally, this evaporation produces the fresh fuel vapor and small droplets which are then available for entrainment in the manner first stated. As a result, the interaction of the aerodynamically induced recirculation zones and the small droplets and fuel vapor in the boundary of the spray are pivotal to the stabilization of the combustor.

5. Conclusions

The present study compares the characterization of a spray in an isothermal chamber and a swirl-stabilized combustor. The following conclusions have resulted from this study:

a. Spray performance under reacting conditions in a swirl-stabilized combustor is substantially different than the performance in an isothermal spray chamber. Except for the initial SMD, no correlation is evident between the two environments.

b. The interaction between the spray and combustor aerodynamics substantially affects the spray performance. Hence, spray performance in a reacting flow is a function of combustor design and operating conditions as well as nozzle design and operating conditions.

c. In the present study, the spray structure is transformed from solid cone in an isothermal chamber to hollow cone in a swirl-stabilized combustor. The radial spread and variation in SMD is markedly influenced by the presence of heat release and aerodynamically induced recirculation. The photographically deduced cone angle in the combustor is not indicative of the radial spread of the spray. The droplets and fuel vapor in the widened boundary of the spray are, in the case of the present experiment, important to combustor stability and overall performance.

d. In-situ measurements of droplet size and droplet velocity in a practical combustion environment are required to characterize the performance of an atomizer. Phase Doppler interferometry, along with photographic analyses, show promise for providing the required data. Outstanding questions remain, however, and the

technique awaits additional verification under reacting flow conditions.

E. TASK 5: WALL JET DILUTION

1. Introduction

Practical gas turbine combustors are characterized by a complex (i.e., turbulent and recirculating) flowfield with a distributed reaction stabilized by the interaction of swirling air and discrete wall jets. In the case of aircraft combustors, fuel is introduced as a spray-atomized liquid. Although research is conducted in full-scale hardware, relatively simple bench scale laboratory analogues are regularly used (e.g., References 23, 32, and 33) as an aid to understanding the complex nature of these reacting flows. Simplified laboratory combustors are valuable due to their amenability to modeling and optical access for laser diagnostics but sacrifice, as a result, the full complement of geometrical and operational features dominant in practical combustors. In contrast, full-scale combustors preclude the use of in-situ optical diagnostics and have poorly defined boundary conditions. In addition, operation is expensive due to their large scale.

To address these issues, a model combustor was developed to provide a bridge between practical combustors and simplified laboratory burners (Figure 37). The combustor incorporates discrete wall jets, as well as swirl and liquid spray atomization, and has been designed to operate at both atmospheric and elevated pressures. The goal is to establish a laboratory combustor geometry, representative of practical combustors, yet amenable to optical access and modeling. In addition to describing the design, the evolution and evaluation of the protype are described and a detailed characterization of the combustor flowfield structure is presented, using an array of diagnostics for two different practical fuels. These fuels are a petroleum-derived JP-4 and a high-aromatic JP-5. The diagnostics include laser anemometry for axial and azimuthal velocity, laser intensity ratioing based upon Mie scattering for soot particle size and number density, and a thermocouple probe for temperature.

(a) Side View

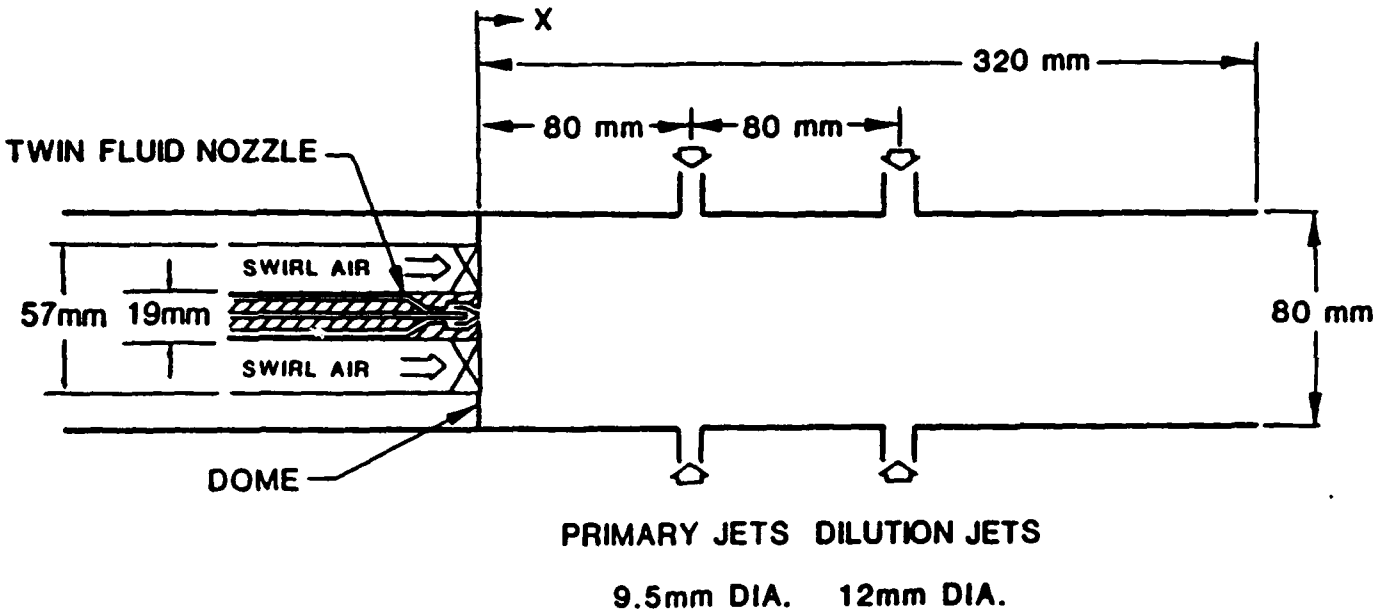

(b) End View

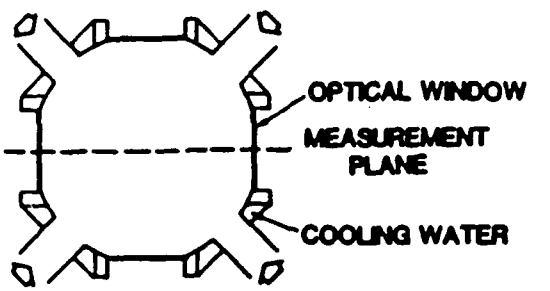

Figure 37. Task 5: Wall Jet Can Combustor (WJCC).

2. Combustor Design

a. Background

The design of the present combustor evolved from a more simplified, axisymmetric can combustor configuration. A full description of the design process may be found in Reference 35; a brief description of the design evolution and final results is presented here.

The axisymmetric can combustor (Figure 1) operates at atmospheric pressure and bulk velocities up to 15 m/s. The module has been used for a number of turbulent transport (e.g., References 7 and 23) and fuel effects studies (e.g., References 7, 16, and 29). Rather than using discrete wall jets, the dilution air is introduced through an annular shroud to provide closure to the swirl generated recirculation zone, retain clean and well described boundary conditions, produce an axisymmetric flow, and maintain the optical access windows cool and clean.

The aim of the "wall jet" can combustor design is to extend the axisymmetric configuration to more accurately represent the aerodynamics of a practical combustor, to wit the introduction of discrete wall jets to properly represent the primary and secondary regions of a gas turbine combustor.

b. Design Approach

The approach adopted for the design of the wall-jet can combustor (WJCC) consisted of four steps. First, for the purposes of continuity, the swirl vane design and duct diameter of the axisymmetric can combustor were retained. Secondly, a detailed design assessment was undertaken to establish a range of candidate values for the following geometric and operating variables:

- The number and location of jet rows;
- The number of wall jets per row;
- The jet and bulk flow velocities;
- The flow splits: primary jet-swirl and dilution jet-swirl ratios;
- The dome design;
- The primary and dilution jet diameters; and
- The nozzle spray angle.

Third, isothermal testing and reacting flow testing were conducted with a prototype Kimax® glass model to finalize the design. Fourth, based on the

prototype tests, a final design was adopted and the model combustor was fabricated out of stainless steel for a detailed characterization.

c. Detailed Design Assessment

(1) Number and Location of Jet Rows. The detailed design assessment was based upon two sources of information: (1) combustor design texts such as Reference 34, and (2) the input of various government and industry combustor designers. Although older combustors generally use three rows of jets, creating a primary, secondary, and dilution zone, the higher exit temperatures of present day combustors are forcing modern designs to two rows of wall jets (Reference 12). This has a secondary benefit of simplifying the flowfield from a laboratory standpoint. However, row locations are less well defined and, although separating the holes by one flame tube diameter is a general rule of thumb, testing is necessary to determine the exact location. Candidate locations are listed in Table 7.

TABLE 7. TASK 5: PARAMETER VARIATION, WJCC PROTOTYPE TESTS

Parameter	Variation
Jet Row Location	x/R = 2.0, 4.0; x/R = 1.0, 3.0
Primary Jet Diameter (mm)	7.0; 9.5
Dilution Jet Diameter (mm)	9.5; 12
Primary-to-Swirl Flow	2.5 - 1.75
Dilution-to-Swirl Flow	3.2 - 2.75
Primary Jet Velocity (m/s)	92 - 33
Dilution Jet Velocity (m/s)	72 - 50
Dome Angle (degrees)	step; 30; 45
Nozzle Spray Angle (degrees)	45; 60
Overall Stoichiometry (ϕ)	0.3; 0.4
Bulk Velocity (m/s)	7.5; 10

(2) Number of Wall Jets Per Row. While can combustors use six to eight jets per row (Reference 34) four jets were selected for the WJCC

to maintain optical access. Prototype testing was necessary to assess the acceptability of four jets.

(3) Jet and Bulk Flow Velocities. Jet velocities in practical combustors are on the order of 100 m/s, and this predicated the choice of jet sizes for prototype testing detailed in Table 7. Bulk velocities tested were nominally 10 m/s, but tests were also conducted at 7.5 m/s to provide a direct comparison with the nominal baseline condition used in the axisymmetric can combustor.

(4) Flow Splits. From literature sources and expert input (Reference 35), the primary zone stoichiometry of the model combustor was based on the sum of the swirler air and 40 percent of the primary jets, the latter of which was accepted to be the amount recirculating. The flow splits were established to provide a roughly stoichiometric primary zone with overall equivalence ratios ranging from 0.3 to 0.4 (Table 7). Fifteen percent (15%) of the total air flow was partitioned to the swirler.

The combustor dome was tested in both a step configuration, and two conical configurations angled at 30 and 45 degrees. Step domes are closer to current practical combustor design and allow easier modeling, but conical domes reflect configurations used historically.

(5) The Nozzle Spray Angle. Two spray angles were considered that encompass values employed in practical systems: 45 degrees and 60 degrees. The narrower angle provides stable operation in the axisymmetric can combustor while a larger angle was anticipated as necessary in the wall jet due to the wider recirculation associated with the step expansion. For both nozzles, an atomizing air-fuel ratio of 3.0 by mass was utilized which, as demonstrated in earlier tests, produced the optimum atomization quality (Figure 19).

d. Prototype Tests

Testing was conducted with short runs in a Kimax® glass prototype WJCC (Figure 38). This combustor allowed varying the parameters over the ranges listed in Table 7 while providing full optical access for observations and photography. The parameters held constant are presented in Table 8. The prototype testing was conducted with a petroleum derived JP-4.

The nozzle angle was first evaluated. The narrow nozzle was unsuitable. In particular, a stable flame could not be sustained. The wide nozzle, in contrast, produced a stable reaction for the full range of

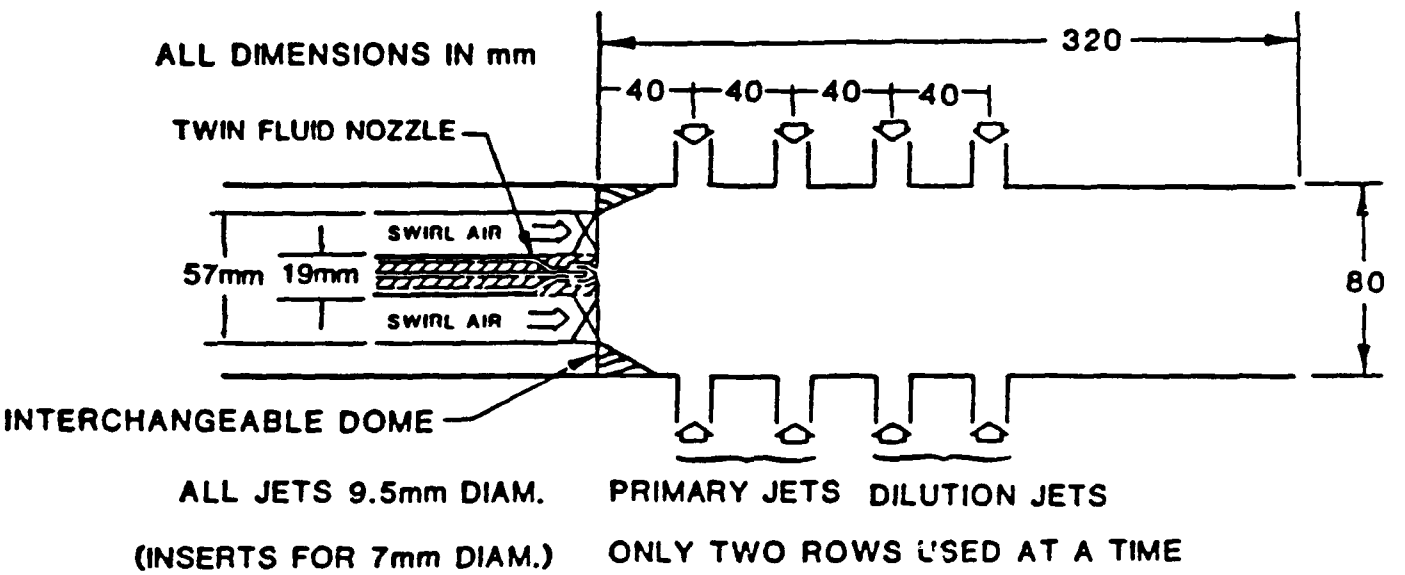

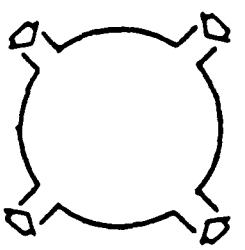

Figure 38. Task 5: Prototype WJCC Design.

parameter variation. Still photography revealed that the flame was symmetric. Gas sampling was next conducted to determine which set of parameters was the most efficient. The dome geometry and jet diameters made little difference in combustion efficiency, but the jets located at x/R = 2.0 and 4.0 were significantly more efficient (98 percent) than those located at x/R = 1.0 and 3.0 (83 percent). In addition, a primary jet-swirl flow ratio of 2.5 was more efficient (98 percent) than a flow ratio of 1.75 (96.5 percent).

TABLE 8. TASK 5: PARAMETER CONSTANTS, WJCC PROTOTYPE TESTS

1. Two rows of jets
2. 4 jets per row
3. 60 degree swirl vanes
4. ϕ = 1.0 in primary zone
5. Nozzle atomizing air-fuel ratio = 3.0
6. Parker Hannifin air assist nozzle
7. Air inlet temperature = 21 °C

As a result of the prototype evaluation, the set of parameters first identified for the combustor characterization was:

- Number and location of jet rows: two at x/R = 2.0 and 4.0.
- Number of wall jets per row: four.
- Primary and dilution jet diameters: 9.5 and 12.0 mm, respectively.
- Primary jet-swirl and dilution jet-swirl ratios: 2.5 and 3.2, respectively.

This design information was used to fabricate a stainless steel module.

F. TASK 6: SIMULATION OPTIMIZATION

1. Introduction

Under this task, the combination of atomizer operating condition, and air flow splits in the WJCC was established that provides the best possible simulation of actual aircraft gas turbine performance. Using this

configuration, the sooting performance was determined and critically compared to the two-dimensional can configuration. Such an assessment was critical to establishing the extent to which the ASCC --- a configuration desirable for laboratory studies of modeling, diagnostic development, and fuel effects --- simulates the combustor performance of practical devices. In addition to sooting behavior, hi-speed photography served as a principal diagnostic tool in assessing and documenting the documents of the WJCC.

2. Approach

The stainless steel module was characterized for a swirl air flow of 0.0057 m^3/s, a primary jet air flow of 0.0142 m^3/s through four 9.5 mm diameter jets, and dilution air flow of 0.018 m^3/s through four 12.0 mm diameter jets. This corresponds to a nominally stoichiometric primary zone, assuming 40 percent of the primary jet air recirculates and an overall equivalence ratio of 0.3. Bulk reference velocity was 7.5 m/s with an inlet temperature of 21°C. Water cooling was a total of 2.5 liters/min with a temperature rise of 30°C from an inlet value of 21°C. The wide angle twin-fluid air-assist Parker Hannifin nozzle was operated at a nozzle air-fuel ratio of 3.0 and a liquid mass flow rate of 3.27 kg/hr. Operation in these tests was at one atmosphere. In the interest of improved optical access, simplicity, and consistency with modern combustor design, the characterization was conducted for the step dome configuration. The characterization consisted of a detailed flowfield mapping of velocity, temperature, and soot particulate for a petroleum-derived JP-4 (Table 9). Data were obtained at seven axial locations and, at each axial location, at the centerline and ten equally spaced radial points or nineteen equally spaced points across the diameter for symmetry checks.

3. Results

a. Nonreacting Flow

Flow velocity measurements for axial velocity were made in the combustor for the air flow rates of the baseline run condition. The nozzle was not employed; the primary purpose of the test was to ascertain the symmetry and general character of the aerodynamic field in the absence of reaction. Figure 39 shows the full-diameter, axial mean and rms velocity fields for a measurement plane bisecting the orthogonal jets.

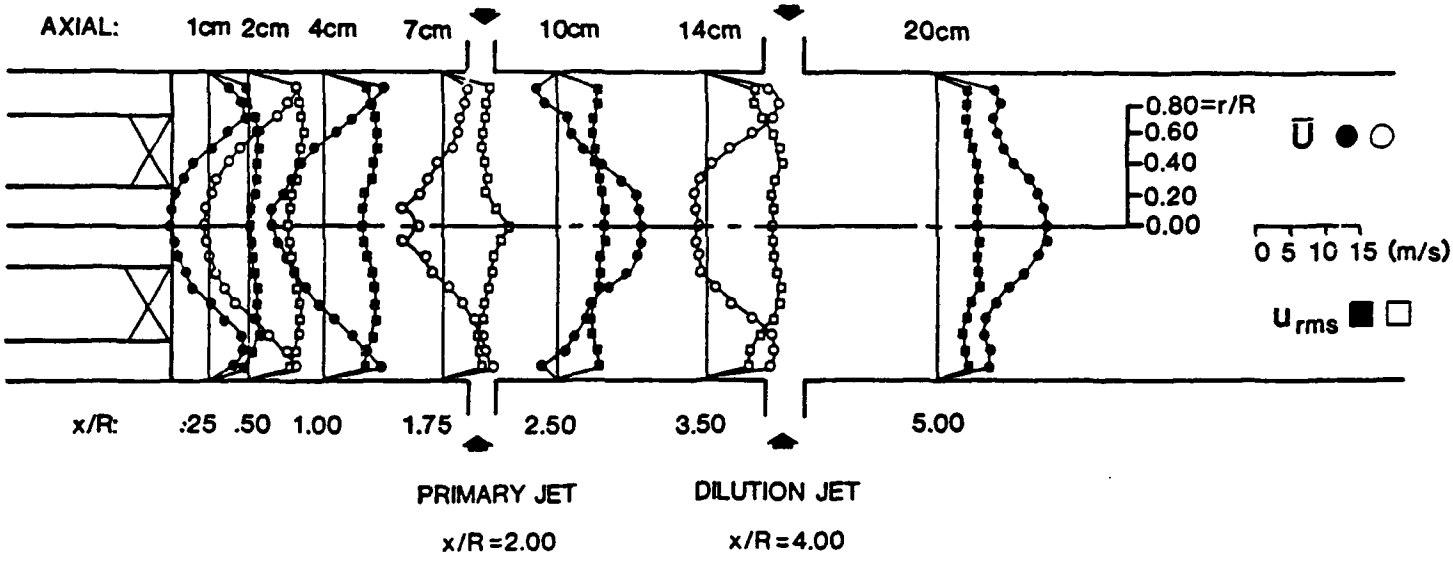

Figure 39. Task 6: Baseline Axial and Azimuthal Velocity Field (Nonreacting).

TABLE 9. TASK 5: FUEL PROPERTIES

Property	JP-4
Specific Gravity	0.7557 (20°C)
Flash Point (°C)	-23
Heat of Combustion (MJ/kg)	43.64
Smoke Point (mm)	25
Hydrogen (Weight Percent)	14.48
Viscosity (Centistokes)	0.9546 (20°C)
Initial Boiling Point (°C)	25
50% of Distillation (°C)	160
End Boiling Point (°C)	281
Total Aromatics (%)	9.7

Examining the axial velocities, excellent symmetry is displayed throughout the flow. An on-axis recirculation zone is formed between the nozzle face and the primary jets. The corner recirculation zone induced by the step dome does not extend to the first axial station surveyed, x/R = 0.25. The elevated centerline velocities immediately downstream of the two jet rows, and the reverse flow centerline velocities at x/R = 1.75 and

3.50 upstream of the jets are evidence of the penetration of the primary and dilution jets to the centerline. Rms velocities remain relatively uniform across the combustor.

b. Reacting Flow

(1) Aerodynamic Field. Figure 40 depicts the axial and azimuthal mean and rms velocity fields for JP-4 fueled combustion. First examining the axial velocity field, an on-axis recirculation zone is formed on centerline between x/R = 0.50 and 1.75. There is evidence of high mean and rms velocity droplets at the x/R = 0.25 and 0.50 regions. This is indicated in the figures by dashed lines. These high values are attributed to multiple particles in the laser anemometer probe volume for very high spray densities. A corner recirculation zone, promoted by the step expansion is noted at the x/R = 0.25, r/R = 0.60 in the dome region.

The jet blockage is evidenced by the sharply accelerated near wall flows at x/R = 1.75, 2.50 and 5.00. At x/R = 2.50 and 5.00, the jets' penetration to centerline is revealed in the accelerated centerline flow. Rms velocities are high throughout the flow, due to the intense mixing created by the discrete jets.

The azimuthal velocity field shows reasonable symmetry in the dome region for such a complex, three-dimensional flow (Figure 40). In particular, the primary zone region shows the persistence of swirl at the x/R = 0.25, 0.50, 1.00, and 1.75 stations. Downstream of the primary jets, the swirl is all but eliminated by blockage of the jets. The generally positive value and peak of the azimuthal velocity at the centerline at x/R = 1.75, 2.5, and 5.00 reflect an upward, buoyancy flow at these locations. The rms velocities are again fairly constant across the flow.

(2) Temperature Field. Figure 41 depicts the temperature field. A cold core is formed, as evidenced by the 300°C centerline temperature. There is a relatively hot (800°C) primary zone between x/R = 0.50 and 1.00, where the on-axis recirculation zone is located. The hollow cone nature of the nozzle is illustrated at x/R = 0.25 by the depression in the temperature profiles. The progression of temperature is similar to a practical gas turbine with temperatures remaining elevated in the secondary zone coincident with the burnout of carbon monoxide and soot. The dilution jets then provide the additional oxidant necessary to cool the flow.

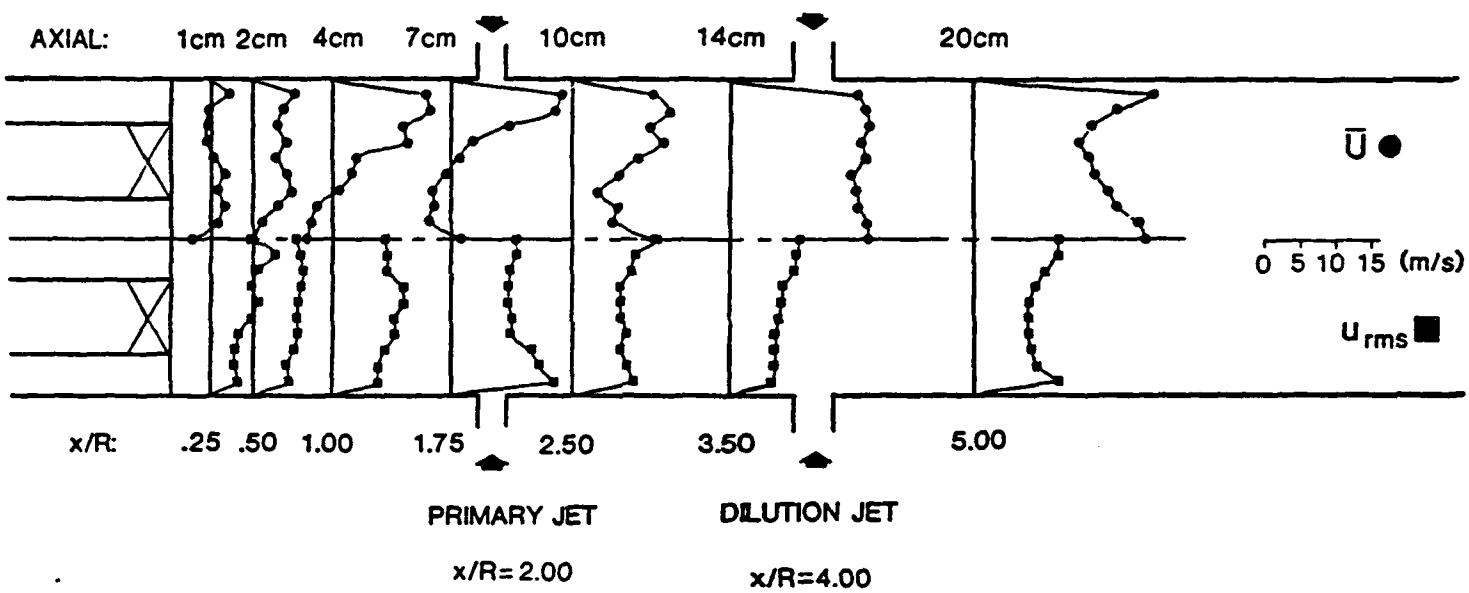

Figure 40. Task 6: Baseline Axial Velocity Field (JP-4, ϕ = 0.3).

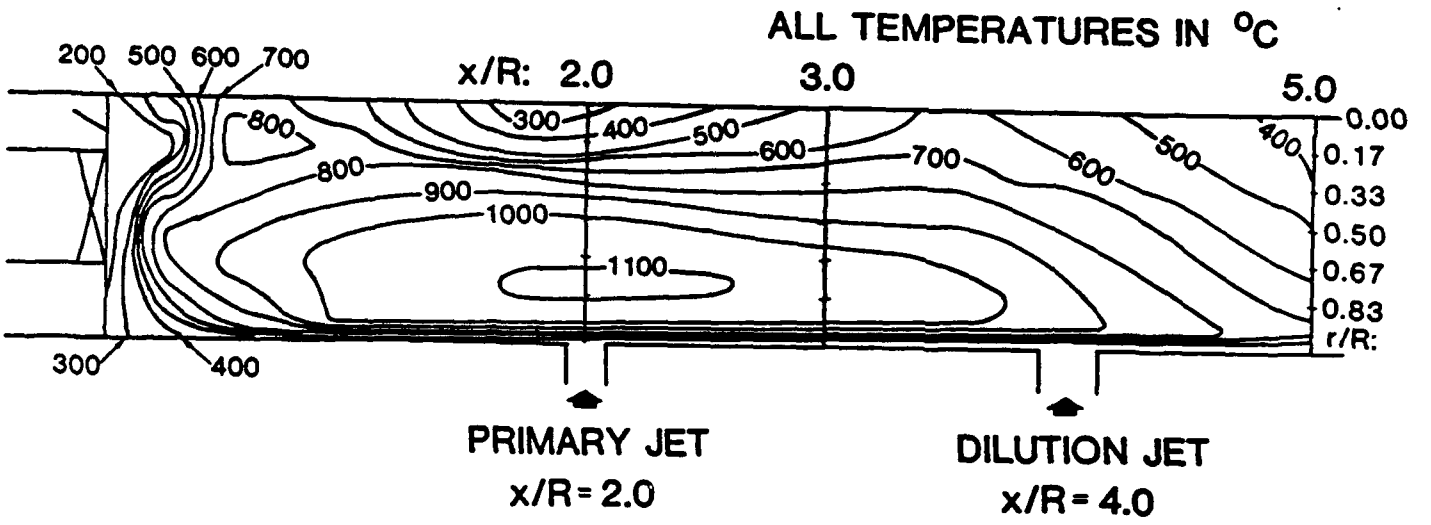

Figure 41. Task 6: Baseline Temperature Field (JP-4, ϕ = 0.3).

At an overall equivalence ratio of 0.3, a final temperature of 825°C can be predicted for JP-4 based on overall adiabatic conditions and no disassociation. The exit plane has an area averaged exit temperature of 543°C. Since temperature is uncorrected for radiation, and the combustor is not adiabatic, a measured temperature lower than the calculated would be expected. Hence, the measured temperatures appear reasonable. In addition, the temperature profile is only in the measurement plane, and it is uncertain if higher temperatures might be found elsewhere in the three dimensional field present at x/R = 5.00.

Using a similar adiabatic flame temperature calculation for the peak primary zone temperatures found in the combustor, the 1100°C peak temperatures correspond to $\phi = 0.39$. Although this value would again be expected to be low due to heat flux and radiation losses, it clearly indicates that the average equivalence ratio in the combustor is lean. Hence, even though the extent of reaction in the primary zone has not been ascertained (i.e., excessive levels of carbon monoxide could persist), the evidence points to more air than expected being entrained from the primary jets into the primary zone. The strong jet penetration to centerline could well be responsible for this.

(3) Soot Field. Figure 42 depicts the soot field. The distribution covers the agglomerate size window of 0.08 to 0.38 μm soot. Primary particles physically collected in the ASCC are ≈ 0.05 μm diameter. The distributions are peaked toward the small end of the size range. The population peaks in the outer region of the flow at x/R = 2.00. By the time x/R = 5.00 is reached the soot is almost completely burnt out. The overall number density of soot is much lower than that of Reference 35 in the axisymmetric combustor for the same fuel and stoichiometry. This indicates the effectiveness of staging the air injection via discrete wall jets in promoting the oxidation of soot.

c. Correlation to Practical Hardware

Because of a size similar to the WJCC and operation at atmospheric pressure, the data from a Lycoming combustor studied in Reference 36 form an attractive basis for comparison to the present data. It should be noted that it is operated at somewhat higher velocities (18.6 m/s) than the 7.5 m/s of the WJCC. Also there are six jets with higher velocities in three rows.

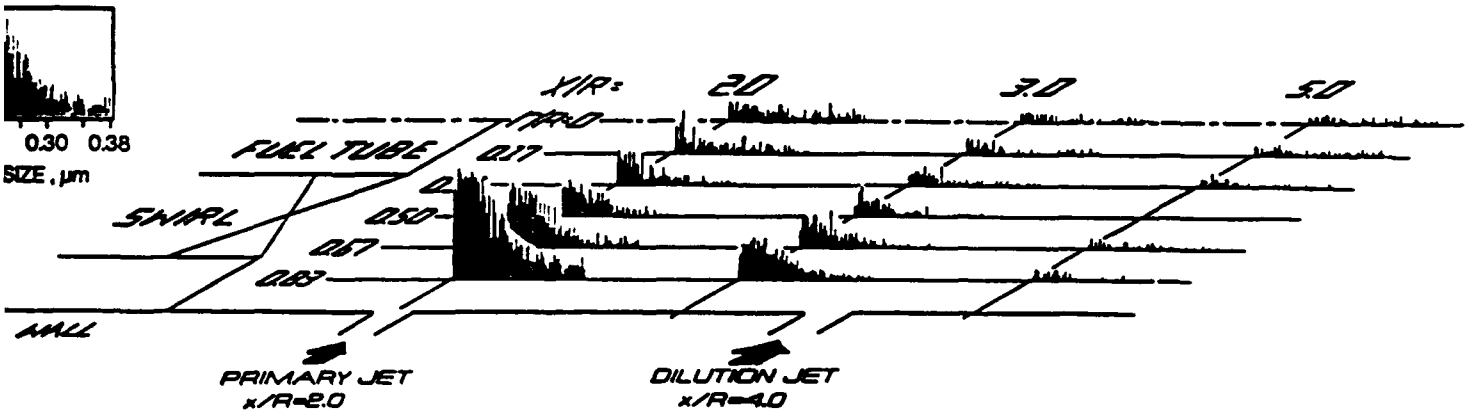

Figure 42. Task 6: Baseline Soot Field (JP-4, ϕ = 0.3).

Temperature profiles for a $\phi = 0.21$ are shown in Figure 43a. The first temperature traverse shows a primary zone with core temperatures of 700 to 900°C which corresponds well to the x/R = 0.50 to 1.00 locations in the WJCC. At the wall, the temperatures decrease significantly. A lack of symmetry is displayed in the temperature contours, revealing the three dimensional nature of the flowfield. The second traverse, in the primary jet plane, shows distinct evidence of a cold 200°C core, with high temperatures at the wall between the jets, just as in the WJCC. Again substantial asymmetry is seen. The third traverse, in the plane just prior to the dilution jets, but far downstream of the secondary jets, shows continued existence of a cold core at 450°C and higher temperatures near the walls. This is again quite similar to the WJCC, but the temperatures of 1300 - 1600°C are significantly higher, although this is prior to the dilution jets and would be expected to reach lower values further downstream. Notably, the temperature profile is nearly symmetric at this point.

Figure 43b depicts the exit temperature profile for this combustor at $\phi = 0.42$, but otherwise unchanged flow conditions (Reference 37). For this higher equivalence ratio, exit temperatures range from 475 to 950°C, which aligns fairly well to the exit temperatures seen in the WJCC for a $\phi = 0.3$. Figure 43b also shows the exit temperature profile for the two WJCC run conditions.

The Lycoming and WJCC data comparison must be qualitative. The nozzles have different design and performance characteristics, and no wall cooling is utilized in the Lycoming combustor. Additionally, three wall jets are used in the Lycoming combustor. Despite these discrepancies, the two combustors show remarkably similar trends and tendencies.

A means of comparing the performance of the WJCC to the performance of practical combustors is conducted by using empirical efficiency correlations such as those of Reference 38. These are based upon large scale practical combustors such as the F-101, T-63, and TF-41. By making appropriate assumptions for mixing times, kinetic times, length scales, and droplet evaporation times, an empirical efficiency value of 97.7 percent is obtained for the wall-jet can combustor. This

(a) Temperature Profiles

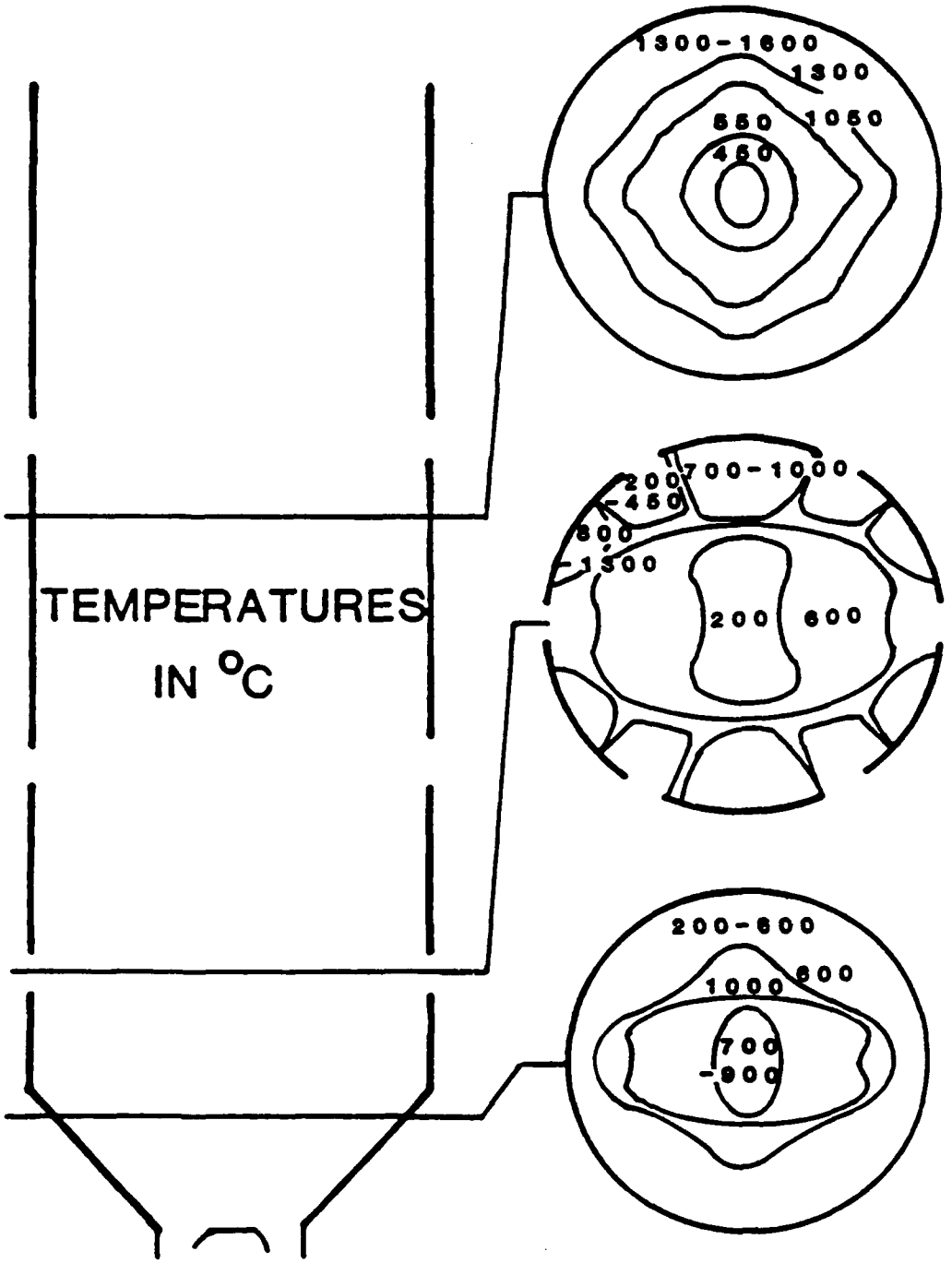

Figure 43. Task 6: Practical Combustor Temperature Fields.

(b) Exit Plane Temperature Profiles

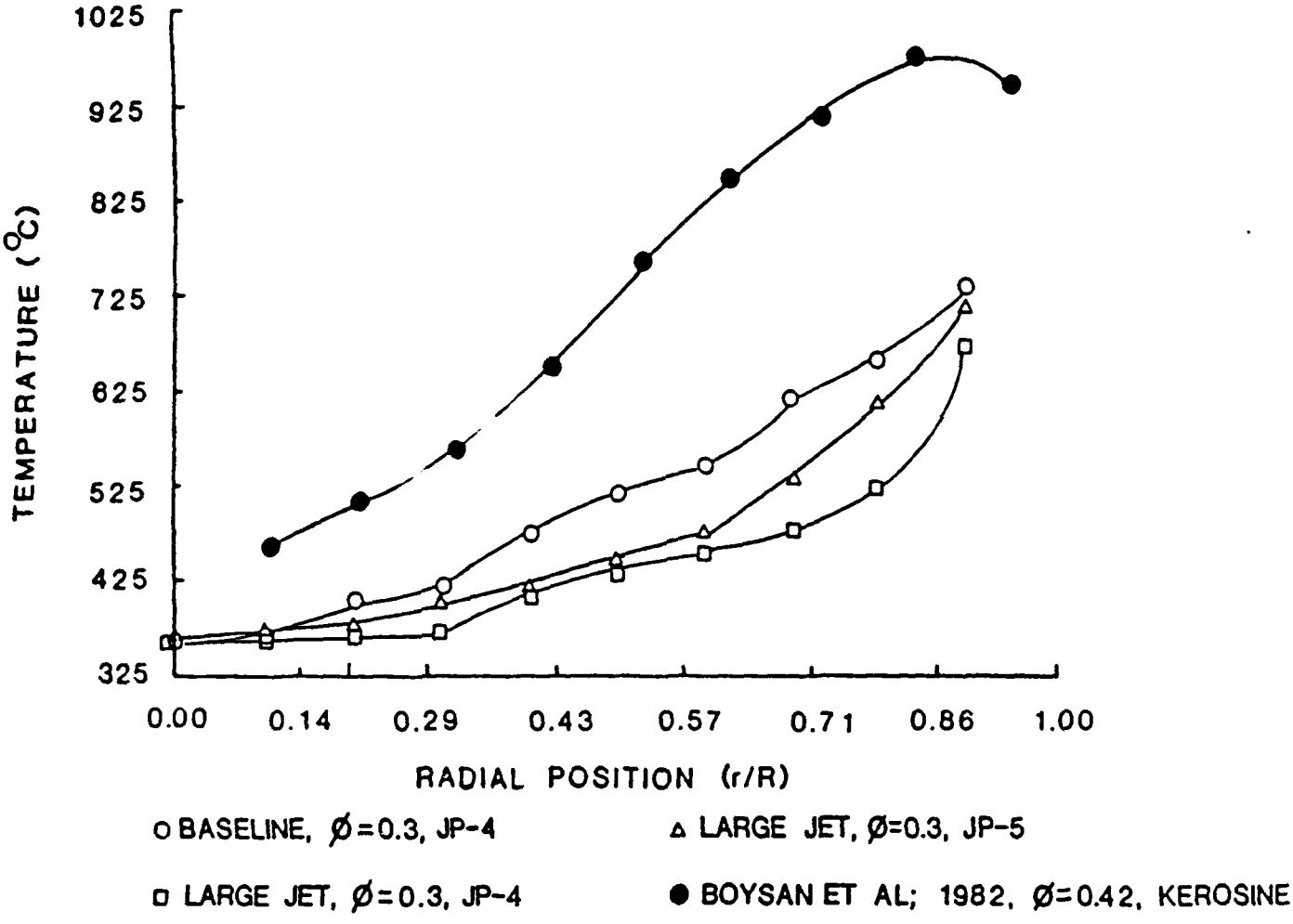

Figure 43. Task 6: Practical Combustor Temperature Fields (concluded).

agrees well with the value of efficiency deduced from a sample gas analysis of 97.6 percent for JP-4. Furthermore, actual operating conditions of practical combustors fall near the point calculated from the correlation (Figure 44). This lends credence to the WJCC serving as a model gas turbine combustor.

4. Summary and Conclusions

A model combustor has been designed to simulate gas turbine combustion performance while providing access needed for optical diagnostics. To assess combustor performance, in-flame measurements of velocity, temperature and soot have been acquired in a swirl and wall-jet-stabilized, spray-atomized model laboratory combustor. From the characterization results presented here, the following conclusions may be deduced:

a. The progression of temperature in the combustor is similar to a practical combustor; with the reaction initiated in the primary zone, continuing in the secondary zone and cooling occurring in the dilution zone where final soot burnout occurs.

b. The temperature fields reveal the presence of a relatively cold core.

c. Primary zone temperatures indicate a lean primary zone: the primary jets display substantial backmixing creating this lean condition.

d. The WJCC is a representative model of a gas turbine combustor.

e. In cold flow, excellent axial symmetry is displayed; reacting flow reveals asymmetries tied to nozzle effects and/or buoyancy.

f. The staging of air injection through the use of discrete wall jets, with the strong mixing and penetration created by these jets, is effective in promoting the oxidation of soot for the range of fuels tested.

g. The effect of fuel composition change is seen primarily in the aerodynamic and soot fields; the temperature field remains substantially unchanged.

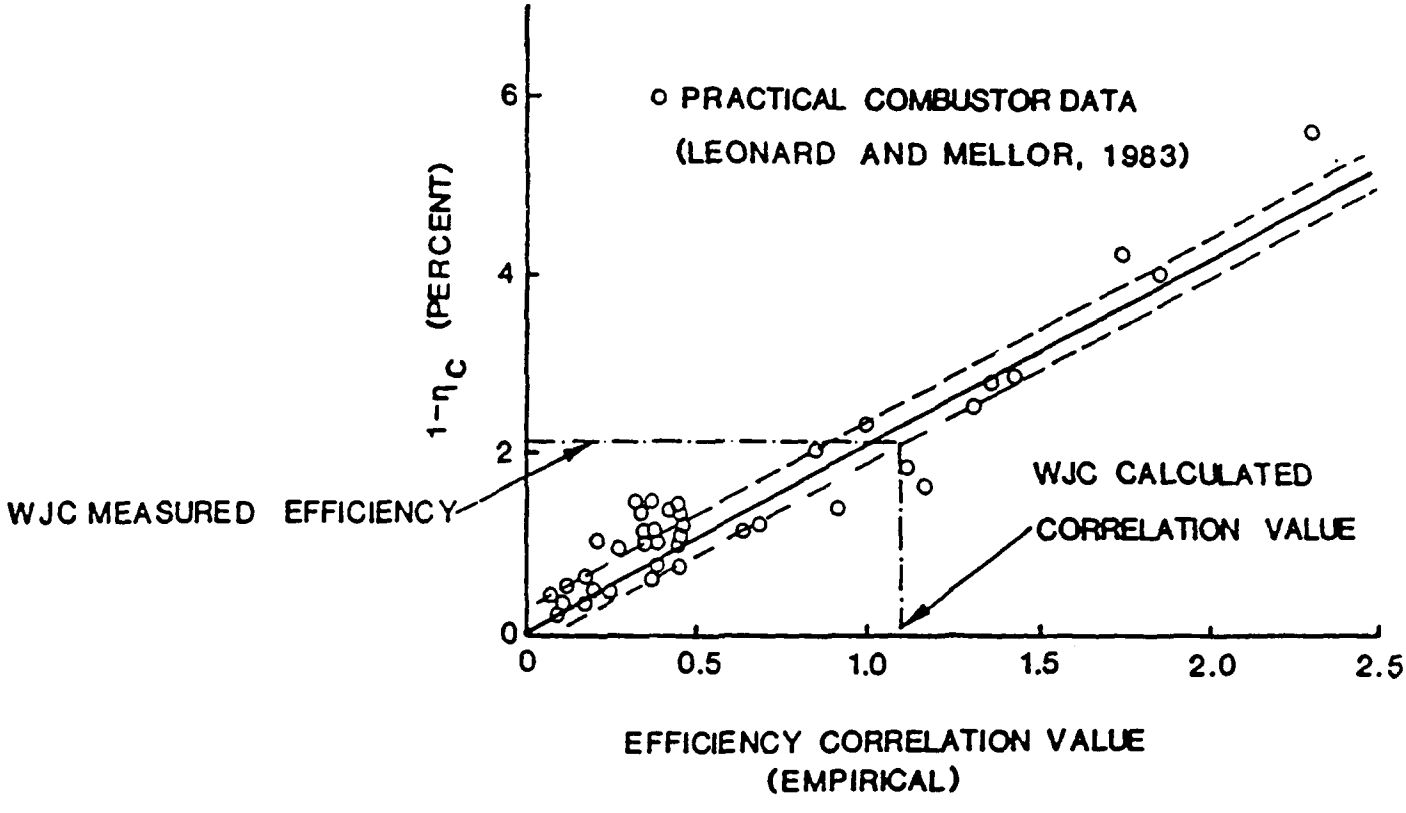

Figure 44. Task 6: Experimental Correlations.

h. The WJCC compares well with selected practical combustors from both an experimental and empirical standpoint.

SECTION V
CONCLUSIONS

The conclusions for each task are delineated in Section III. The salient conclusions for the program are summarized below:

1. The sampling conditions (e.g., sample cooling rate, charge grounding) of an extractive probe used for the extraction of soot particulate can dramatically modify soot morphology from that which exists prior to extraction. Precautions are required to insure that probe sampling conditions are set to preclude transformation of soot morphology during transport.
2. The blending of a fuel surrogate to simulate a petroleum derived JP-4 is viable. In the present study, a surrogate comprised of fifteen constituents of pure hydrocarbons accurately simulates the combustion performance of the parent JP-4, as well as the chemical and physical properties with the sole exception of smoke number. The smoke number of the surrogate is significantly higher than the parent. Correspondingly, the soot produced under combustion conditions is substantially lower for the surrogate.
3. Doping of the surrogate with small (~1.5% by weight) of select compounds suspected as effective in the formation of soot can, in fact, increase the yield of soot.
4. A Wall Jet Can Combustor (WJCC) has been designed with clean boundary conditions, optical access, and performance that reflects the basic characteristics of practical gas turbine can combustors. These attributes are attractive for the acquisition of data for the verification and development of numerical codes, and for the adaptation of optical probes for the study of the active physical and chemical processes.
5. Isothermal characterization of spray behavior, while instructive, does not reflect the performance of the atomizer in the presence of reaction and the complex aerodynamics representative of the dome region of gas turbine combustors. In-situ measurements are required, and

the phase Doppler interferometer shows promise in providing the needed measurements.

6. The behavior of sprays is likely dependent upon the specific characteristics of the combustor in which they are operated. The close coupling between the dome region aerodynamics and spray behavior suggest, as noted above, that in-situ measurements are required in the practical environment to fully establish the performance of an atomizer, and the relationship of the performance to the overall stability and emissions of the combustor.

7. The spatial distribution of soot, as well as the soot yield in a complex flow combustor, is a function of not only fuel molecular structure and fuel loading, but of flow aerodynamics and pattern of fuel injection. This conclusion points to (1) the importance of aerodynamics and nozzle performance, alone and in combination, in controlling the amount of soot produced, and (2) the requirement of spatially resolved, nonintrusive optical measurements to guide combustor design, nozzle design, and fuel property specification for future design, and fuel property specifications for future fuels and advanced propulsion systems.

8. The performance of the model gas turbine can combustors used in the present study are especially sensitive to the atomizing air conditions of the fuel nozzle. Relatively small changes in the atomizing flow rate, for example, profoundly impact the soot performance. These results suggest that (1) atomizing air can be an important variable in the optimization of combustor performance, and (2) the atomizing air can be used as a vehicle for the development of adaptive control strategies.

SECTION VI

REFERENCES

1. Brum, R.D., and Samuelsen, G.S. (1982a). Assessment of a Dilute Swirl Combustor as a Bench Scale, Complex Flow Test Bed for Modeling, Diagnostics, and Fuel Effects Studies, AIAA Paper 82-1263, Presented at the AIAA/SAE/ASME Joint Propulsion Conference, Cleveland, June.

2. Brum, R.D. and Samuelsen, G.S. (1982b). "Two-Component Laser Anemometry Measurements in a Non-Reacting and Reacting Complex Flow Model Combustor," WSS/CI Paper 82-53.

3. Jackson, T.A. and Samuelsen, G.S., "Performance Comparison of Two Interferometric Drop Sizing Techniques," In Chigier, N. and Steward, G.W. (Eds.), Proceedings of the SPIE -- The International Society for Optical Engineering, Vol., 573, Particle Sizing and Spray Analysis, 75-79, 1985.

4. Jackson, T.A. and Samuelsen, G.S., "Droplet Sizing Interferometry: A Comparison of the Visibility and Phase Doppler Techniques," **Applied Optics**, Vol. 26, June 1987, pp. 2137-2143.

5. Hack, R.L. (1983). "Extractive and Nonintrusive Optical Measurements of Soot and Probe Perturbation in a Swirl-Stabilized Combustor," Master's Thesis, University of California, Irvine.

6. Himes, R.M., Hack, R.L., and Samuelsen, G.S. (1984). Chemical and Physical Properties of Soot as a Function of Fuel Molecular Structure in a Swirl-Stabilized Combustor, **Journal of Engineering for Gas Turbines and Power**, Vol. 106, pp. 103-108.

7. LaRue, J.C., Seiler, E.T., and Samuelsen, G.S., "Momentum and Heat Flux in a Swirl-Stabilized Combustor," Twentieth Symposium (International) on Combustion, The Combustion Institute, 1985, pp. 277-285.

8. Hack, R.L., Samuelsen, G.S., Poon, C.C., and Bachalo, W.D. (1981). An Exploratory Study of Soot Sample Integrity and Probe Perturbation in a Swirl-Stabilized Combustor, **Journal of Engineering for Power**, Vol. 103, pp. 179-771.

9. Ikioka, L.M., Brum, R.D., and Samuelsen, G.S., "A Laser Anemometer Seeding Technique for Combustion with Multiple Stream Injection," **Combustion and Flame**, Vol. 49, 1983, pp. 155-162.

10. Bachalo, W.D. and Houser, M.J.,: **Optical Engineering**, 23, 583 (1984).

11. Glassman, I., and Yaccarino, P. (1981). The Temperature Effect in Sooting Diffusion Flames. Eighteenth Symposium (International) on Combustion, The Combustion Institute, pp. 1175-1183.

12. Blazowksi, W.S., "Future Jet Fuel Combustion Problems and Requirements," **Prog. Energy Combust. Sci.**, Vol. 4, pp. 177-199, 1978.

13. Schirmer, R.M. (1972). "Effect of Fuel Composition on Particulate Emission from Gas Turbine Engines," in Emissions from Continuous Combustion Systems, Plenum Press, New York, pp. 189-210.

14. Clark, V.A. Leonard, J.A., and Mellor, A.M. (1981). "Soot Loadings, Radiation Intensities, Gaseous Species Concentrations and Temperatures in a Quasi-Steady Spray Flame," in Particulate Carbon Formation During Combustion, Plenum Press, New York.

15. Jackson, T.A. and Samuelsen, G.S., "Spatially Resolved Droplet Size Measurements," **Journal of Engineering for Gas Turbines and Power**, Vol. 108, Jan 1986, pp. 196-203.

16. Wood, C.P., and Samuelsen, G.S. (1985). Optical Measurements of Soot Size and Number Density in a Spray-Atomized, Swirl-Stabilized Combustor, **Journal of Engineering for Gas Turbines and Power**, Vol. 107, pp. 38-47.

17. Smith, R.A. (1985). "Extractive Probe Perturbation and Soot Sample Integrity in a Swirl-Stabilized Combustor," Master's Thesis, University of California, Irvine.

18. Cooper, H.B.H., and Rossano, A.T., (1971). Source Testing for Air Pollution Control, Environmental Research and Applications, Inc., Wilton, Connecticut.

19. Churchill, A.V., DeLaney, C.L. and Lander, H.R. (1978). "Future Aviation Turbine Fuels," J. Aircraft, Vol. 15, No. 11, pp. 731-734.

20. Prado, G.P., Lee, M.L., Hites, R.A., Hoult, D.P., and Howard, J.B. (1976). "Soot and Hydrocarbon Formation in a Turbulent Diffusion Flame," Sixteenth Symposium (International) on Combustion. The Combustion Institute, pp. 649-661.

21. Wyatt, W.R., Clark, J.A., Peters, J.E., and Mellor, A.M. (1979). "Size Distribution and Surface Area Measurements of Gas Turbine Combustor Smoke," Journal of Energy, Vol. 3, No. 5, pp. 285-290.

22. Samuelsen, G.S., Wood, C.P., and Jackson, T.A. (1983). "Optical Measurements of Soot Size and Number Density in a Complex Flow, Swirl-Stabilized Combustor," AGARD preprint 353. Presented at the NATO/AGARD Propulsion and Energetics Panel 62nd Symposium on Combustion Problems in Turbine Engines, Cesme, Turkey, October.

23. Brum, R.D. and Samuelsen, G.S., "Two-Component Laser Anemometry Measurements of Non-Reacting and Reacting Complex Flows in a Swirl Stabilized Model Combustor," **Experiments in Fluids**, Vol. 5, 1987, pp. 95-102.

24. Sawyer, R.F. (1972). "Experimental Studies of Chemical Processes in a Model Gas Turbine Combustor," Emissions From Continuous Combustion Systems, edited by W. Cornelius and W.G. Agnew, Plenum Publishing Co., New York, pp. 243-254.

25. Fenton, D.L., Luebcke, E.H., and Norstrom, E. (1979). "Physical Characterization of Particulate Material From a Turbine Engine," ASME Paper 79-GT-179.

26. Jackson, T.A., and Samuelsen, G.S. (1984). An Evaluation of Fuel Spray Performance in a Swirl Stabilized Combustor Using Optical Methods for Drop Sizing, presented at the AIAA/SAE/ASME 20th Joint Propulsion Conference, Cincinnati, June.

27. Kramlich, J.C., Heap, M.P., Seeker, W.R., and Samuelsen, G.S.: **Twentieth Symposium (International) on Combustion**, p. 1991, The Combustion Institute, 1984.

28. Rizk, N.K. and Lefebvre, A.H.: **J. Propulsion**, 1, 200 (1985).

29. Wood, C.P., Smith, R.A., and Samuelsen, G.S. (1985). Spatially-Resolved Measurements of Soot Size and Population in a Swirl-Stabilized Combustor, Proceedings of the Twentieth Symposium (International) on Combustion, The Combustion Institute, pp. 1083-1094.

30. Dodge, L.G.: **Optical Engineering, 23, 626** (1984).

31. Jackson, T.A. and Samuelsen, G.S., "Detailed Characterization of an Air Assist Atomizer and Its Use in a Swirl Stabilized Combustor," AIAA 85-1811, July 1985.

32. Gouldin, F.C., Depsky, J.S., and Lee, S.L., "Velocity Field Characteristics of a Swirling Flow Combustor," **AIAA Journal**, Vol. 23, No. 1, p. 95, January, 1985.

33. Lilly, D.G., "Investigations of Flowfields Found in Typical Combustor Geometries," NASA Contractor Report 3869, 1985.

34. Lefebvre, A.H., Gas Turbine Combustion, McGraw-Hill, New York, 1983.

35. Rudoff, R.C., "Design, Evaluation, and Characterization of a Gas Turbine Model Laboratory Combustor with Discrete Wall Injection," Master's Thesis, UCI Combustion Laboratory Report UCI-ARTR-86-1, Department of Mechanical Engineering, University of California, Irvine, CA, 92717, 1986.

36. Swithenbank, J., Turan, A., and Felton, P.G. Three-Dimensional Two-Phase Mathematical Modelling of Gas Turbine Combustors. Gas Turbine Combustor Design Problems, Edited by A.H. Lefebvre, Hemisphere Publishing, pp. 249-314, 1980.

37. Boysan, F., Ayers, W.H., Swithenbank, J., and Pan, Z. Three-Dimensional Model of Spray Combustion in Gas Turbine Combustors. J. Energy, Vol. 6, No. 6, pp. 368-375, 1982.

38. Leonard, P.A., and Mellor, A.M. Correlation of Gas Turbine Combustor Efficiency. J. Energy, Vol. 7, No. 6, pp. 596-602, 1983.

(The reverse of this page is blank.)